

Copyright
by
Pamela Lynn Gay
2002

This Dissertation Committee for Pamela Lynn Gay Certifies that this is the approved version of the following dissertation:

Using Radio Sources to Find Galaxy Clusters

Committee:

Gary Hill, Supervisor

John Kormendy, Co-Supervisor

Edward L. Robinson

J. Craig Wheeler

Hugo Martel

Steven Rawlings

Using Radio Sources to Find Galaxy Clusters

by

Pamela Lynn Gay, B.S. M.A.

Dissertation

Presented to the Faculty of the Graduate School of

The University of Texas at Austin

in Partial Fulfillment

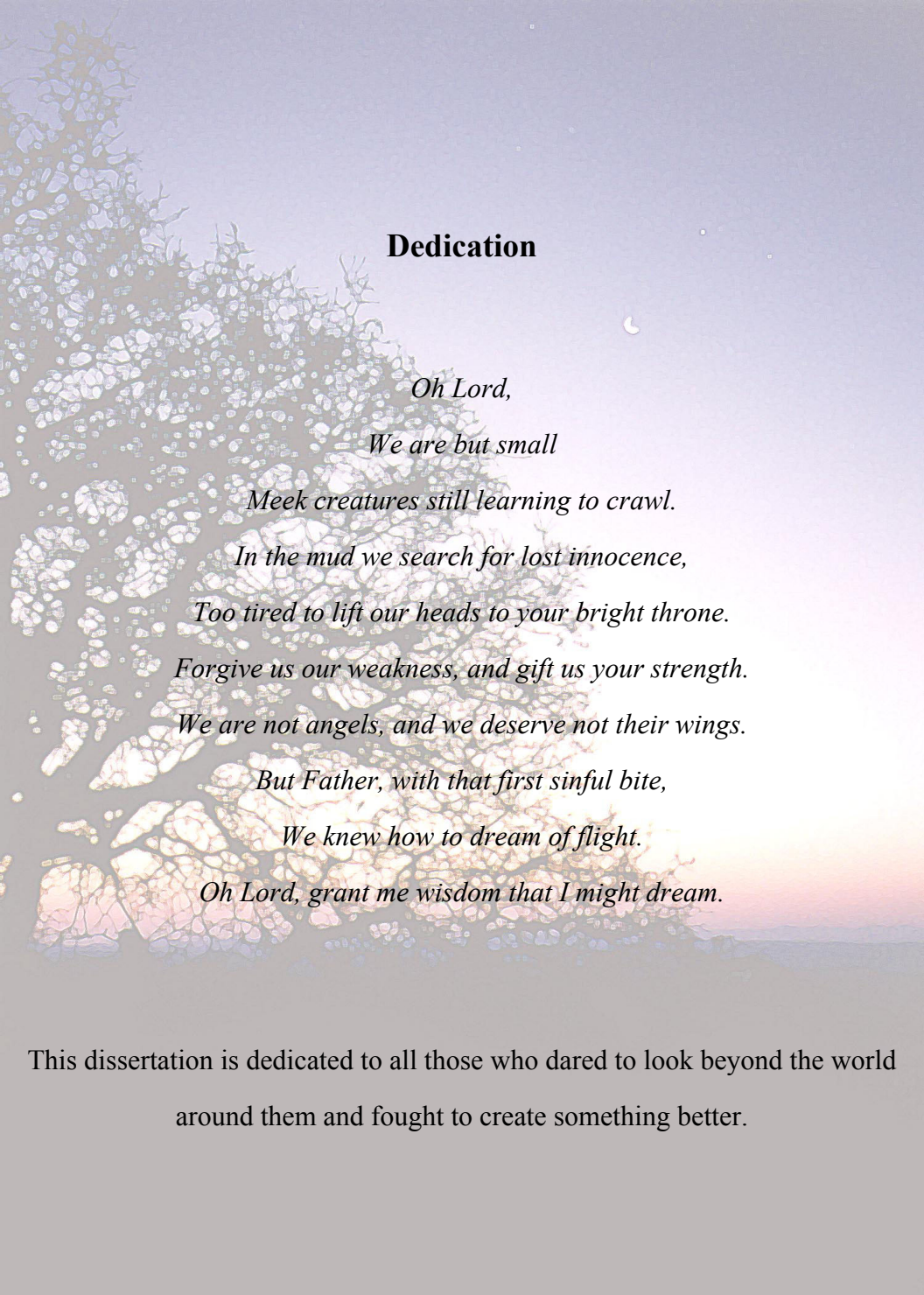
of the Requirements

for the Degree of

Doctor of Philosophy

The University of Texas at Austin

December, 2002



Dedication

*Oh Lord,
We are but small
Meek creatures still learning to crawl.
In the mud we search for lost innocence,
Too tired to lift our heads to your bright throne.
Forgive us our weakness, and gift us your strength.
We are not angels, and we deserve not their wings.
But Father, with that first sinful bite,
We knew how to dream of flight.
Oh Lord, grant me wisdom that I might dream.*

This dissertation is dedicated to all those who dared to look beyond the world
around them and fought to create something better.

Acknowledgements

My committee provided invaluable service throughout the past four years. Specifically, I would like to thank Rob Robinson for pointing me towards extragalactic research, and who listened to a myriad of random problems and offered levelheaded support. I thank Gary Hill for proposing this topic and being patient with me as I have transitioned from stars to galaxies. Last, but far from least, I thank John Kormendy for helping me find ways to do things I enjoy, while keeping me focused on finishing this dissertation and finding a future.

I would like to acknowledge the people who helped me observe just because they wanted to: to David Fisher, Brian Faitt and the dead mouse they disposed of for me; to Rebecca Christian who kept me sane through two weeks of fires, dust, lightening and all other manner of natural observing disasters; and to Kelley Knight who introduced me to tomatillos and helped me see possibilities.

This dissertation was made possible by three people: Julie Szebehely, who brought me vanilla cokes and forced me to ride horses when she found me arguing verbally with IRAF; my Dad who did all the things a dad sometimes needs to do; and Chris Wilkinson who supported me in the face of many storms.

Using Radio Sources to Find Galaxy Clusters

Publication No. _____

Pamela Lynn Gay, Ph.D.

The University of Texas at Austin, 2002

Supervisors: Gary Hill and John Kormendy

In this work, we studied the feasibility of using radio source overdensities to find moderate redshift galaxy clusters. We define an overdensity as five NVSS radio sources contained in a 6-arcmin \times 6-arcmin box, and find a lower-limit cluster finding rate of 21%. The clusters we identified have low to moderate redshifts ($z < 0.5$), are observationally average when compared to clusters from the literature, have low richnesses, and have an estimated two physically associated radio sources.

While creating comparison samples from the literature we noted two significant trends: (1) the radio source R-z relation breaks down with decreasing $S_{1.5}$ values and (2) the B-O effect appears to be a function of both redshift and cluster richness.

We find that the brightest radio sources in the sky, those drawn from the 3CR and 6C catalogues, have a different relationship between redshift and R magnitude than lower flux sources ($S_{1.5} < 200$ mJy). Furthermore, sources drawn from the NVSS catalogue show increased scatter in their R-z relationship with decreasing flux, and the high resolution high sensitivity FIRST catalogue shows only a modest R-z relationship. We feel that only sources with $S_{1.5} \geq 10$ mJy from the NVSS catalogue can be used with any reliability to constrain the redshift of a radio-optical source.

The observed dependence of the B-O effect on redshift and richness is a reflection of field galaxy infall rates changing with redshift, the ability of the cluster environment to trigger and/or suppress star formation, and cluster sizes. A rich red cluster can only minimally be blue enhanced by field galaxy infall. Additionally, the primary mechanisms for triggering star formation – interactions and tidal effects – are most effective in systems with low velocity dispersions and a diffuse ICM; e.g. in lower richness clusters. Ram pressure stripping, which truncates star formation, is most effective in high mass systems. Thus, star formation is most likely to be triggered and last in lower richness clusters, while in high richness clusters, what star formation is able to occur is quickly extinguished. These effects are not found in groups, which have widely varying blue fractions.

Table of Contents

Acknowledgments	v
Abstract	vi
List of Tables	x
List of Figures	xii
Chapter 1: Listening for Clusters	1
Radio Source Distribution	7
Overdensity Search Technique	9
Initial Observations	14
Summary	14
Chapter 2: Defining Signal	17
Deep Images	17
Wide-field Images	20
Data Reduction: 2.7-m + IGI	23
Data Reduction: 0.8-m + PFC	26
Image Co-addition	28
Standard Calibrations	30
Summary	35
Chapter 3: Cluster Characteristics	39
Redshifts	39
Brightest Cluster Galaxies	43
Radio Sources	46

Richness.....	59
Color Distributions.....	63
Summary.....	63
Chapter 4: All the Pretty Colors.....	68
Measurements.....	69
The Literature.....	71
Summary.....	80
Chapter 5: A Few Brief Words in Closing.....	82
Appendix 1: Region 1.....	86
Appendix 2: Region 2.....	103
Appendix 3: TOC J1602.8 + 4338.....	121
Appendix 4: TOC J1620.9 + 4442.....	123
Appendix 5: TOC J1626.1 + 4859.....	125
Appendix 6: TOC J1705.8 + 3657.....	127
Special Acknowledgements.....	129
Bibliography.....	130
Vita.....	137

List of Tables

Table 1-1:	Richness & distance class distributions for a sample of 50 Abell clusters containing radio sources.....	5
Table 1-2:	Comparison between actual and expected overdensity distributions.....	8
Table 1-3:	Summary of overdensity positions and radio source number.....	11
Table 1-4:	Known clusters near radio overdensities.....	13
Table 2-1:	Clusters selected for detailed study.....	18
Table 2-2:	Adopted cluster redshifts.....	19
Table 2-3:	Log of observing conditions.....	22
Table 2-4:	Final co-added image seeing and area.....	29
Table 2-5:	Log of standard star observations.....	32
Table 2-6:	Limiting magnitudes for each field.....	38
Table 3-1:	Redshifts of objects in field of clusters.....	40
Table 3-2:	TOC brightest cluster galaxy R-magnitudes.....	46
Table 3-3:	The standard deviation about the R – z relationship for N NVSS sources.....	48
Table 3-4:	Radio sources within $2 R_{\text{Abell}}$ of TOC clusters.....	52
Table 3-5:	R30, N30 and Field galaxy densities.....	60
Table 4-1:	f_B for TOC clusters.....	71
Table 4-2:	Fitting parameters for $f_B = m z + b$	72

Table A1-1: Complete list of Region 1 overdensities.....	88
Table A1-2: List of known clusters in Region 1.....	101
Table A2-1: Complete list of Region 2 overdensities.....	105
Table A2-2: List of known clusters in Region 2.....	116
Table A3-1: Basic Data.....	121
Table A3-2: Standard Star Corrections.....	121
Table A3-3: Image characteristics.....	122
Table A4-1: Basic Data.....	123
Table A4-2: Standard Star Corrections.....	123
Table A4-3: Image characteristics.....	124
Table A5-1: Basic Data.....	125
Table A5-2: Standard Star Corrections.....	125
Table A5-3: Image characteristics.....	126
Table A6-1: Basic Data.....	127
Table A6-2: Standard Star Corrections.....	127
Table A6-3: Image characteristics.....	128

List of Figures

Figure 1-1: Redshift vs. richness for galaxy clusters found around radio sources	6
Figure 1-2: Overdensities rejected after visual inspection	10
Figure 1-3: ZwCl 1639.9+3805 with ODs marked	15
Figure 2-1: B-R-I matched images of clusters selected for detailed analysis	18
Figure 2-2: B-R-I matched images of comparison fields	19
Figure 2-3: Fiery sunset and stormy sunrise	21
Figure 2-4: Wide area image of TOC J1602.8 + 4338	23
Figure 2-5: Raw vs. reduced IGI images	25
Figure 2-6: Raw vs. reduced PFC images	27
Figure 2-7: Examples of images not used	28
Figure 2-8: A plot of measured magnitudes vs. aperture for 5 stars	30
Figure 2-9: Differences between Landolt's published magnitudes for standard stars, and the magnitudes calculated using determined constants	31
Figure 2-10: Difference between PFC standardized and instrumental B, R and I magnitudes + determined constant term for all shared objects images	36
Figure 2-11: Number of objects vs. magnitude for TOC J1602.8+4338	37

Figure 3-1:	TOC J1626.1+4859. Main image is from PFC data, and inset is an IGI image of the cluster.....	41
Figure 3-2:	TOC J1705.8+3657. Main image is from PFC data, and inset is an IGI image of the cluster.....	42
Figure 3-3:	Magnitude vs. redshift for BCGs.....	44
Figure 3-4:	PL95 brightest cluster galaxy sample.....	45
Figure 3-5:	Redshift vs. R-magnitude for 6C and 3CR galaxies.....	47
Figure 3-6:	Redshift vs. R-magnitude for NVSS galaxies.....	49
Figure 3-7:	Redshift vs. R-magnitude for FIRST galaxies.....	50
Figure 3-8:	Comparison of R mag. vs. redshift for 3CR, 6C, NVSS and FIRST.....	50
Figure 3-9:	R – z plot of optical magnitudes of TOC radio sources and cluster redshifts.....	51
Figure 3-10:	Central Region of TOC J 1602+4338 at $z = 0.416$	57
Figure 3-11:	Central Region of TOC J 1620.9+4442 at $z = 0.215$	58
Figure 3-12:	Radial galaxy density for TOC 1620.9+4442.....	61
Figure 3-13:	Number of field galaxies as a function of R-magnitude.....	62
Figure 3-14:	R_{30} vs. N_{30} for the 33 clusters from BO84, and the TOC sample.....	64
Figure 3-15:	Cluster Color Diagrams.....	64
Figure 3-16:	Rest frame Color Distribution for all TOC Clusters.....	66
Figure 4-1:	Plot of points BO84 used to show the B-O effect.....	68
Figure 4-2:	Collection of published blue fractions from literature.....	69

Figure 4-3:	Comparison of our f_B value with those from the literature.....	73
Figure 4-4:	Trend of f_B with z for entire cluster data set.....	73
Figure 4-5:	f_B trends for various Abell Richnesses.....	74
Figure A1-1:	Map of Region 1.....	87
Figure A2-1:	Map of Region 2.....	104

Chapter 1: Listening for Clusters

Galaxy clusters are scientifically important on a variety of scale sizes, acting as laboratories for the study of galaxy evolution in diverse density environments and as test particles that help to trace out the evolution of the large-scale structure of the universe. Spatial statistics on galaxy clusters can be used to constrain cosmological parameters (Bahcall and Fan 1998; Kauffmann 1995; Bahcall 1988), as well as the universe's dark matter distribution and baryon fraction (Allen et al. 2002; Schindler 2001; Navarro, Frenk & White 1997). The recent discovery of massive clusters at high redshifts (Fairley et al. 2002; van Dokkum et al 2001; Yamada et al. 2001; Cagnoni et al. 2001) has worked with supernovae results (Perlmutter et al. 1999; Riess et al. 1998) and observations of the cosmic microwave background (Netterfield et al. 2002; Melchiorri et al. 2000) to demonstrate that we live in a low Ω_M universe.

The newly discovered population of high- z clusters has cosmological implications and provides a new tool for studying the evolution of galaxies in moderate to high-density environments (10-100s of galaxies Mpc^3). In the local universe, populations of galaxies in clusters are markedly redder than the field, and galaxy clusters contain almost no spiral galaxies. The Butcher-Oemler effect (hereafter B-O effect – Butcher and Oemler 1984) demonstrates that with increasing redshift, galaxy clusters contain higher and higher fractions of blue galaxies. The exact cause of the bluing and the relationship between cluster density and blue fraction is still unclear.

Looking at our own local universe, we observe that as cluster densities decrease from Abell-like systems to small groups such as our own Local Group, the fraction of disk galaxies begins to more closely resemble that of the field. Most large studies of the B-O effect have focused on massive clusters (Fairley et al. 2002; Ellingson, et al. 2001; Margoniner et al. 2001; Margoniner and de Carvalho 2000; Metevier et al. 2000; Lubin 1996; Dressler and Gunn 1992), and this may distort our understanding of any physical mechanisms behind the B-O effect. There are two reasons: the massive clusters of yesterday do not evolve into the same massive clusters of today, and the physical mechanisms (if any) behind the Butcher-Oemler effect may have different strengths in different density environments.

Possible mechanisms for the B-O effect include cluster infall (Ellington et al. 2001; Rakos et al. 2000; Kaufmann 1995), galaxy harassment (Fujita 1998; Rakos et al. 2000), and galaxy-galaxy interactions and mergers (Nelson et al. 2002; van Dokkum 1999; Kaufmann 1995). The general picture is one of disk galaxies falling into a cluster potential and undergoing triggered star formation due to ram pressure,¹ galaxy harassment² and galaxy-galaxy interactions and mergers. These same “bluing” mechanisms lead to the eventual loss of the galaxies’ spiral structure and reddening. This picture, combined with the

¹ Ram Pressure: As galaxies fall into / orbit thru clusters, their speed relative to the ICM creates a pressure front that will flow around the galaxy or blow through it. This may initially double star formation rates, can remove some or all of the galaxies ISM, and may transform spiral galaxies into S0s. (Gunn & Gott 1972; Dressler & Gunn 1983; Abadi, Moore & Bower 1999; Fujita 2001)

² Galaxy Harassment: High-speed interactions between galaxies disrupt their structure, drive gas into galaxy cores, and cause star formation. Multiple interactions can strip out all the galaxy’s gas and end all star formation (Moore, Lake & Katz 1998).

observation that some clusters have large blue fractions at high redshifts, implies that perhaps there was a higher rate of cluster infall at higher redshifts. This picture is not without problems, however.

There is some evidence in the literature that perhaps what is being observed is not a bluing of all galaxy cluster populations with look-back time, but rather an effect created by studying intrinsically different objects in different epochs. Andreon and Etori (1999) studied the X-ray properties of the clusters in Butcher and Oemler sample and conclude, "... the BO sample is not formed from the same class of objects observed at different look-back times." Studies of similar objects at varied redshifts do not demonstrate an increase in blue fraction that is significantly different than that expected from passive evolution (Fairley et al 2002; Andreon and Etori 1999; Allington-Smith et al. 1993). This suggests that either the BO effect is limited to certain types of galaxy clusters or that it is not a physical effect at all.

To understand what is going on, the blue galaxy fraction of clusters must be explored in the 2-dimensional-phase space of redshift and cluster size. The blue fraction must be measured in a consistent way that takes into account the difference in cluster volume as a function of cluster size. This requires a cluster sample that is unbiased in both redshift and density. Unfortunately, there is no simple way to create such a data set.

At this time, the majority of clusters are being found using time consuming large-area photometric and X-Ray surveys that are limited in their ability to find low richness clusters and groups. The optical imaging surveys,

such as the Las Campanas Distant Cluster Survey (Gonzalez 2001), the Sloan Digital Sky Survey (Kim et al. 2002) and the Palomar Distant Cluster Survey (Postman 1996) are naturally biased towards rich, bright and/or centrally concentrated clusters because these stand out the strongest against the foreground and background galaxy distributions. X-Ray surveys, such as the Einstein EMSS Survey (Gioia et al. 1990, Stocke 1991), the Catalogue of ROSAT galaxy clusters (Vikhlinin et al. 1998), and the ROSAT brightest cluster and Extended Bright Cluster Samples (Ebeling et al. 1998, 2000) are biased towards evolved, high-mass systems at low to moderate redshifts. To understand the distribution of clusters across a wide range of masses, concentrations and redshifts, a technique for finding clusters without these biases is required. While new spectroscopic surveys, such as the 2-degree Field Galaxy Redshift Survey (2dFGRS — de Propris et al 2002), should be completely unbiased, they are extremely time consuming and at this time do not probe even moderate ($z > 0.15$) redshifts.

A possible timesaving technique is to search for clusters around radio sources. Galaxy clusters have often been serendipitously found around strong radio sources (see Owen 1996 for a review). In a 1.5 GHz VLA survey of 58 Abell clusters between $-30^\circ \geq \text{Dec} \geq 35^\circ$ that each contain one strong steep-spectrum³ ($\alpha \leq -0.9$) radio source, Slee et al. (1998) find an average of two radio galaxies per cluster. These galaxies were concentrated towards the cluster centers, and while the survey contained clusters spanning a large range in Abell

³ The distribution of energy from synchrotron radiation in a radio source can be represented by a spectral index α where: $\epsilon_\nu \propto \nu^{-\alpha}$. ϵ_ν is the synchrotron emissivity, and ν is the frequency.

Table 1-1: Richness & distance class distributions for a sample of 50 Abell clusters containing radio sources. Data from Slee et al. (1996).

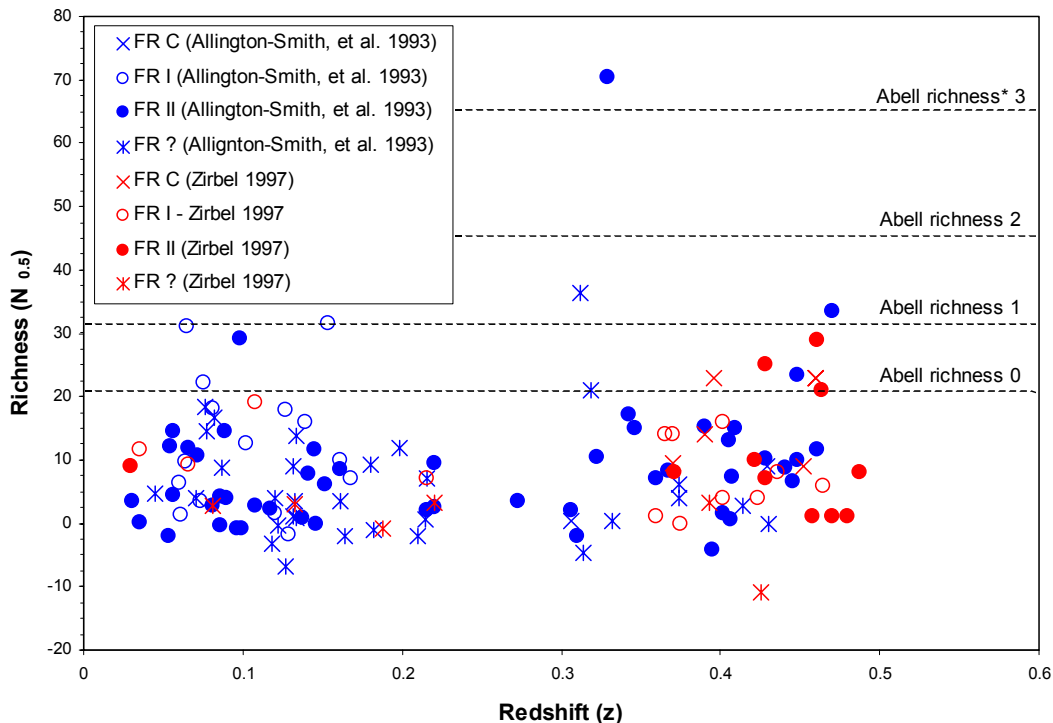
Richness	# of	Distance	# of
0	20	1	1
1	22	2	2
2	5	3	11
3	1	4	12
4	2	5	15
5	0	6	9

richness and distance classes, the majority (42 out of 50) of the clusters were richness class 0 or 1 and they tended towards higher distance classes (see Table 1-1). This implies that

clusters containing radio sources have lower richnesses and radio selected clusters should tend towards higher redshifts. These results are consistent with studies of radio galaxy environments done by Zirbel (1997), Allington-Smith et al. (1993), Hill and Lilly (1991). These papers found that radio sources avoid high density environments in the local universe, and that even at $z \sim 0.4$, the radio source environments were on average less rich than Abell class 0 (see Fig. 1-1). Furthermore, no correlation between a cluster's radio source properties or X-Ray luminosity has been identified (Feigelson et al 1982; Burns et al. 1994). These results imply that radio sources can be used to create galaxy cluster catalogues that are not biased towards the richest or most evolved clusters..

Using radio sources to find galaxy clusters is not a novel idea. Blanton, et al. (2001) used bent doubles from the Faint Images of Radio Sky at Twenty-centimeters (FIRST - Becker et al. 1995) radio survey to identify double-lobed radio galaxies with jets contorted by the intra-cluster medium (ICM) of rich clusters. While this technique is very successful, the necessity of resolving radio lobes limits its application to lower redshifts. In a different study, Zanichelli et al. (2001) looked for clusters around 661 radio sources from the New VLA Sky

Figure 1-1: Redshift vs. Richness for galaxy clusters found around radio sources. Abell richness divisions are derived from Abell's definitions (Abell 1958) and the relationship $N_{\text{Abell}} = 0.35 (N_{0.5})^{1.4}$ (Allington, et al. 1993).



Survey (NVSS – Condon et al. 1998) and found 171 cluster candidates (a success rate of 26%). Of these candidates, 76 (44%) were associated with known clusters. 11 additional cluster candidate fields were spectroscopically studied, and 9 (82%) of these identified a cluster and the radio source at the same redshift. In the 2 other fields, clusters were found, but they had redshifts different from those of the radio source. These results demonstrate that radio sources can be used to effectively find galaxy clusters at least to $z \sim 0.5$.

The $\sim 25\%$ cluster rate of Zanichelli et al.'s work still implies that roughly three-fourths of the telescope time used to observe a set of potential cluster fields

would go wasted. While this is better than the success rate of drift scanning⁴ optical surveys (see discussion below) it is still not ideal. In this work we will outline a technique that employs overdensities of multiple radio sources in the NVSS survey to find cluster candidates.

In this dissertation, I will outline our new technique for identifying galaxy clusters and discuss the characteristics of a subset of our clusters in comparison to well-studied galaxy clusters at similar redshifts. In this chapter, I will outline our selection method and preliminary statistics on its efficiency. Chapter 2 will review data reduction techniques and our observation set. Chapters 3 will discuss our results for 4 clusters we observed in detail, and chapter 4 will compare these clusters to other clusters at similar redshifts. Chapter 4 also contains a detailed review of cluster galaxy populations as a function of richness and redshift as taken from the literature. Particular emphasis will be placed on understanding cluster galaxy populations in terms of their blue fraction (Butcher & Oemler 1984) and radial population gradients.

Unless noted, cosmological parameters of $H_0 = 65 \text{ km sec}^{-1} \text{ Mpc}^{-1}$, $\Omega_m = 0.3$, $\Omega_\Lambda = 0.7$ and $q_0 = -0.15$ are assumed. K-corrections are taken from Fujita et al (1995). Angular and luminosity distances were calculated using software provided by Hugo Martel (2002) and based on Premadi et al. (1998).

RADIO SOURCE DISTRIBUTION

Our technique is based on very simple logic: if clusters are often found around isolated radio sources, we should be able to increase our probability of

⁴ Drift Scanning Surveys: Surveys employing specialized CCD electronics and tracking rates that scan such that the CCD is readout at the same rate that an object moves across the chip.

finding galaxy clusters by looking around concentrations of radio sources. In our initial survey, our goal was to find galaxy clusters at the distance $0.35 \leq z \leq 0.6$. At these redshifts, AGN radio galaxies have a range in brightness $18.38 \pm 0.59 \leq R \leq 19.22 \pm 0.59$ (Machalski & Condon 1999), making them

Table 1-2: Comparison between actual and expected overdensity distributions. The source samples contained 20,762 sources in 734.4 deg^2 . The expected number comes from a random distribution.

# of Sources	# of Actual Overdensities	# of Expected Overdensities
0	68,806	92,454
1	32,660	17,231
2	8,238	1,605.8
3	1,440	99.764
4	231	4.6485
5	17	0.1733
6	3	0.0054
7	1	0.0001
8	0	0.0000

easily observable in single 900 second observations using the McDonald Observatory Harlan J. Smith 2.7-m telescope and the Imaging Grism Instrument (IGI). The Abell cluster radius ($1.5 \text{ h}^{-1} \text{ Mpc}$) in this redshift band is $7.2 - 5.3$ arcmin, which is well matched to IGI's $7\text{-arcmin} \times 7\text{-arcmin}$ field of view (FoV).

To find clusters in this redshift region, we examined the frequency of finding n radio sources in a $6\text{-arcmin} \times 6\text{-arcmin}$ box and looked for an n that produced significantly more overdensities than expected from a random distribution. Our radio sources were taken from the NVSS catalogue. In the test region $00:00:00 \leq \alpha \leq 03:00:00$ and $30:00:00 \leq \delta \leq 40:00:00$, we found 20,762 sources with $S_{1.5} \geq 2.0 \text{ mJy}$. We sampled this region 111,396 times with sample boxes that overlapped by no more than 70% and compared our observed clustering distribution to that of an artificial data set of the same area, with the same number of sources distributed randomly (see Table 1-2).

Differences between the actual and random distributions arise from the physical clustering of sources. It is well understood that radio sources clump at the 2-source level with a slope in the correlation function similar to that of the general galaxy population (Blake & Wall 2002). Directly determining higher-order correlation functions is complicated by multi-lobed radio galaxies being catalogued as multiple radio sources and by the tendency of radio sources with different powers to prefer different environments at different redshifts (Zirbel 1997; Hill & Lilly 1991). Rather than directly calculating progressively higher-order correlation functions that attempt to take these dependences into account, we have looked for significant divergences between the random and observed source distributions. At the ≥ 5 sources per box frequency, we find 21 overdensities compared to the expected 0.18, and we chose 5 sources per 6-arcmin \times 6-arcmin box as our overdensity minimum size.

OVERDENSITY SEARCH TECHNIQUE

For our observational study, we selected two regions of the sky that are accessible to the fixed-altitude Hobby-Eberly Telescope (HET - Glaspey 1998) at McDonald Observatory, and that are included in the NVSS catalogue. These regions are: $16:00:00 \leq \alpha \leq 17:00:00$ by $35:00:00 \leq \delta \leq 60:00:00$ (hereafter, region 1) and $01:30:00 \leq \alpha \leq 03:00:00$ by $30:00:00 \leq \delta \leq 40:00:00$ (hereafter, region 2). A C program, FindOD (Gay 2002) was written to find overdensities from source lists produced using NVSSlist (Cotton 1998). This software finds all the sources within a 5 arcmin radius around a given radio source, and then looks for a combination of that source and four or more other sources that will fit inside

a $6\text{-arcmin} \times 6\text{-arcmin}$ box. While inefficient in terms of CPU cycles, this algorithm creates a complete list of overdensities from an input radio source catalogue. Clusters separated by less than 1 arcmin were removed by hand. The resulting overdensity catalogues can be found in Appendices 1 and 2.

Once the overdensity (OD) catalogues were produced, NVSS, FIRST and Second Digital Sky Survey (DSS2 – McLean 2000) images of the ODs were visually inspected for local galaxies over-resolved into multiple radio sources, obvious double-lobed radio galaxies broken into multiple sources, and radio overdensities that can be completely identified from DSS2 images (see Figure 1-2). We also compared the positions of our overdensities to the positions of known clusters listed in NASA’s Extragalactic Database (NED). The ODs from regions 1 and 2 and their number of NVSS radio sources, are given in Table 1-3. Table 1-4 lists the name, OD-cluster separation and redshifts for any known clusters within 20-arcmin ($1.5h^{-1}$ Mpc at $z = 0.1$ is 19.4 arcmin) of an OD.

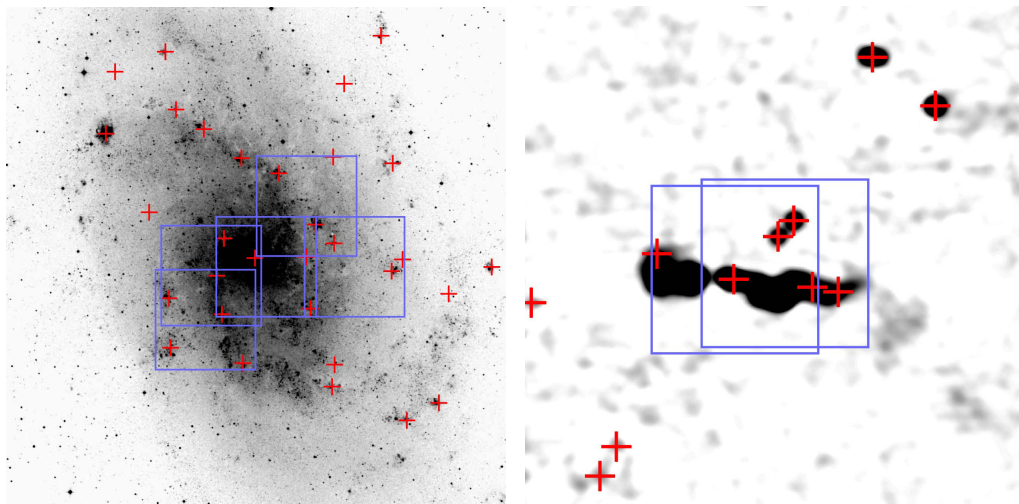


Figure 1-2: Overdensities rejected after visual inspection. a: (left) Along with finding potential galaxy clusters, our technique “discovered” M33. b: (right) Fields with obvious double lobes, such as TXS 0217+367, shown here, were given low/no observational priority.

Table 1-3: Summary of Overdensity Positions and Radio Source Number.
a - Region 1 Summary. # refers to the number of NVSS radio sources in the OD.
TOCC stands for Texas-Oxford Cluster Candidate.

Name	#	Name	#
TOCC 0130.9 +3609	5	TOCC 0211.2 +3521	5
TOCC 0131.9 +3737	5	TOCC 0212.7 +3342	5
TOCC 0133.4 +3039	6	TOCC 0214.0 +3316	5
TOCC 0133.6 +3043	5	TOCC 0214.9 +3326	5
TOCC 0133.8 +3039	6	TOCC 0215.0 +3129	5
TOCC 0134.3 +3049	5	TOCC 0217.1 +3134	5
TOCC 0135.3 +3004	5	TOCC 0220.2 +3701	5
TOCC 0137.0 +3013	5	TOCC 0221.1 +3025	5
TOCC 0137.3 +3338	6	TOCC 0221.7 +3200	5
TOCC 0137.4 +3319	5	TOCC 0223.1 +3245	5
TOCC 0138.1 +3309	6	TOCC 0227.0 +3407	5
TOCC 0138.2 +3727	5	TOCC 0227.4 +3440	5
TOCC 0138.5 +3723	5	TOCC 0227.4 +3441	5
TOCC 0138.5 +3323	5	TOCC 0229.8 +3111	5
TOCC 0139.3 +3226	5	TOCC 0232.4 +3425	5
TOCC 0139.3 +3229	5	TOCC 0233.4 +3021	6
TOCC 0139.5 +3625	5	TOCC 0233.6 +3560	6
TOCC 0139.8 +3309	5	TOCC 0233.8 +3510	5
TOCC 0141.0 +3015	5	TOCC 0234.2 +3132	5
TOCC 0142.1 +3219	5	TOCC 0234.3 +3852	5
TOCC 0142.3 +3548	5	TOCC 0234.9 +3136	5
TOCC 0143.0 +3140	5	TOCC 0240.2 +3005	5
TOCC 0146.1 +3746	5	TOCC 0240.2 +3625	5
TOCC 0146.6 +3654	5	TOCC 0245.5 +3344	5
TOCC 0148.0 +3050	5	TOCC 0245.9 +3910	5
TOCC 0148.0 +3053	5	TOCC 0246.5 +3629	5
TOCC 0148.1 +3048	6	TOCC 0246.7 +3025	5
TOCC 0153.7 +3106	5	TOCC 0246.9 +3642	5
TOCC 0153.9 +3748	5	TOCC 0247.8 +3753	5
TOCC 0154.0 +3554	5	TOCC 0249.4 +3647	5
TOCC 0154.0 +3557	6	TOCC 0249.9 +3026	5
TOCC 0155.2 +3345	5	TOCC 0250.2 +3043	5
TOCC 0156.8 +3205	5	TOCC 0253.3 +3836	5
TOCC 0156.8 +3207	6	TOCC 0256.3 +3828	5
TOCC 0158.4 +3901	5	TOCC 0256.7 +3652	8
TOCC 0207.4 +3653	5	TOCC 0256.8 +3032	5
TOCC 0209.4 +3729	6	TOCC 0259.5 +3559	5

Table 1-3 (continued)

b: Region 2 Summary. # refers to the number of NVSS radio sources in the OD.

Name	#	Name	#
TOCC 1601.1 +4413	6	TOCC 1629.1 +4335	5
TOCC 1601.5 +4602	5	TOCC 1629.9 +4514	5
TOCC 1601.7 +4522	5	TOCC 1630.6 +3512	5
TOCC 1602.0 +4242	5	TOCC 1633.2 +4438	5
TOCC 1602.0 +4240	5	TOCC 1636.3 +4912	5
TOCC 1602.8 +4338	5	TOCC 1636.1 +3824	5
TOCC 1603.7 +3539	5	TOCC 1636.8 +4215	5
TOCC 1604.2 +3726	5	TOCC 1638.6 +3607	5
TOCC 1604.2 +3730	6	TOCC 1641.5 +3749	5
TOCC 1604.3 +3730	5	TOCC 1641.5 +3748	5
TOCC 1604.3 +3728	5	TOCC 1642.1 +3928	5
TOCC 1605.0 +4339	5	TOCC 1644.4 +3739	5
TOCC 1605.0 +4337	5	TOCC 1646.0 +4610	5
TOCC 1606.1 +4303	6	TOCC 1646.6 +3626	5
TOCC 1608.6 +4801	5	TOCC 1648.2 +4701	6
TOCC 1610.3 +4754	5	TOCC 1649.1 +3846	7
TOCC 1610.7 +4929	5	TOCC 1649.1 +3844	5
TOCC 1610.8 +4021	5	TOCC 1649.5 +4817	5
TOCC 1612.6 +4313	5	TOCC 1649.5 +4815	5
TOCC 1615.6 +3820	5	TOCC 1649.8 +4955	5
TOCC 1617.3 +3510	5	TOCC 1649.9 +4734	5
TOCC 1617.3 +3506	5	TOCC 1649.9 +4127	5
TOCC 1617.6 +3503	5	TOCC 1650.5 +4511	6
TOCC 1620.1 +4229	5	TOCC 1651.8 +3527	5
TOCC 1620.9 +4442	5	TOCC 1654.0 +3846	5
TOCC 1620.9 +4445	5	TOCC 1654.8 +4002	5
TOCC 1623.1 +4114	5	TOCC 1654.8 +4258	5
TOCC 1625.3 +4055	5	TOCC 1655.1 +4600	5
TOCC 1625.7 +4029	5	TOCC 1655.4 +4601	5
TOCC 1626.1 +4859	6	TOCC 1656.0 +4438	5
TOCC 1626.1 +4901	6	TOCC 1658.3 +4900	5
TOCC 1626.7 +3615	5	TOCC 1659.0 +3518	5
TOCC 1627.1 +4826	5	TOCC 1659.1 +3518	5
TOCC 1629.1 +4338	5	TOCC 1659.6 +3734	5

Table 1-4. Known Clusters near Radio Overdensities.

References are given in Appendices 1 and 2. Separations are in arcmin.

Name	Nearest/Notes	z	Sep.
Region 1			
TOCC 0155.2 +3345	1RXS J015505.4+335452	0.092	10.1
TOCC 0154.0 +3557	ABELL 0262	0.0163	18.1
TOCC 0153.9 +3748	ABELL 0263		15.8
TOCC 0156.8 +3207	ABELL 0278	0.0891	9.3
TOCC 0156.8 +3205	ABELL 0278	0.0891	10.6
TOCC 0246.9 +3642	RXC J0246.0+3653	0.0488	15.4
TOCC 0143.0 +3140	ZwCl 0140.1+3144		18.7
TOCC 0153.7 +3106	ZwCl 0150.9+3050		1.3
TOCC 0229.8 +3111	ZwCl 0226.5+3111		14.4
TOCC 0240.2 +3625	ZwCl 0237.6+3618		8.1
TOCC 0245.5 +3344	ZwCl 0242.2+3323		9.0
Region 2			
TOCC 1642.1 +3928	[VMF98] 186	0.47	10.1
TOCC 1608.6 +4801	ABELL 2157		14.5
TOCC 1615.6 +3820	ABELL 2167		16.2
TOCC 1620.1 +4229	ABELL 2179	0.136	4.1
TOCC 1623.1 +4114	ABELL 2187	0.1836	12.9
TOCC 1627.1 +4826	ABELL 2195		8.1
TOCC 1629.1 +4338	ABELL 2198	0.0798	16.0
TOCC 1629.1 +4335	ABELL 2198	0.0798	18.6
TOCC 1654.8 +4002	ABELL 2235	0.1511	1.6
TOCC 1602.0 +4240	GHO 1559+4242		8.8
TOCC 1602.0 +4242	GHO 1559+4242		9.8
TOCC 1606.1 +4303	GHO 1604+4303	0.897	7.8
TOCC 1605.0 +4337	GHO 1604+4331		16.6
TOCC 1605.0 +4339	GHO 1604+4331		18.7
TOCC 1601.5 +4602	ZwCl 1559.3+4615		7.7
TOCC 1612.6 +4313	ZwCl 1612.1+4320		12.8
TOCC 1617.6 +3503	ZwCl 1615.8+3505	0.0302	6.3
TOCC 1617.3 +3506	ZwCl 1615.8+3505	0.0302	8.5
TOCC 1617.3 +3510	ZwCl 1615.8+3505	0.0302	9.6
TOCC 1620.9 +4442	ZwCl 1619.5+4445		4.1
TOCC 1620.9 +4445	ZwCl 1619.5+4445		7.6
TOCC 1636.3 +4912	ZwCl 1633.5+4916		14.0
TOCC 1641.5 +3749	ZwCl 1639.9+3805		10.1
TOCC 1641.5 +3748	ZwCl 1639.9+3805		11.5
TOCC 1648.2 +4701	ZwCl 1646.4+4659		8.3

INITIAL OBSERVATIONS

Observational priority was given to fields that did not contain bright stars, obvious jets or extended radio emission. A complete list of observations is given in tables A1-1 and A2-1 in the appendices. We initially tried to observe OD fields for 900 s in R. If the observer⁵ felt that the field looked promising or was unable to identify any of the radio sources in the raw images, the fields were observed for another 900 seconds in R, and where time allowed, also in I.

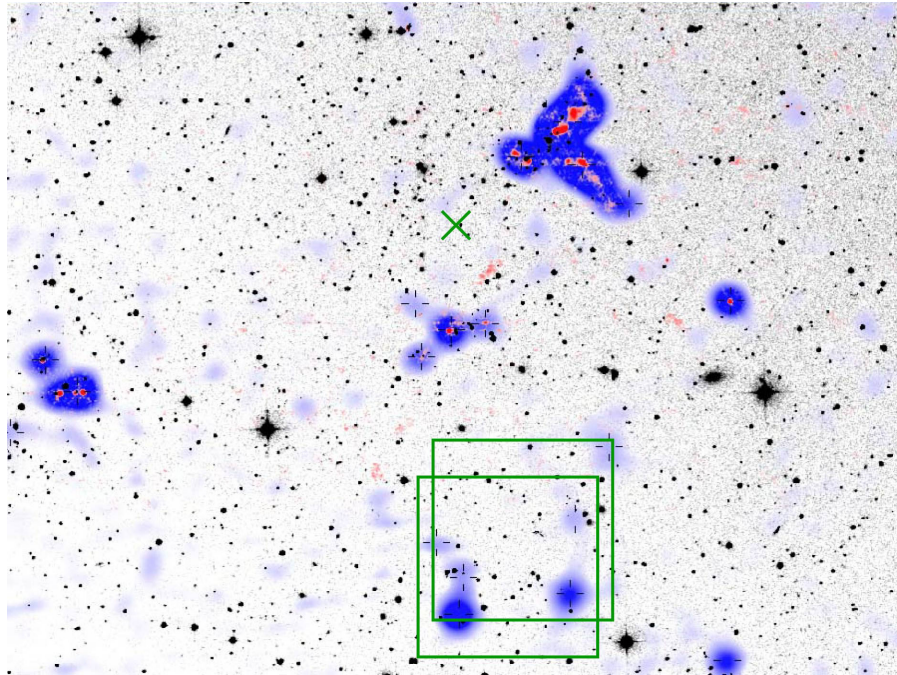
From our two regions, we observed 42 fields, including 2 Zwicky Cluster fields, for a minimum of 900 seconds. Of these, 19, including the Zwicky Clusters, appeared significantly richer than comparison fields and the remaining fields. We were able to confirm via further photometry and spectroscopy that 6 of these richer fields contain clusters.

SUMMARY

We found a total of 142 radio ODs in two regions that totaled 348 square degrees. Of these, 24 ODs (17%) aligned with known low ($z < 0.2$) redshift clusters (see Fig. 1-3). An additional 5 of 42 observed fields (12%) were confirmed to contain new clusters and 13 OD fields (31%) appeared optically richer in galaxies than the field and are considered good candidates for future observations. This puts a lower limit on our success rate of 20% (29/142), although it must be noted that we have not confirmed that the radio source overdensities are physically associated with any of the clusters. Assuming that half of the candidates contain clusters and that the unobserved fields have a

⁵ Data was taken by Marcel Bergmann, Steve Croft, Pamela Gay and Joseph Tufts, with assistance from Rebecca Christian, David Fisher, Kelley Knight and Marsha Wolf.

Figure 1-3: ZwCl 1639.9+3805 with ODs marked. Overdensities (green boxes) are centered 10.1 and 11.5 arcmin from the cluster center (green \times). NVSS radio maps are overlaid in blue, and FIRST radio maps are overlaid in red.



cluster frequency similar to that of the observed fields, we can expect a success rate of 35-45%.

Several observed fields contained no identifiable optical matches for the radio sources. We believe that these fields may be associated with extremely high-redshift objects, but follow-up observations have been inconclusive. These blank fields do not show the Sunyaev-Zeldovich⁶ effect (Cotter 2002).

Our technique is at least as successful as looking around individual NVSS sources, and potentially much more successful if overdensities are optically

⁶The Sunyaev-Zeldovich (S-Z) effect is a reduction in brightness of the CMB caused by Compton-Scattering by electrons in the hot intracluster medium.

observed until all the radio sources in a field are optically identified. We stress that 20% is simply a lower limit, but even this rate is significantly more successful than optically scanning the sky. In the Palomar Distant Cluster Survey (PDCS – Postman et al. 1996) of 5.1 square degrees, 47 clusters with redshifts $\leq 0.4^7$ were found. This region is equivalent to ~ 435 IGI fields, and if we had surveyed this region, we could only have expected to observe a cluster 11% of the time. This leads us to believe that our technique is at least twice as successful as optically surveying the sky, and potentially much more successful. Further study into the success rate of this technique at higher redshifts is needed.

⁷ They gave photometric redshifts to the nearest tenth.

Chapter 2: Defining Signal

Observations for this project were taken in three phases: OD preliminary observations (Chapter 1), deep imaging of selected clusters and comparison fields, and wide-field observations of regions surrounding clusters and comparison fields. In this chapter we describe comparison field selection and the observations made in the final two observational phases. Data reduction techniques, magnitude determinations, and standard calibrations are also discussed.

DEEP IMAGES

We selected four overdensities with apparent clusters for detailed photometric observations and spectroscopic confirmation (see Table 2-1 and Figure 2-1). Redshifts were provided by Gary Hill, and will be described in Chapter 3 (see Table 2-2). For each of the clusters, we selected a comparison field which was used to statistically correct for field galaxies in our cluster fields (see Figure 2-2). The selected comparison fields met the following criteria: they contained no bright stars; they were ~ 20 arcmin from the corresponding clusters; and there were no known clusters within 20 arcmin of their centers. Deep photometry with $0.65 \text{ arcsec pixel}^{-1}$ resolution was obtained for the cluster and comparison fields using IGI with the Harlan J. Smith 2.7-m telescope at McDonald observatory. We attempted to obtain limiting magnitudes in our final co-added images of $B = 24.5$, $R = 22.0$, and $I = 23.0$ with better than 3 arcsec seeing. This corresponds to $M_B = -18.4$, $M_R = -20.2$ and $M_I = -19.0$ at $z = 0.45$.

Table 2-1 – Clusters selected for detailed study. Epoch is J2000.
 TOC is our IAU approved acronym for Texas Oxford Cluster.

Name	Optical Center		Radio Center		Radio dist. (")	# Radio	Comparison Field		Comp dist. (")
	RA	DEC	RA	DEC			RA	DEC	
TOC J 1602.2 +4338	16:02:51.51	+43:35:05	16:02:48	+43:38:19	3.29	5	16:02:51	+43:55:05	20.00
¹ TOC J 1620.9 +4442	16:20:54.54	+44:42:00	16:20:53	+44:41:35	0.48	5	16:20:50	+45:02:48	20.85
TOC J 1625.7 +4900	16:25:44.44	+49:00:04	16:26:03	+48:58:40	4.84	6	16:25:52	+49:20:05	20.11
TOC J 1706.0 +3657	17:06:01.01	+36:57:28	17:05:50	+36:58:30	2.97	5	17:05:44	+37:17:30	20.44

Figure 2-1: B-R-I matched images of clusters selected for detailed analysis. Colors are mapped as follows: B → Blue, R → Green, I → Red.

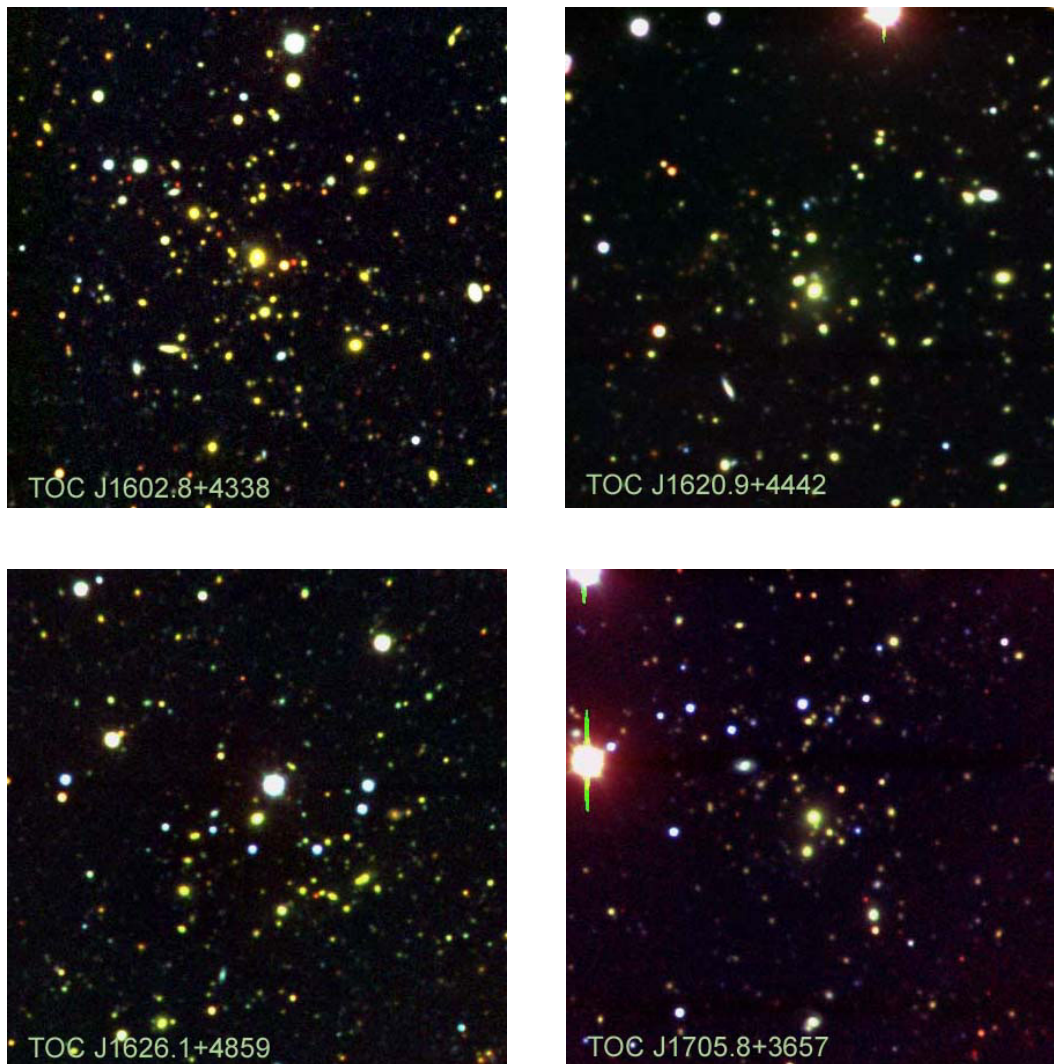


Table 2-2: Adopted Cluster Redshifts

Name	Redshift	
	z	err (z)
TOC J 1602.9+4335	0.416	0.004
¹ TOC J 1620.9+4442	0.215	0.001
TOC J 1626.1+4859	0.40	0.01
TOC J 1706.0+3657	0.167	0.002

Figure 2-2: B-R-I matched images of comparison fields. From top left and going clockwise these are the comparison fields for: TOC J1602.9+4335, TOC J1620.9+4442, TOC J1625.7+4900, TOC J1706.0+3657. Colors are mapped as follows: B \rightarrow Blue, R \rightarrow Green, I \rightarrow Red.



These observational limiting magnitudes were chosen to allow us to study the Butcher-Oemler effect in our clusters. The B-O effect describes the observation that many distant clusters have a larger blue galaxy fraction than local clusters. This fraction is measured using all galaxies with $M_V > -18.5$, which corresponds to a limit of $M_R = -19.1$ and $M_B = -17.5$ for an elliptical galaxy with $B-R = 1.57$, or $M_R = -18.8$ and $M_B = -18.23$ for an irregular galaxy with $B-R = 0.58$.

During the time allocated for these observations, this observer experienced a string of amazingly bad weather and bad atmospheric conditions (see Figure 2-3 and Table 2-3). The resulting final images had less than ideal seeing, and their limiting magnitudes were lower than anticipated (see “Summary” in this chapter). As luck would have it, 2 of our 4 clusters were at lower than expected redshifts, so we still achieved our desired limiting absolute magnitudes.

WIDE-FIELD IMAGES

The limited size of the IGI FoV makes accurate determination of the bright galaxy luminosity distribution impossible. To statistically correct for potential field galaxies in our cluster images, we need to understand the field galaxy luminosity distribution across a wide range of magnitudes. The bright and rare galaxy population was measured using the McDonald Observatory 0.8-m telescope and Prime Focus Camera (Claver 1996). The FoV was $55\text{-arcmin} \times 55\text{-arcmin}$, allowing us to observe fields containing both the cluster and comparison fields (see Figure 2-4). Wide-field PFC observations produced final co-added images with nominal limiting magnitudes of $B = 22$ and $R = 21.5$ with seeing $< 3.5\text{-arcsec}$. While better seeing was desired, the weather did not provide it.

In addition to being necessary to determine the field LF, the wider field of the PFC allowed us to better understand the angular extent of our clusters on the sky. The PFC was also used to observe Landolt standards (Landolt 1992). Comparison between the deep IGI observations and PFC observations allowed all images to be placed on a standard photometric system as described below.



Figure 2-3: Fiery Sunset and Stormy Sunrise. Extensive forest fires cause the glow on the hills in the top picture.

Table 2-3: Log of Observing Conditions

Date	Instrument	Seeing	Weather	Region	Notes	Observer	
10/16/1998	2.7-m	IGI	2.3	clouded up	1	1, 4	Croft, Gay, Hill
10/17/1998	2.7-m	IGI	2.2	clouded up	1	1, 4	Croft, Gay, Hill
01/14/1999	2.7-m	IGI	~2	clear	1	1, 3	Bergmann, Croft, Hill, Tufts
01/15/1999	2.7-m	IGI	3.0	clear	1	1, 3	Bergmann, Croft, Hill, Tufts
01/16/1999	2.7-m	IGI	2.4	clear	1	1, 3	Bergmann, Croft, Hill, Tufts
01/18/1999	2.7-m	IGI	~2	clear	1	1, 3	Bergmann, Croft, Hill, Tufts
04/15/1999	2.7-m	IGI	2.3	high clouds	2	1, 3	Bergmann, Croft, Gay
04/16/1999	2.7-m	IGI	2.0	clear	2	1	Croft, Gay
04/17/1999	2.7-m	IGI	1.7	clear	2	1, 3	Croft
04/18/1999	2.7-m	IGI	1.7	partly cloudy	2	1	Croft
05/11/1999	2.7-m	IGI	2.3	high clouds	2	1, 2	Croft
05/12/1999	2.7-m	IGI	2.0	hazy	2	1	Croft
05/13/1999	2.7-m	IGI	1.6	partly cloudy	2	1	Croft
05/14/1999	2.7-m	IGI	1.6	partly cloudy	2	1, 2	Croft
05/15/1999	2.7-m	IGI	1.8	clouded up	2	1, 4	Croft
05/16/1999	2.7-m	IGI	1.6	clear	2	2, 3	Croft
10/15/1999	2.7-m	IGI	1.5	clear	2	1, 3	Croft
12/31/1999	2.7-m	IGI	2.0	partly cloudy	1	1, 3	Gay, Fisher
01/01/2000	2.7-m	IGI	2.0	partly cloudy	1	1, 3	Gay, Fisher
01/03/2000	2.7-m	IGI	2.6	partly cloudy	1	1, 3	Gay, Fisher
01/04/2000	2.7-m	IGI	3.0	hazy	1	1, 3	Gay, Fisher
01/05/2000	2.7-m	IGI	2.0	clear	1	1, 3	Gay, Fisher
01/06/2000	2.7-m	IGI	2.0	clear	1	1, 3	Gay, Fisher
05/07/2000	2.7-m	IGI	3.3	partly cloudy	2	2	Gay
05/08/2000	2.7-m	IGI	3.0	hazy/dusty	2	1, 2	Gay
05/09/2000	2.7-m	IGI	2.7	hazy/dusty	2	2, 4	Gay
05/09/2000	2.7-m	IGI	2.7	hazy/dusty	2	2, 4	Gay
10/26/2000	2.7-m	IGI	2.4	partly cloudy	1	2, 4	Gay
10/29/2000	2.7-m	IGI	3.0	high wind	1	2, 4	Gay
10/20/2000	2.7-m	IGI	2.5	clear	1	2	Gay
04/23/2001	0.8-m	PFC	variable	clouds/high wind	2	2, 4	Gay
04/24/2001	0.8-m	PFC	3.0	photometric	2	2, 4	Gay
04/25/2001	0.8-m	PFC	2-3	cirrus everywhere	2	2	Gay
04/28/2001	2.7-m	IGI	variable	partly cloudy	2	2, 4	Gay
05/23/2001	0.8-m	PFC	2.8	clear	2	2	Christian, Gay
05/24/2001	0.8-m	PFC	2.8	clear	2	2	Christian, Gay
05/25/2001	0.8-m	PFC	2.8	partly cloudy	2	2	Christian, Gay
05/26/2001	2.7-m	IGI	2.0	mostly clear, ash	2	2	Christian, Gay
05/27/2001	2.7-m	IGI	1.6	partly cloudy, ash	2	2, 4	Christian, Gay
05/28/2001	2.7-m	IGI	2.0	partly cloudy, ash	2	2, 4	Christian, Gay
05/31/2001	0.8-m	PFC	2.6	high ash	2	2, 4	Gay
06/01/2001	0.8-m	PFC	2.8	high ash	2	2, 4	Gay
06/02/2001	0.8-m	PFC	2.8	high ash	2	2, 4	Gay
06/23/2001	2.7-m	IGI	2.6	high ash	2	2	Gay
06/25/2001	2.7-m	IGI	2.5	high ash	2	2, 4	Gay
06/26/2001	2.7-m	IGI	2.6	high ash	2	2, 4	Gay
06/27/2001	2.7-m	IGI	2.6	high ash	2	2, 4	Gay
06/28/2001	2.7-m	IGI	2.5	high ash	2	2, 4	Gay

Notes: 1-Preliminary OD observations, 2-Cluster Observations, 3-Night split with other projects, and 4-Significant time/data lost to conditions.

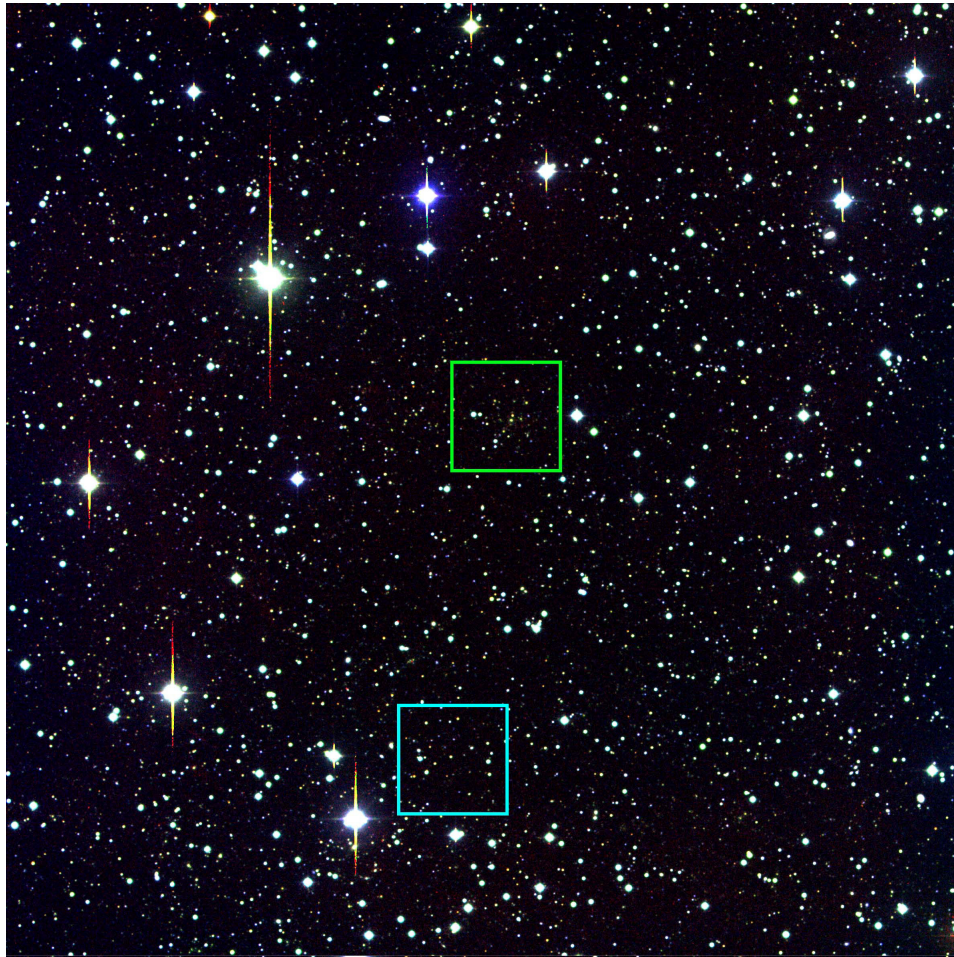


Figure 2-4: Wide area image of TOC J1602.8 + 4338. The cluster is outlined in green and the comparison field is marked in light blue.

DATA REDUCTION: 2.7-M + IGI

Data reduction was performed using IRAF. At the beginning and end of each night, 15 dome flats were obtained per filter and a similar number of bias images were taken daily. All calibration images were overscan-corrected and trimmed using `ccdproc`. Bias and flat master images were created by average combining image using `combine`. Bad pixels were rejected using `avesigclip` which rejects pixels above or below n -sigma, where we used $n = 3$.

In IGI, the filters lay in the focal plane. This causes all dust to appear as resolved lumps of particulate in images. Occasionally, dust grains would fall onto the filters during the night. If the dust patterns stayed the same all night, morning and evening flats were combined and the same master flat was used for all images. If the dust pattern changed, the combined flat with the closest matching dust pattern was applied to the image. Master bias images and master flats were subtracted and divided through the data appropriately with `ccdproc`.

The flat board used with this telescope + instrument combination is not illuminated evenly, and while the dome flats are necessary for removing dust patterns and correcting for differences in sensitivity in the CCD, they can not be used to correct for vignetting and they introduce a lumpiness in the background of images. In addition to these problems, residual fringe patterns created by night-sky lines were present in I-band science images (see Figure 2-5) and not in I-band flats. As a result, images needed further corrections after flat-field applications.

To remove these effects, sky flats and fringe images were created. Each night, all long (≥ 300 s) science images for each filter were combined using `combine` with `minmax` rejection, which rejects pixels above or below user input values. This creates an image containing only the background pattern and I-band fringes. For B-band and R-band image sets, where there were no fringes, this image was normalized to 1 and divided into all the science images. For I-band exposures, the image was boxcar-smoothed to create a sky flat without fringes. This image was divided into the original illumination correction image to create a fringe frame. The sky flat was divided into the science images, and the fringe

frame was scaled to the sky of each image and subtracted. The sky was added back in as a constant to produce the final images. These images were flat to <1% corner to corner.

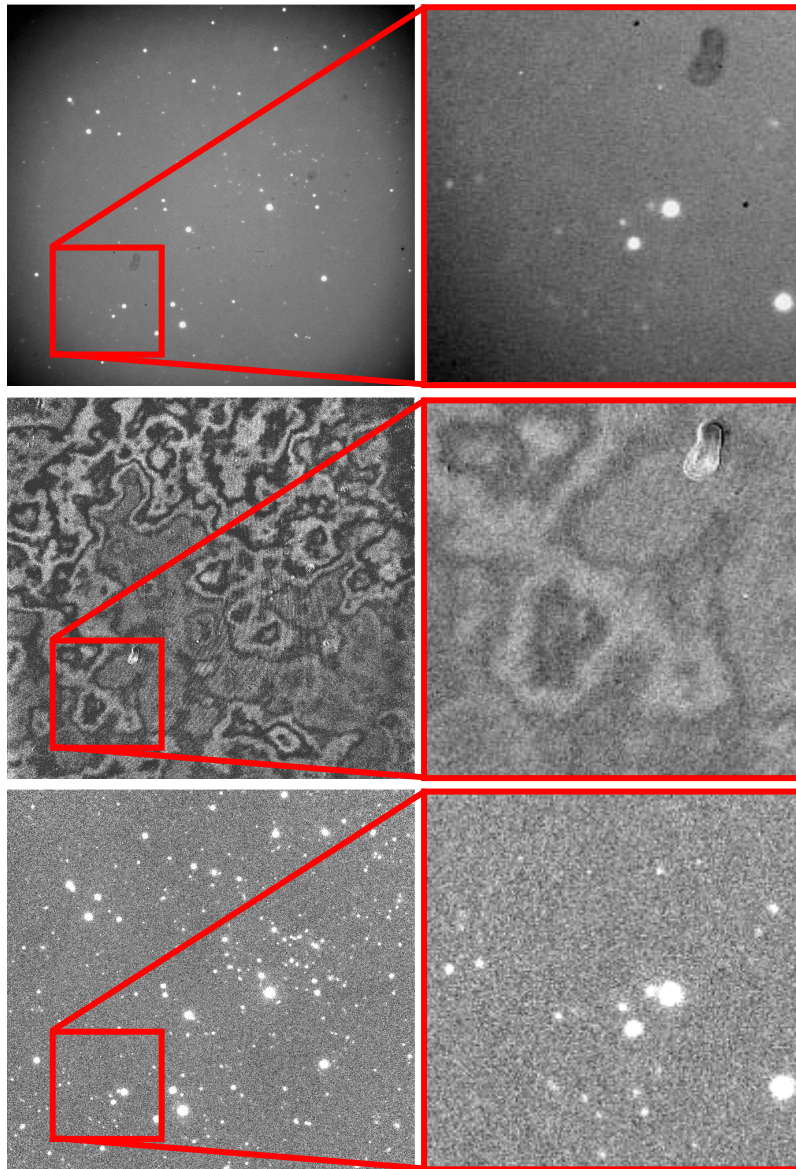


Figure 2-5: Raw vs. reduced IGI images. top: Raw I-band image D14. Middle: Fringe frame created by combining 35 I-band exposures. Bottom: Same exposure after bias, flat field and fringe corrections. Images on the left are full frame (706×661) and on the right they are 191×191 pixels.

DATA REDUCTION: 0.8-M + PFC

The prime focus camera on the McDonald Observatory 0.8-m telescope produces clean images that are devoid of fringes in all standard filters. The filter set and CCD are well protected from dust and other changeable defects and flats are typically unchanged for more than a week at a time. The stability of this instrument allowed us to take sets of 15 flats per color every other evening. Bias images were also taken, and generally all bias and flat images from a run were combined using the `combine` routine and `avsigclip` pixel rejection. The only exception to this occurred after a filter wheel mal-function required removal of the wheel and remounting of the filters. In this case, all flats prior to the failure were combined, and all flats after the failure were combined.

In addition to getting bias and flat calibration images, the slow opening and closing speed of the PFC shutter requires that shutter correction images be observed and applied to all short images. The master shutter correction image was created from the quotient of two 10 second images averaged together and the average of ten 1 second exposures. This shutter correction image was multiplied into all science and flat images after being scaled to the image exposure times.

These calibration images were applied using `ccdproc` after bad columns and pixels were corrected using `fixpix`. After overscan and bias subtraction, trimming, and the application of shutter correction and flat field images, a residual gradient was present in many images. This gradient is generally related to actual gradients in the sky due to moonlight or clouds. These gradients were fit with a

plane and subtracted off using an IRAF routine called `resgradcor` (Bergmann 1998). Final PFC images were flat to $< 1\%$ (see Figure 2.6).

Figure 2-6: Raw vs. reduced PFC images. (top) 801×801 pixel section from a raw PFC image. (bottom) Same section after all reductions. Bad columns were fixed with `fixpix`, and diagonal features were corrected with flat fielding. The top images are 801×801 sections and the bottom images are 201×201 image sections.

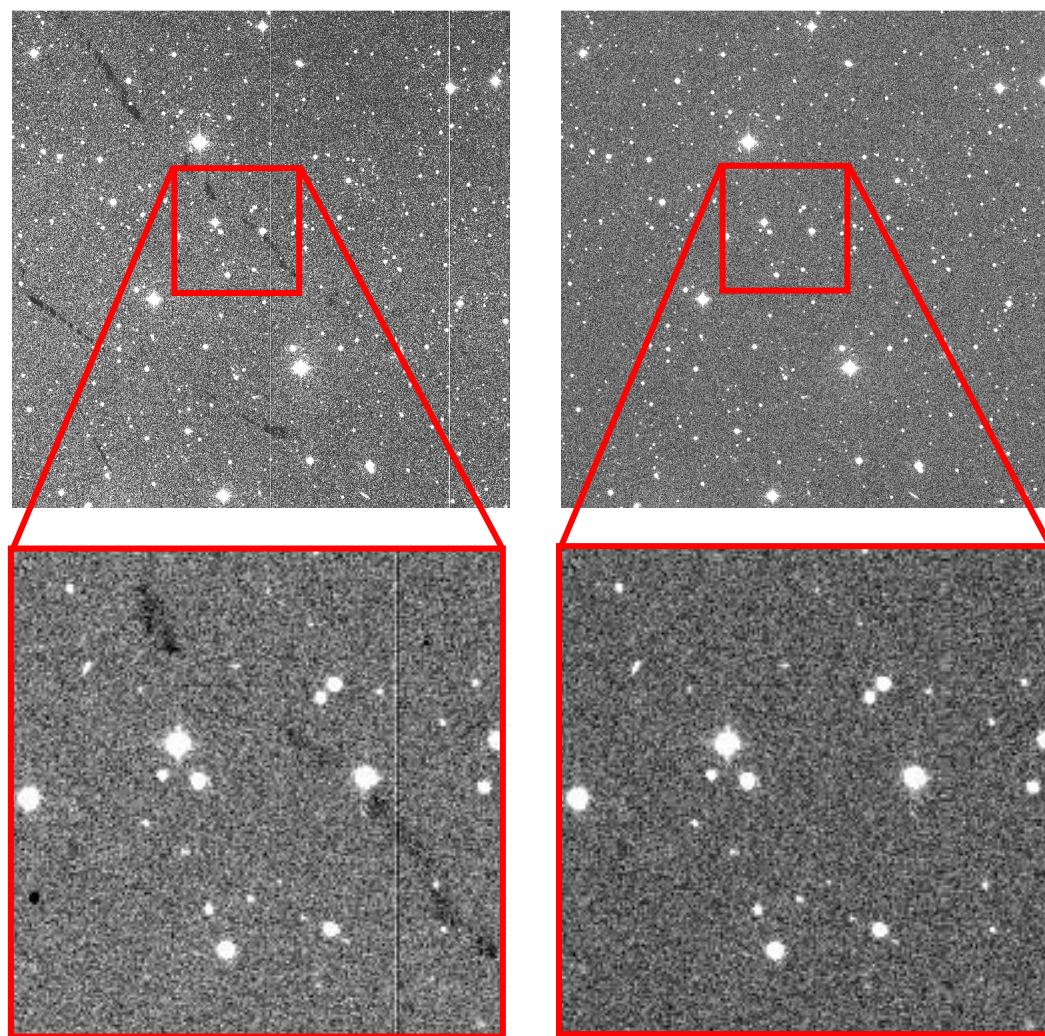
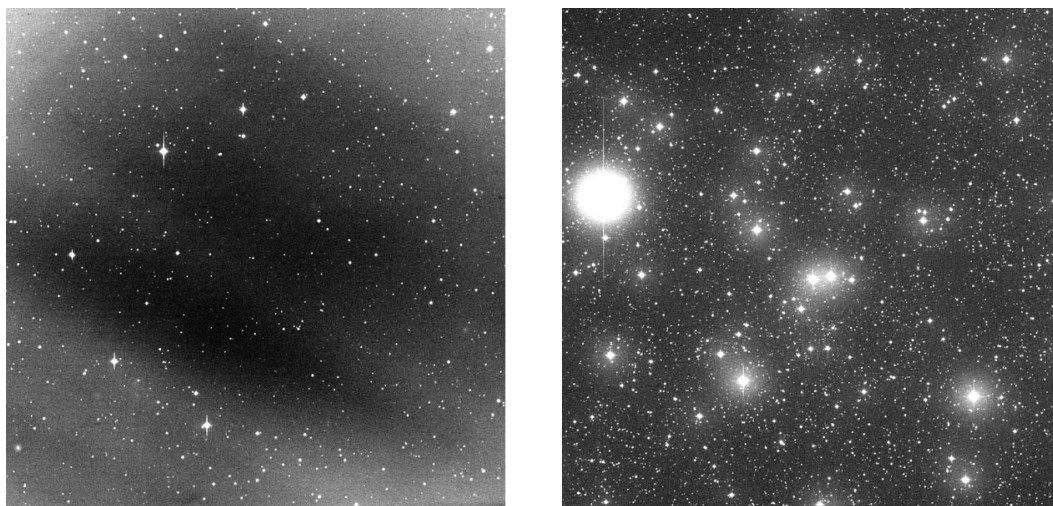


IMAGE CO-ADDITION

All data, irregardless of the conditions during observations, were reduced. Not all of these data were suitable for inclusion in creating the final coadded images. Images containing obvious clouds obscuring the field unevenly (see Figure 2-7a) or that were taken immediately before or after a passing cloud were eliminated. Images with large halos around bright objects were also not used (see Figure 2-7b) Images were also required to have seeing less then 3.5 arcsec.⁸ and reasonable transparency when compared to other images of the same field. Images were aligned and then co-added using the `imcoadd` routine in IRAF's `gemini` package (see Table 2-4). Minmax rejection was used during image coaddition to eliminate cosmic rays.

Figure 2-7: Examples of images not used. a: (left) Fields containing striations and obscured regions due to clouds. b: (right) Fields containing halos around bright objects.



⁸ In 5 of the 36 image sets this limit had to be raised because there were few or no images with seeing ≤ 3.5 arcsec. See Appendices 3-6 for details on individual image sets.

Table 2-4: Final Co-added Image Seeing and Area

Field	Instrument	Filter	Seeing (pixels)	Seeing (arcsec.)	Area (deg. ²)
TOC J 1602.8 +4338	IGI	B	1.98	3.05	0.008
TOC J 1602.8 +4338	IGI	R	1.96	3.02	0.008
TOC J 1602.8 +4338	IGI	I	1.95	3.00	0.008
TOC J 1602.8 +4338 comp	IGI	B	2.21	3.40	0.009
TOC J 1602.8 +4338 comp	IGI	R	1.66	2.55	0.009
TOC J 1602.8 +4338 comp	IGI	I	2.10	3.23	0.009
TOC J 1602.8 +4338	PFC	B	3.75	2.78	0.535
TOC J 1602.8 +4338	PFC	R	3.69	2.73	0.535
TOC J 1602.8 +4338	PFC	I	3.82	2.83	0.535
TOC J 1620.9 +4442	IGI	B	2.34	3.59	0.011
TOC J 1620.9 +4442	IGI	R	2.08	3.20	0.011
TOC J 1620.9 +4442	IGI	I	2.16	3.32	0.011
TOC J 1620.9 +4442 comp	IGI	B	2.27	3.49	0.010
TOC J 1620.9 +4442 comp	IGI	R	1.17	1.80	0.010
TOC J 1620.9 +4442	PFC	B	3.69	2.74	0.466
TOC J 1620.9 +4442	PFC	R	3.27	2.42	0.466
TOC J 1620.9 +4442	PFC	I	3.84	2.84	0.466
TOC J 1626.1 +4859	IGI	B	2.18	3.35	0.010
TOC J 1626.1 +4859	IGI	R	2.05	3.16	0.010
TOC J 1626.1 +4859	IGI	I	1.81	2.78	0.010
TOC J 1626.1 +4859 comp	IGI	B	2.61	4.01	0.013
TOC J 1626.1 +4859 comp	IGI	R	1.77	2.72	0.013
TOC J 1626.1 +4859 comp	IGI	I	2.32	3.57	0.013
TOC J 1626.1 +4859	PFC	B	3.30	2.44	0.476
TOC J 1626.1 +4859	PFC	R	3.44	2.55	0.476
TOC J 1626.1 +4859	PFC	I	4.60	3.41	0.476
TOC J 1705.8 +3657	IGI	B	2.23	3.43	0.011
TOC J 1705.8 +3657	IGI	R	1.98	3.04	0.011
TOC J 1705.8 +3657	IGI	I	1.94	2.98	0.011
TOC J 1705.8 +3657 comp	IGI	B	2.23	3.43	0.010
TOC J 1705.8 +3657 comp	IGI	R	2.14	3.30	0.010
TOC J 1705.8 +3657 comp	IGI	I	2.43	3.73	0.010
TOC J 1705.8 +3657	PFC	B	3.46	2.56	0.477
TOC J 1705.8 +3657	PFC	R	3.66	2.71	0.477
TOC J 1705.8 +3657	PFC	I	5.05	3.74	0.477

STANDARD CALIBRATIONS

On the night of April 24, 2001 five Landolt fields and the cluster-comparison fields were repeatedly observed in Johnson-Kron-Cousins broadband BRI filters (see Table 2-5). Instrumental magnitudes for stellar objects in all fields were determined using the DAOPhot aperture photometry package in IRAF. Measured seeing during this night was 3.2 ± 0.3 arcsec FWHM with 1.35 arcsec pixel⁻¹ resolution. A 15 pixel aperture radius was adopted (see Figure 2-8), and a 5 pixel wide sky annulus with a 20 pixel inner radius was used.

These data were used to fit the constants in the following equations:

$$mB = [(B-R) + R] + x_1B + x_2B \times \text{Airmass} + x_3B \times (B-R),$$

$$mR = R + x_1R + x_2R \times \text{Airmass} + x_3R \times (B-R),$$

$$mI = [R - (R - I)] + x_1I + x_2I \times \text{Airmass} + x_3I \times (R-I),$$

where the x_1 terms are the constant terms, the x_2 terms are the airmass terms, and the x_3 terms are the color terms. The resulting magnitudes had an error of typically (see Figure 2-9): $\text{error}(BR) \sim \pm 0.05$ mag, $\text{error}(R) \sim \pm 0.04$, and

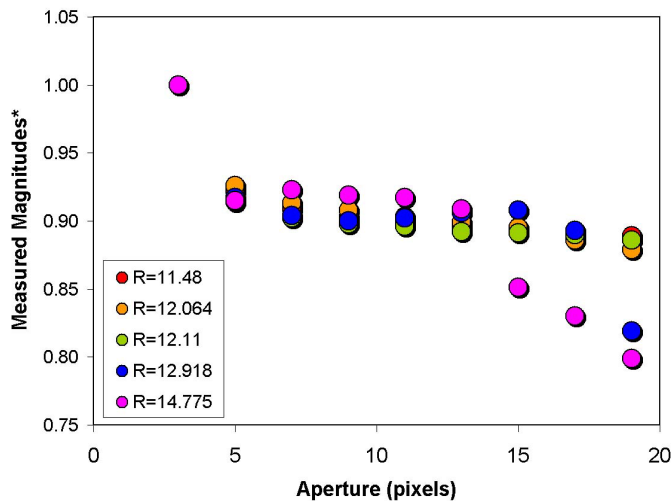
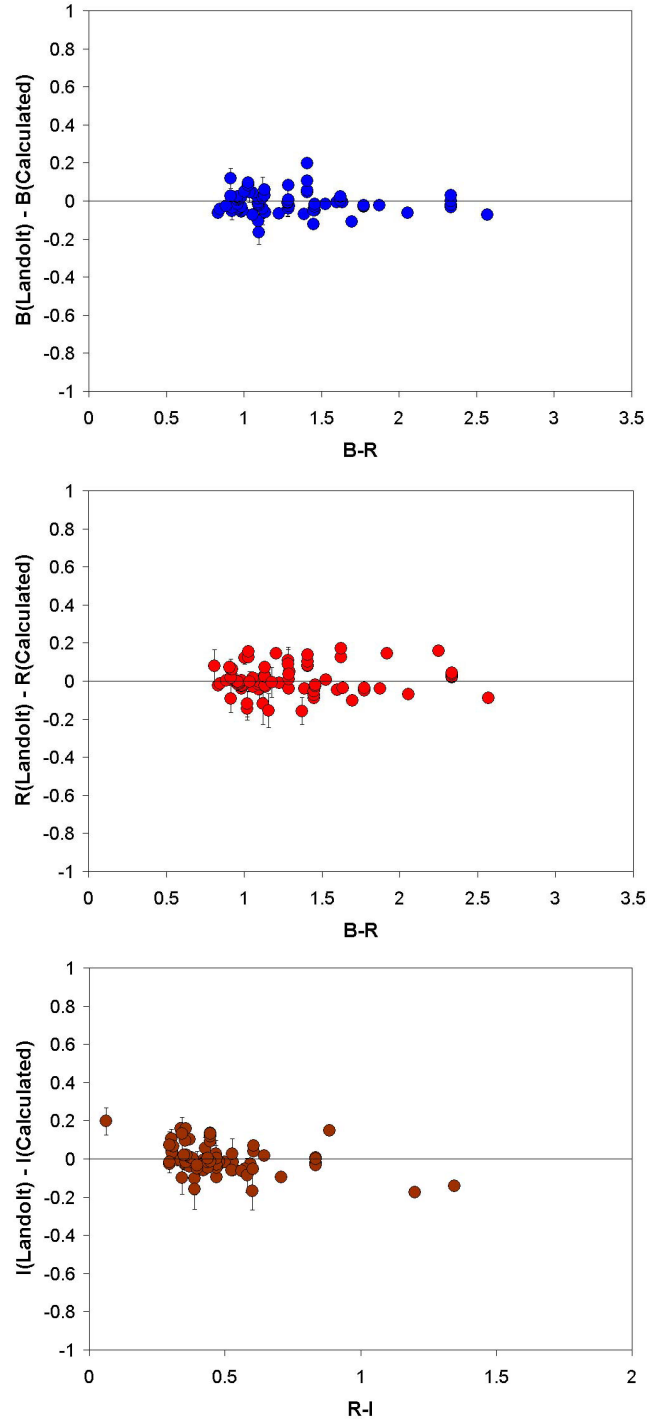


Figure 2-8: A plot of measured magnitudes vs. aperture for 5 stars. Actual magnitudes are given in the color key. While the size of the aperture was changed for each measurement, the sky annulus was held constant.

*The measured 3-arcsec aperture instrumental magnitude for each star was set to 1 for comparison purposes.

Figure 2-9: Differences between Landolt's published magnitudes for standard stars, and the magnitudes calculated using determined constants.



error(RI) $\sim \pm 0.04$ when the published and calculated magnitudes for the Landolt stars were compared. There was no discernable offset between the two magnitude sets. These constants were used to convert the wide-field single exposure instrumental magnitudes to a standard system.

Table 2-5: Log of standard star observations

Field	Filter	UT	Airmass
NGC 4147	R	05:44	1.042
NGC 4147	B	05:48	1.047
NGC 4147	I	05:56	1.055
SA 107	R	06:06	1.417
SA 107	B	06:11	1.396
SA 107	I	06:16	1.375
TOC J 1602.8 +4338	R	06:22	1.170
TOC J 1602.8 +4338	B	06:30	1.150
TOC J 1602.8 +4338	I	06:42	1.130
SA 107	R	06:53	1.266
SA 107	B	06:57	1.255
SA 107	I	07:03	1.244
TOC J 1620.9 +4442	R	07:07	1.121
TOC J 1620.9 +4442	B	07:16	1.105
TOC J 1620.9 +4442	I	07:27	1.090
TOC J 1626.1 +4859	R	07:39	1.104
TOC J 1626.1 +4859	B	07:48	1.093
TOC J 1626.1 +4859	I	07:59	1.083
SA 110	R	08:10	1.772
SA 110	B	08:14	1.729
SA 110	I	08:21	1.680
SA 107	R	08:26	1.166
SA 107	B	08:30	1.166
SA 107	I	08:36	1.167
TOC J 1705.8 +3657	R	08:41	1.037
TOC J 1705.8 +3657	B	08:50	1.029
TOC J 1705.8 +3657	I	09:01	1.021
SA 110	R	10:09	1.230
SA 110	B	10:14	1.219
SA 110	I	10:20	1.210
SA 107	R	10:25	1.351
SA 107	B	10:30	1.369
SA 107	I	10:36	1.389

In order to place our co-added PFC and IGI images on a standard system, all the images had to be boot-strapped together using secondary standards within the PFC fields. This was done using SExtractor (Bertin & Arnouts 1996) aperture photometry and the statistical packages available in MS Excel 2000.

Comparison of aperture magnitudes from DAOphot and SExtractor showed a scatter of just 0.02 ± 0.05 magnitudes for objects in the same frame. SExtractor was used because it provides information on whether an object is most

likely a star or a galaxy. It makes this determination using a neural network trained to separate stars from galaxies based on 10 parameters: 8 isophotal areas per object, the object's peak intensity and the image's seeing. These parameters allow the software to take into account that galaxies typically have a flatter radial profile than stars. Its galaxy/star determinations are successful for a large range of magnitudes and in crowded fields. Bertin and Arnout's testing of this software with data from a wide range of telescope+instrument combinations demonstrates a consistent 95% success rate in correctly separating stars from galaxies.

To place the wide-field, co-added data on the same standard magnitude system as the single frame calibration images, SExtractor was used to determine aperture magnitudes for all the stars in both frames. The co-added image was assumed to have the same color term as the single exposure image, and the first 4 magnitudes of stars were used to find the offset between the standard instrumental magnitudes. The scatter in the differences between the single exposure standard magnitudes, and the standard magnitudes for objects in the coadded field were: $\text{error}(B) \pm \sim 0.10 \text{ mag}$, $\text{error}(R) \pm \sim 0.04 \text{ mag}$, and $\text{error}(I) \pm \sim 0.06 \text{ mag}$ (detailed errors for all fields are given in Appendices 3 – 6).

The calibrated, co-added PFC images were then used to calibrate the IGI co-added images. Due to the dearth of stars in the IGI fields, galaxies were incorporated into this fit. We used Kron (Kron 1980) magnitudes for all galaxies throughout this study. The aperture magnitudes we used for the stars are inappropriate for galaxies because the galactic light profiles are a function of galaxy type and redshift, making it impossible to choose an aperture size that is

appropriate for all galaxies in an image. If the aperture is too large the sky will dominate, drastically increasing the noise in the measurement. If the aperture is too small, significant amounts of light may be lost. While isophotal magnitudes are popular for galaxies, they often measure an inconsistent amount of the galaxies' total light. This is because the surface brightness at a given metric distance from a galactic center falls as $(1+z)^4$. This causes the limiting isophot for faint galaxies to contain less of the galaxies' total light than the same limiting isophot will contain for brighter galaxies. Kron's technique measures the flux from galaxies within twice the characteristic radius, r_1 , defined as:

$$r_1 = \frac{\sum rI(r)}{\sum I(r)}.$$

This radius is approximately equal to an object's half-light radius. This radius was selected to minimize the slope of the light growth curve, $l(r)$, at the maximum radius, $2r_1$. The steepness of $l(r)$ is directly related to the error in the measured magnitude, with a flat slope corresponding to a small error. For an aperture of $2r_1$, Kron found that $d \ln l(r) \sim 0.05$. For a 5 kpc exponential disk and 0.6" seeing, Kron states that this technique measures 91-94% of the galaxies' total light in the redshift interval $z = 0.1 \rightarrow 1.9$. Kron magnitudes were chosen in favor of Petrosian magnitudes because they measure a larger fraction of the total light (Blanton et al. 2360).

Once the galaxies' Kron magnitudes were determined, we used the brightest 4 magnitudes of objects to determine the standard calibration constants. A fit was made by forcing all sets of IGI images to have the same color terms and allowing the constant term to vary. The typical final difference in magnitude

between the IGI co-added images and PFC images is 0.1 magnitudes (see Figure 2-10). It should be noted that the error for the DX19 and DX46 comparison fields is much greater. Due to pointing problems, the final coadded PFC images of these regions did not contain the comparison fields. These fields were placed on a standard system using only the single exposure PFC images of Apr 24, 2001. The single exposure contained very few objects that were not saturated in the IGI exposures, and many of these objects had poor signal to noise.

Once each image was calibrated to a standard magnitude system, limiting magnitudes were determined. To do this we created a plot of number of objects vs. magnitude using 0.25 magnitude bins for each image, and assumed 0.5 magnitudes below the turn off (see Figure 2-11) as the limiting magnitude (see Table 2-6 and Appendices 3 – 6).

SUMMARY

We used standard data reduction techniques to produce high-quality co-added images of our cluster and comparison fields. This data was carefully placed on a standard system, with the determined magnitudes of objects appearing in multiple images constantly being compared. We find that our final magnitudes have a typical error of $\leq \pm 0.15$ magnitudes. This is sufficient for our goal of creating galaxy luminosity functions and determining the cluster blue galaxy fractions. While our final images did not meet our initial desired limiting apparent magnitudes, the lower than expected redshifts of the majority of our clusters allowed us to meet our absolute limiting magnitude goals.

Figure 2-10: Difference between PFC standardized and instrumental B, R and I magnitudes + determined constant term for all shared objects images. These plots show that there is no color term in the B or I data ($x_3B=$, $x_3I=0$), and the R data has a color term of $x_3R=-0.14$.

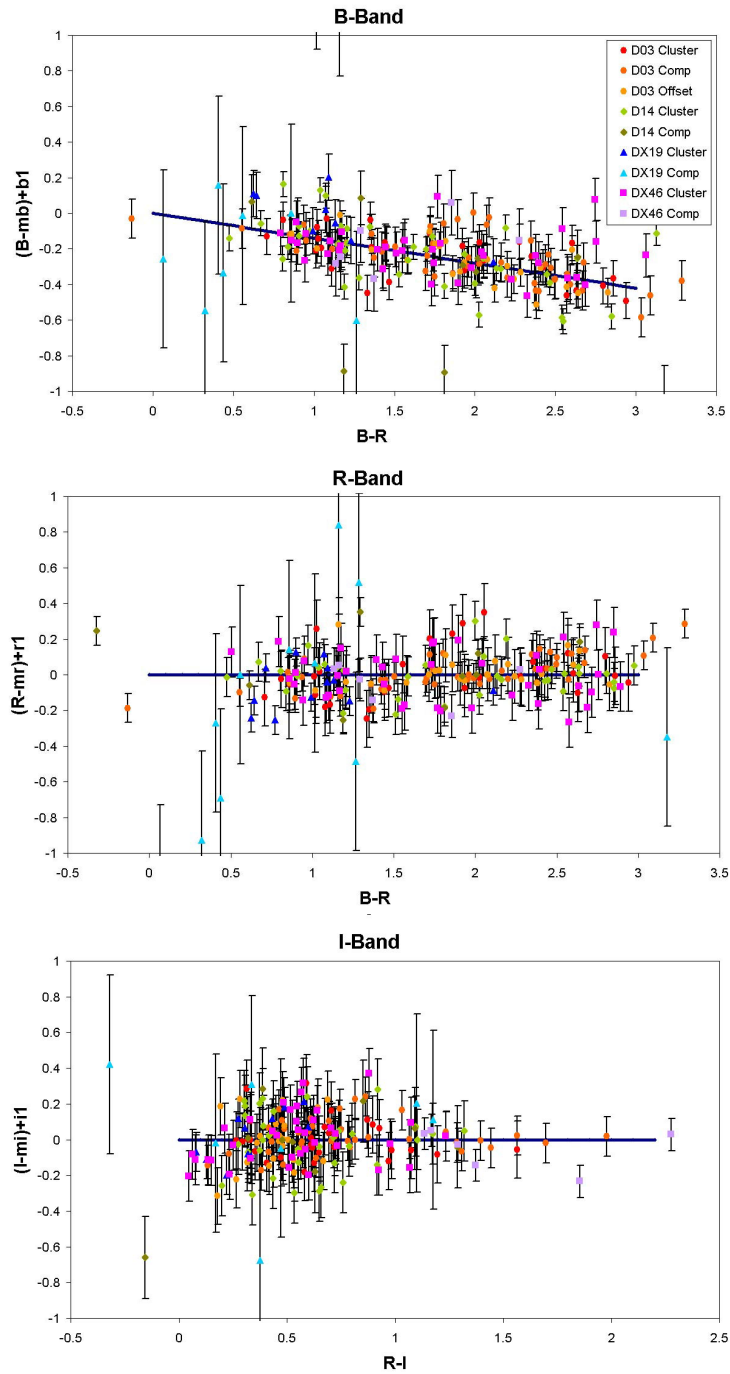


Figure 2-11: Number of Objects vs. Magnitude for TOC J1602.8+4338. The limiting magnitude is taken as 0.5 magnitudes brighter then the turn-down point. These figures show star + galaxy counts.

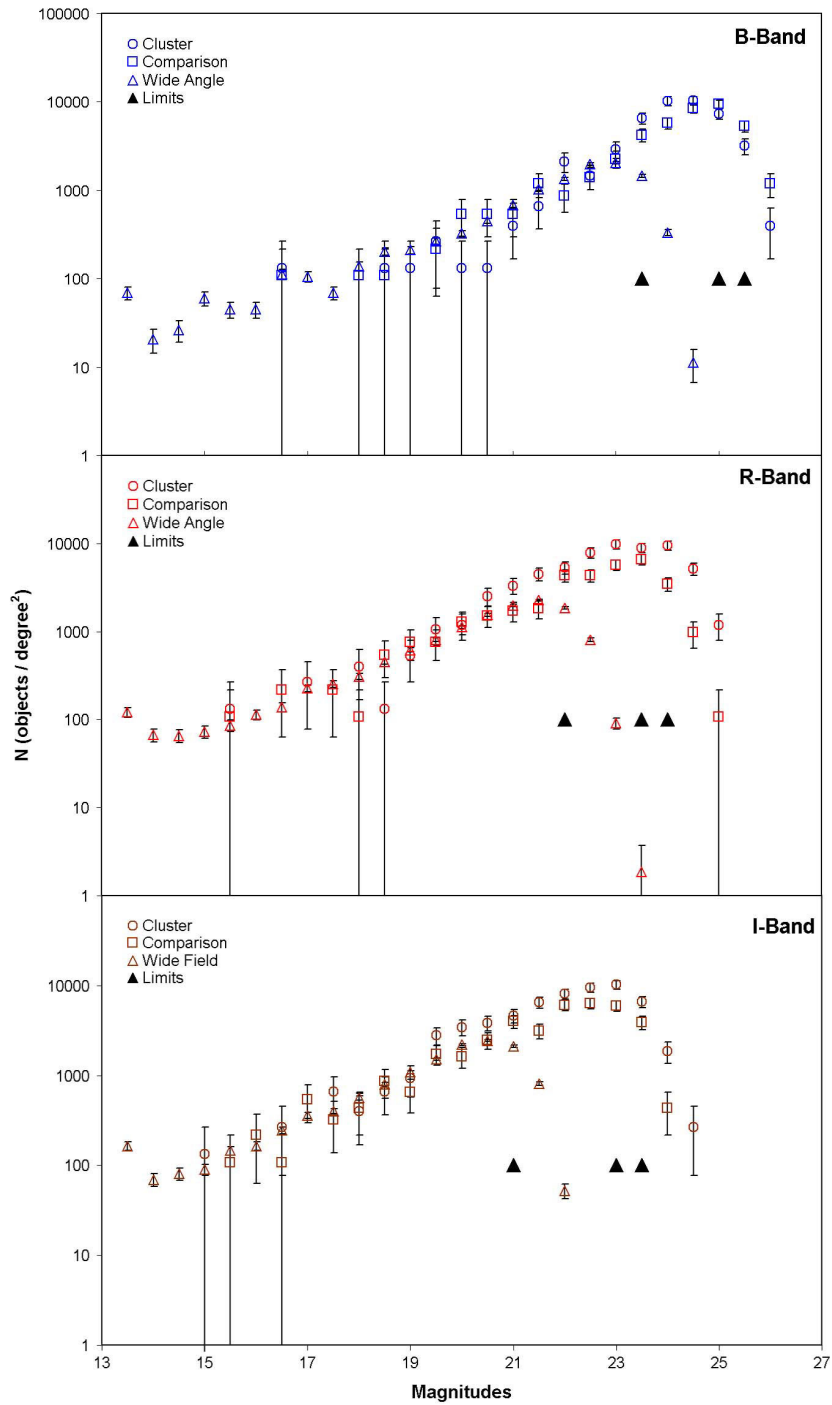


Table 2-6: Limiting Magnitudes for each Field.

Field	Instr.	Filter	Limiting Magnitude
TOC J 1602.8 +4338	IGI	B	25.0
TOC J 1602.8 +4338 comp	IGI	B	25.5
TOC J 1620.9 +4442	IGI	B	24.0
TOC J 1620.9 +4442 comp	IGI	B	24.5
TOC J 1626.1 +4859	IGI	B	24.0
TOC J 1626.1 +4859 comp	IGI	B	23.5
TOC J 1705.8 +3657	IGI	B	24.0
TOC J 1705.8 +3657 comp	IGI	B	24.0
Average	IGI	B	24.3
TOC J 1602.8 +4338	PFC	B	23.5
TOC J 1620.9 +4442	PFC	B	22.5
TOC J 1626.1 +4859	PFC	B	23.0
TOC J 1705.8 +3657	PFC	B	22.0
Average	PFC	B	22.8
TOC J 1602.8 +4338	IGI	R	23.5
TOC J 1602.8 +4338 comp	IGI	R	24.0
TOC J 1620.9 +4442	IGI	R	23.0
TOC J 1620.9 +4442 comp	IGI	R	23.5
TOC J 1626.1 +4859	IGI	R	24.0
TOC J 1626.1 +4859 comp	IGI	R	24.5
TOC J 1705.8 +3657	IGI	R	23.5
TOC J 1705.8 +3657 comp	IGI	R	23.0
Average	IGI	R	23.6
TOC J 1602.8 +4338	PFC	R	22.0
TOC J 1620.9 +4442	PFC	R	21.5
TOC J 1626.1 +4859	PFC	R	22.0
TOC J 1705.8 +3657	PFC	R	22.0
Average	PFC	R	21.9
TOC J 1602.8 +4338	IGI	I	23.5
TOC J 1602.8 +4338 comp	IGI	I	23.0
TOC J 1620.9 +4442	IGI	I	22.5
TOC J 1626.1 +4859	IGI	I	22.0
TOC J 1626.1 +4859 comp	IGI	I	23.0
TOC J 1705.8 +3657	IGI	I	21.5
TOC J 1705.8 +3657 comp	IGI	I	21.5
Average	IGI	I	22.4
TOC J 1602.8 +4338	PFC	I	21.0
TOC J 1620.9 +4442	PFC	I	21.0
TOC J 1626.1 +4859	PFC	I	21.0
TOC J 1705.8 +3657	PFC	I	20.0
Average	PFC	I	20.8

Chapter 3: Cluster Characteristics

In this chapter we will examine our selected clusters' identifying characteristics: spectral redshifts, brightest cluster galaxies, number densities and radio source populations. These features are being studied for the specific purpose of determining if our clusters are in any way unusual. These clusters were found in the direction of concentrations of radio sources on the sky. While it was impossible to a priori know if these radio sources are physically associated with our clusters, this unique alignment raises the possibility that our clusters may have unique galaxy populations. After examining our clusters in detail, we find that our clusters have average characteristics and in no way stand out against large comparison samples taken from the literature.

REDSHIFTS

Redshifts for our clusters were measured using the Hobby-Eberly Telescope (HET) with either the Low-Resolution Spectrograph (LRS) or Multi-Object Spectrograph (MOS) during the instruments' early science or commissioning runs. All data were taken prior to the installation of edge sensors. The data were reduced and provided by Dr. Gary Hill. (see Table 3-1).

As can be seen in Table 3-1, two of our clusters have ambiguous redshift determinations. The brightest cluster galaxy (BCG) in TOC J1705.8+3657 is 2.5 arcmin from the center of ZwCl 1704.1+3700. After examining Palomar sky survey plates of these regions, we feel that we are dealing with two different situations. (1) TOC J1705.8+3657 and ZwCl 1704.1+3700 are the same cluster,

and the other redshifts are field objects, and (2) our TOC J1626.1+4859 measurements are contaminated with field galaxies. Each of these clusters will be discussed in detail throughout this chapter. We have included large field images of each field in Figure 3-1 and Figure 3-2.

Table 3-1: Redshifts of objects in field of clusters

Field	Instr.	z
TOC J 1602.8 +4338	LRS	0.411 ± 0.003
	LRS	0.422 ± 0.003
	<i>mean</i>	0.416 ± 0.004
TOC J 1620.9 +4442 ¹	MOS	0.221 ± 0.003
	MOS	0.216 ± 0.003
	MOS	0.211 ± 0.004
	MOS	0.219 ± 0.004
	MOS	0.214 ± 0.003
	MOS	0.209 ± 0.003
<i>mean</i>	0.215 ± 0.001	
TOC J 1626.1 +4859	MOS	0.410 ± 0.007
	MOS	0.388 ± 0.007
	MOS	0.264 ± 0.003
	MOS	0.27 ± noisy
	<i>mean 1</i>	<u>0.40</u> ± 0.01
<i>mean 2</i>	0.264	
TOC J 1705.8 +3657 ²	MOS	0.165 ± 0.003
	MOS	0.167 ± 0.005
	MOS	0.168 ± 0.002
	MOS	0.193 ± 0.005
	MOS	0.269 ± 0.005
	MOS	0.278 ± 0.001
	MOS	0.281 ± 0.003
	MOS	0.283 ± 0.005
	<i>mean 1</i>	<u>0.278</u> ± 0.004
<i>mean 2</i>	0.167 0.002	

(1) 4.2-arcmin from ZwCl 1619.5+4445.

(2) 2.5-arcmin from ZwCl 1704.1+3700.

Figure 3-1: TOC J1626.1+4859. Main image is from PFC data, and inset is an IGI image of the cluster. Color is produced by mapping the I filter image to red, the R filter image to green and the B filter image to blue.

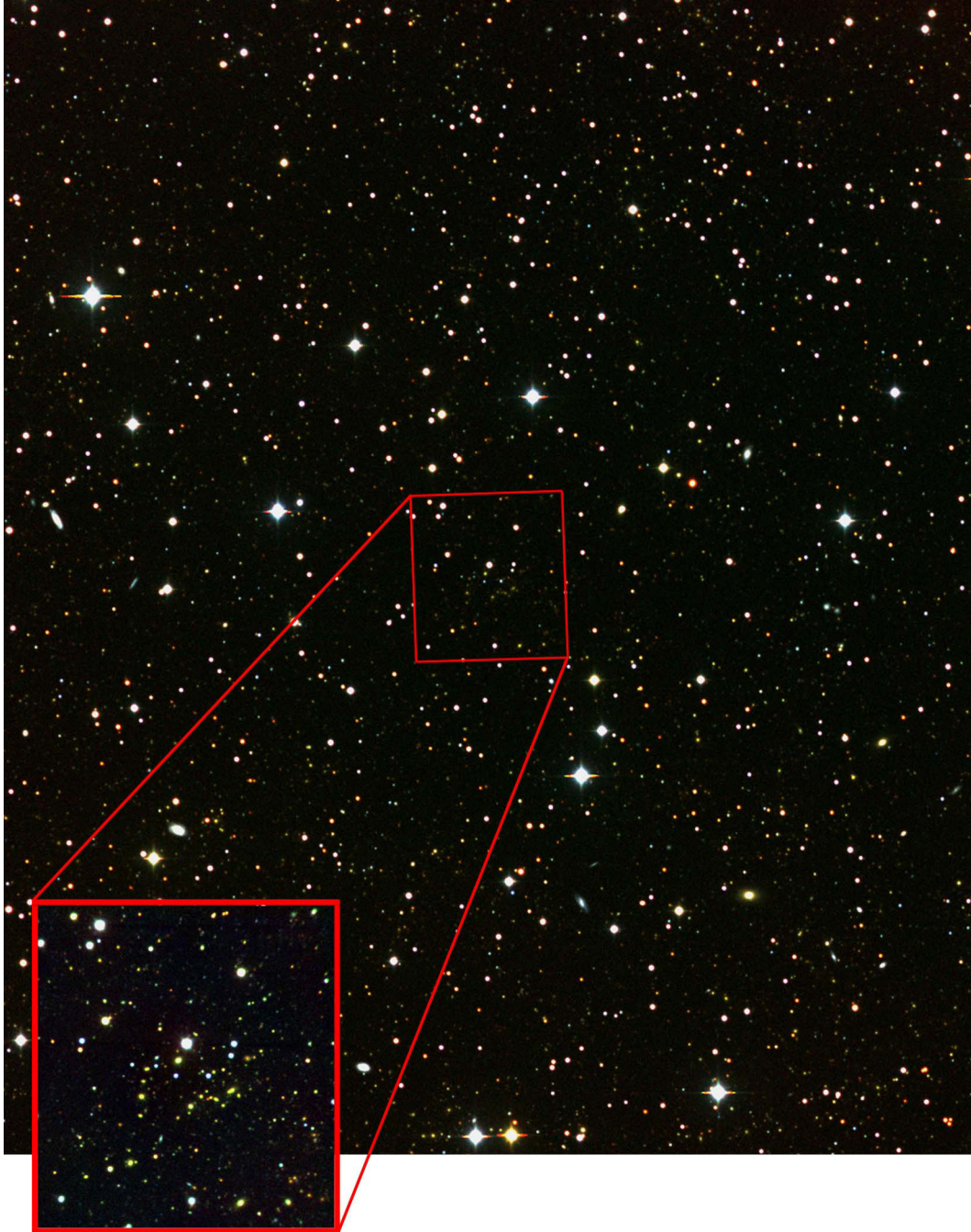
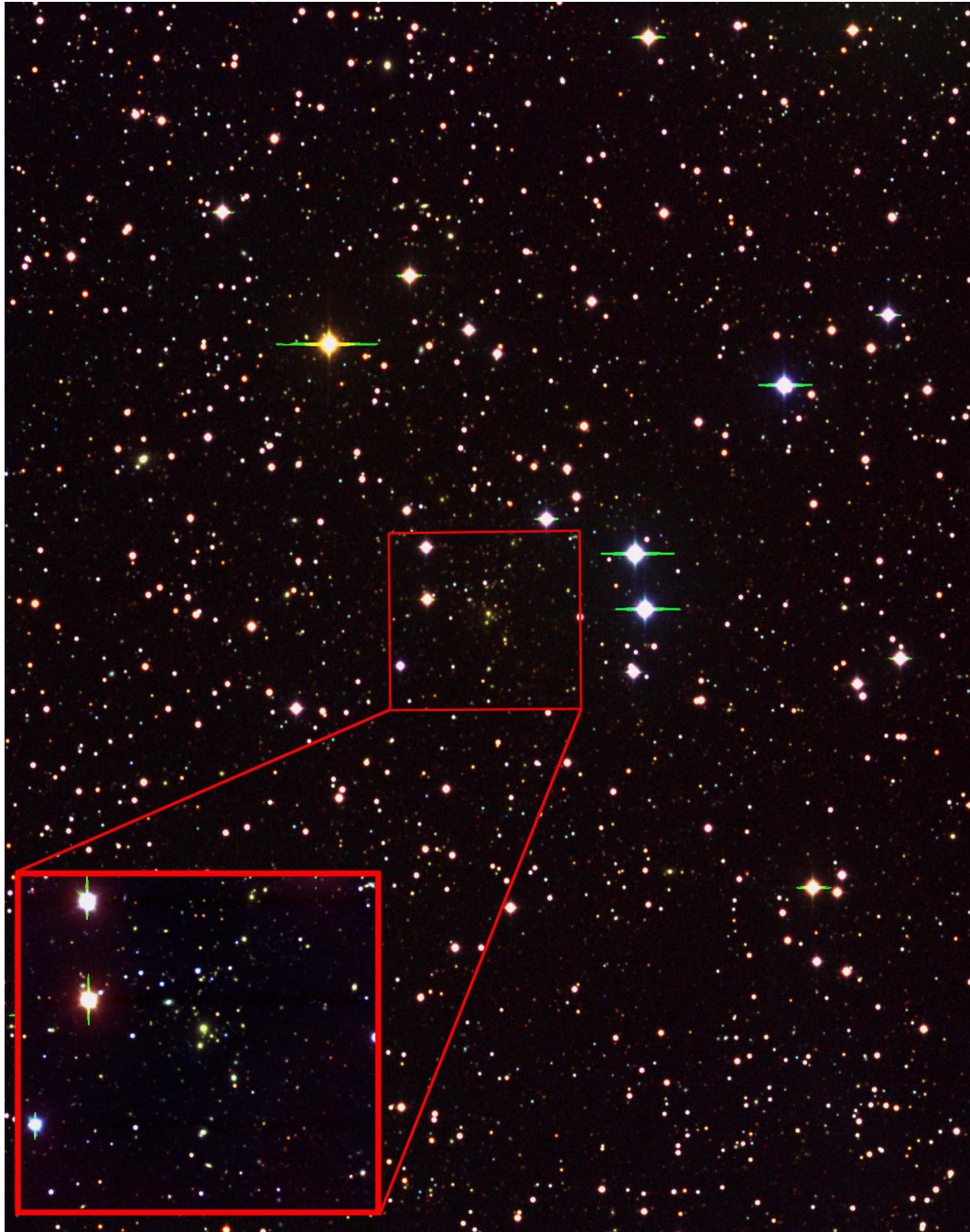


Figure 3-2: TOC J1705.8+3657. Main image is from PFC data, and inset is an IGI image of the cluster. Color is produced by mapping the I filter image to red, the R filter image to green and the B filter image to blue.



BRIGHTEST CLUSTER GALAXIES

In this work, we used the redshift-magnitude relation for BCGs to help us break our redshift ambiguities. The central elliptical galaxies in clusters – also referred to as the brightest cluster galaxies (BCG) – are extremely luminous examples of the elliptical galaxy population. It has long been known that these giants have a well-defined magnitude-redshift relationship (Humason, Mayall & Sandage 1956; Sandage Kristain & Westphall 1976; Hoessel 1980). It has been shown (Nelson et al 2002) that brightest cluster galaxies have magnitudes consistent with passive evolution in high L_X ($L_X > 2 \times 10^{44}$ ergs s^{-1}) clusters and with no evolution in low- L_X clusters. Our clusters with ambiguous redshifts have widely separated pairs of redshifts, and the BCG should clearly determine which redshift is appropriate for each system.

We compared our BCG magnitudes (see Figure 3-3) to the low-redshift data of Postman and Lauer (1995, hereafter PL95) and to the high-redshift data from Nelson et al. (2002, hereafter N02). To assess which redshifts were appropriate for our two ambiguous clusters, we examined the difference between the expected and actual magnitudes for three situations: a no-evolution model, a fit to the PL95 + N02 data, and a passive evolution model. Because our data fall primarily in a redshift gap between the two samples, a robust Kolmogorov-Smirnov (K-S) test could not be done.

Our no-evolution model assumes $M_R = -23.5$ and the E0 K-corrections of Fukugita et al (1995). The absolute magnitude derived from the median value for the PL95 BCG sample uses the apparent magnitudes associated with their largest

aperture radius. This sample shows no luminosity evolution and has a Gaussian magnitude distribution (see Figure 3-4a & b). We use the larger radius aperture because it more closely approximates the BCGs' total magnitudes. It should be noted that the scatter in these magnitudes could be lowered from our 0.63 magnitudes to 0.34 magnitudes by changing the selected aperture radius to a metric radius (see their section 4.1, and Bhavsar 1989). This dims the median absolute magnitude to -22.6 and makes a fit to both the high z and low z samples impossible for a constant or a passive evolution model.

Our passive evolution model is taken from N02 who utilized Bruzual and

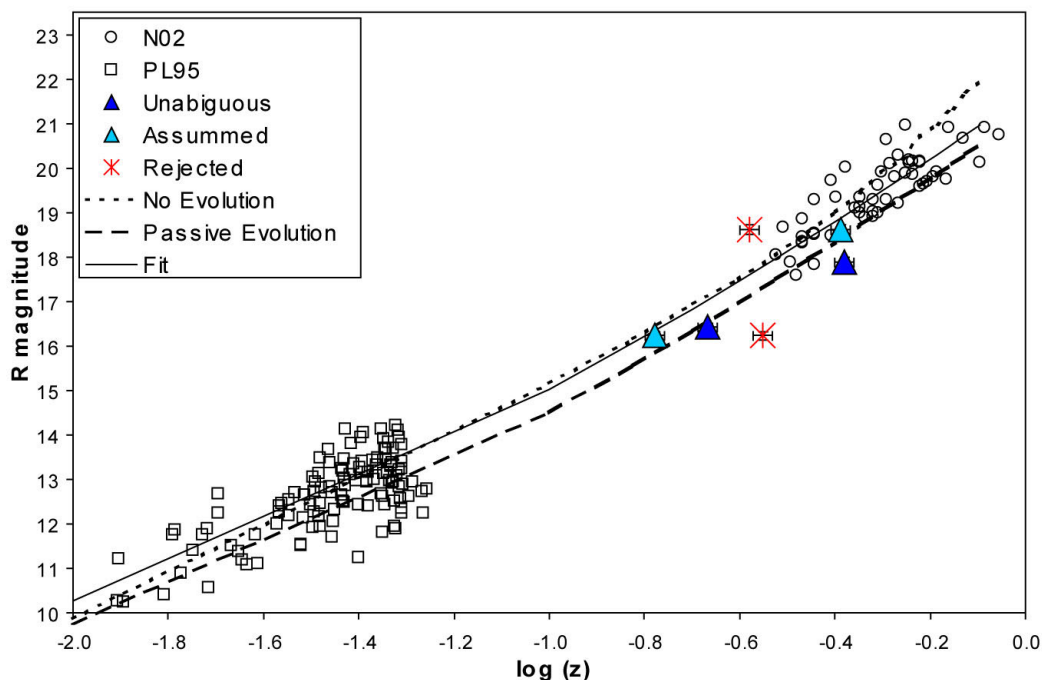
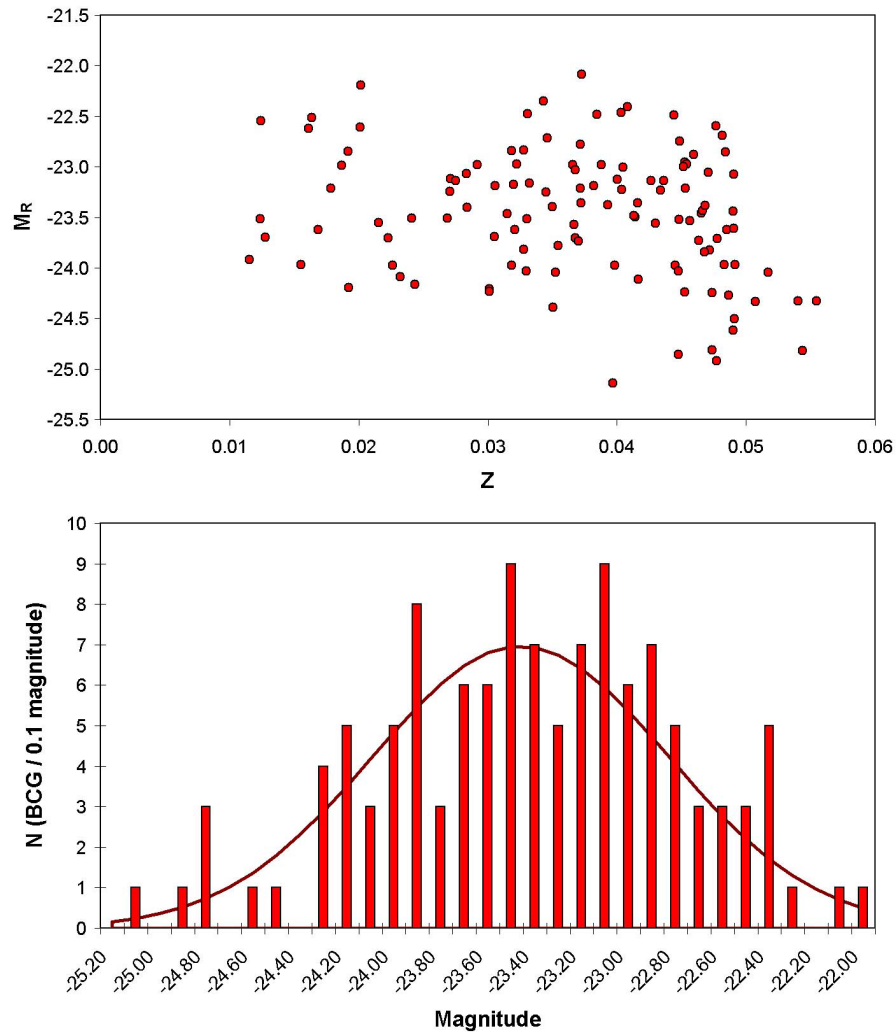


Figure 3-3: Magnitude vs. Redshift for BCGs. The low redshift sample (squares) is from Postman and Lauer 1995 and the high redshift sample (circles) is from Nelson et al. 2002. We have over-plotted both a passive evolution model (long dash), a no evolution model (short dash), and a least squares fit (solid line) for comparison. The dark blue triangles are TOC clusters with known clusters, the light blue triangles are the accepted redshifts for clusters with ambiguous redshifts, and the red stars are rejected redshifts. It should be noted that the BCG in TOC J 1602.8+4338 has nearby neighbors and may not have been completely deblended. This would produce its lower than expected R magnitude.

Figure 3-4: PL95 Brightest Cluster Galaxy Sample. a - (top) The sample shows no clear evidence of luminosity evolution. The best-fit line with a non-zero slope has a coefficient of determination of $R^2 = 0.05$. b - (bottom) The distribution of BCG magnitudes is Gaussian about $R = -23.46$, with $\sigma^2 = 0.63$.



Charlot's (1993) GISSEL96 model. It assumes $z_{\text{formation}} = 2$, a Salpeter initial mass function for masses between 0.1 and $100 M_{\odot}$, and a 10^7 year burst of star formation. A least-squares polynomial fit to N02 and PL95 produced:

$$R(\log z) = 0.9321 (\log z)^2 + 7.5711 (\log z) + 21.674.$$

Table 3-2: TOC Brightest Cluster Galaxy R-magnitudes. The expected – observed (exp.-obs.) differences for a no evolution model (No Ev.), a fit to the PL95 and N02 data and a passive evolution (P.E.) model are shown. We have accepted the redshifts with the smallest residuals as being correct for the 2 clusters with multiple spectroscopic redshifts. It should be noted that the BCG in TOC J 1602.8+4338 has several near neighbors and may have been incompletely deblended, resulting in a brighter than expected (lower) magnitude.

Field	Redshift z	R	No Ev. (exp.-obs.)	Fit (exp.-obs.)	P.E. (exp.-obs.)	Notes
TOC J 1602.8+4338	0.416	17.89	1.23	1.04	0.58	
TOC J 1620.9+4442	0.215	16.42	0.47	0.27	-0.18	
TOC J 1626.1+4859	0.410	<u>18.61</u>	0.47	0.27	-0.18	accepted
	0.264		-0.97	-1.00	-1.48	
TOC J 1705.8+3657	0.167	16.23	0.19	0.12	-0.37	accepted
	0.281		1.64	1.55	1.08	

Comparing our 4 clusters to these 3 R(z) trends, we clearly identified the appropriate redshift for each cluster. In all cases the passive evolution model is the best fit to our clusters' BCG (see Table 3-2), and our accepted and unambiguous redshifts differ from it by no more than 0.58 magnitudes. The standard deviation of the BCG about the fit is 1.56 magnitudes. For the rest of this paper we use the BCG “accepted” redshifts for our clusters with multiple spectroscopic redshifts. It should be noted that the BCG in TOC J 1602.8+4338 has several near neighbors, and may have been inexactly deblended, creating too high a magnitude.

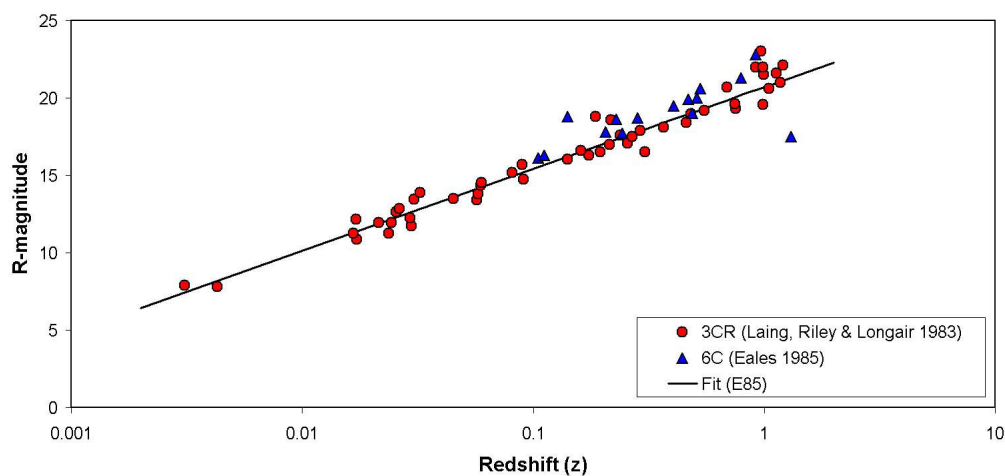
RADIO SOURCES

With our cluster redshifts identified, we can begin to interpret the radio sources aligned with our clusters. Until as recently as 1999, the majority of the optically identified moderate and high z radio sources were radio galaxies with S

> 0.5 Jy. These systems form a collection of elliptical galaxies (Lilly et al. 1984; Lacy et al 2000) that often contain AGN producing central engines or quasars (95%), or more rarely large amounts of star formation (Sadler et al 2002, hereafter S02). Optical studies have shown that their number distribution peaks near a redshift of $z = 1$ (Condon 1984). At low to moderate redshifts ($z < 0.5$) the optical properties of radio source host galaxies are homogenous and do not vary with radio power (Laing et al. 1983; Owen & Laing 1989; Owen & White 1991), and there is a well-defined R magnitude-redshift (R-z) relationship (Eales 1985). Nominally, this relationship should allow us to identify optical objects associated with radio sources as cluster members or non-members by using an object's R-magnitude as a surrogate for a spectral redshift (see Figure 3-5).

As work has been done to identify the host galaxies of the fainter radio sources in the NVSS and FIRST surveys (mJy sources), the radio source host galaxy population has become more diverse (Sadler et al. 2002; Magliocchetti et al. 2000- hereafter M00; Machalski and Condon 1999-hereafter MC99). While

Figure 3-5: Redshift vs. R-magnitude for 6C and 3CR galaxies (Eales 1985)



high power radio sources have a well defined luminosity function associated with AGN, at $L \leq 10^{25} \text{ W Hz}^{-1}$ the radio luminosity function becomes dominated by starburst galaxies (Condon 1992, 1989; Windhorst et al. 1985; Danese et al. 1987), and matches the luminosity function of spiral galaxies. Observationally, this corresponds to a flattening of the differential source count dN/dS below $S \sim 10 \text{ mJy}$ (M00) as late type galaxies – often IRAS galaxies (Franceschini et al. 1988; Benn et al. 1993) – become important. This has the effect of spreading out the R-z relationship for radio sources (see Table 3-3 and Figure 3-6, 3-7, 3-8).

When the high power sources in the 3CR and 6C catalogues are compared with samples from the NVSS and FIRST catalogues, it is apparent that the highest power objects are substantially brighter than lower power radio sources. While the lower power systems do have a solid R-z relationship, its scatter is much larger. This increased R(z) dispersion at fainter radio magnitudes, and the varying optical properties of different types of radio sources makes it impossible for us to clearly identify specific radio sources with our clusters without spectra.

The best we can do is optically identify as many radio sources in our

S_{1.5} mJy	N	Stdev
200 - 300	10	0.087
100-200	27	0.282
50-100	57	0.293
10-50	299	0.326
5-10	248	0.336
< 5	506	0.416

Table 3-3: The Standard Deviation about the R – z relationship for N NVSS sources. Optical identifications are taken from the Las Campanas Redshift Survey (MC99).

cluster fields as possible and consider whether these optical galaxies have colors and magnitudes consistent with radio galaxies from other samples. Sources with $S_{1.5} > 10 \text{ mJy}$ should roughly follow a R-z relationship. The Las Campanas Redshift Survey (LCRS - Shectman et. Al 1996) and the 2-degree Field

Galaxy Redshift Survey (2dFGRS – Colless 1999, Maddox 1998) are ideal for this. MC99 used LCRS to optically identify 1157 NVSS radio sources with limiting magnitudes of $S_{1.4} = 2.5$ and $R = 17.75$. Magleocchetti et al (2002, hereafter M02) used the 2dFGRS to identify 557 radio sources from the FIRST survey with limiting magnitudes of $S_{1.4} = 1$ mJy and $R = 18.6$.

We considered any radio source within 2 Abell Radii ($2 R_{\text{Abell}}$) of a cluster a possible cluster member. While this choice of cut-off radius was somewhat arbitrary, it should be noted that Carlberg et al. (1996) found virial radii, $R_V = 0.785 - 3.156 h^{-1} \text{ Mpc}$ ($<1.54 h^{-1} \text{ Mpc}>$) for 16 X-ray selected galaxy clusters with the same redshift range as our sample. Only one of their clusters, A2390, had a $R_V > 2 R_{\text{Abell}}$. We believe a search for physically associated radio galaxies beyond $2 R_{\text{Abell}}$ is unjustified.

Figure 3-6: Redshift vs. R-magnitude for NVSS galaxies (MC99). The solid line is a fit to the data, $R = 20.5 + 5 \log z + 0.6 (\log z)^2$ and the long dash and short dash represent the 1σ and 3σ standard deviation about the fit.

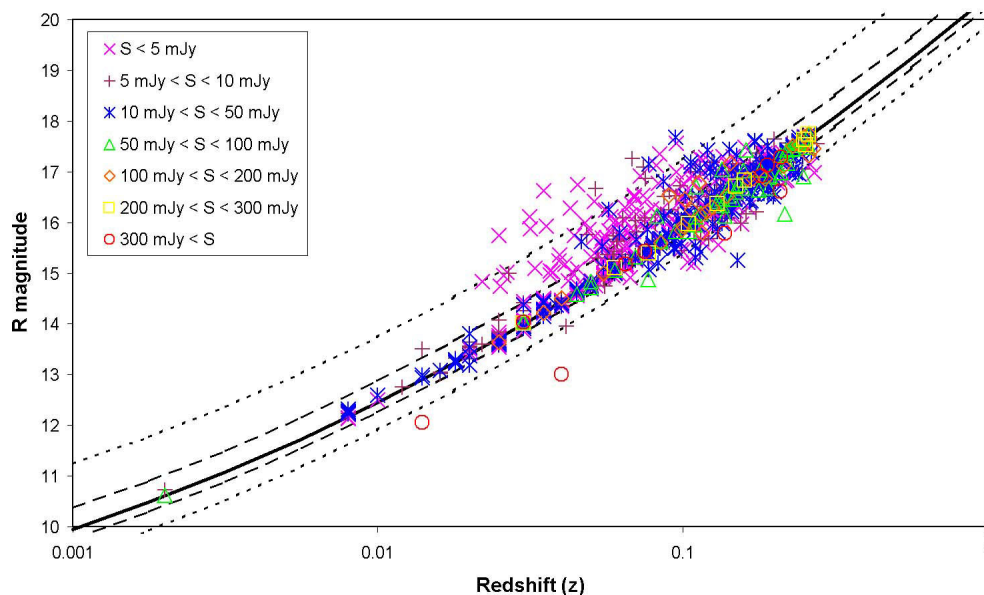


Figure 3-7: Redshift vs. R-magnitude for FIRST galaxies (M02). The lines are as in Fig. 3-6.

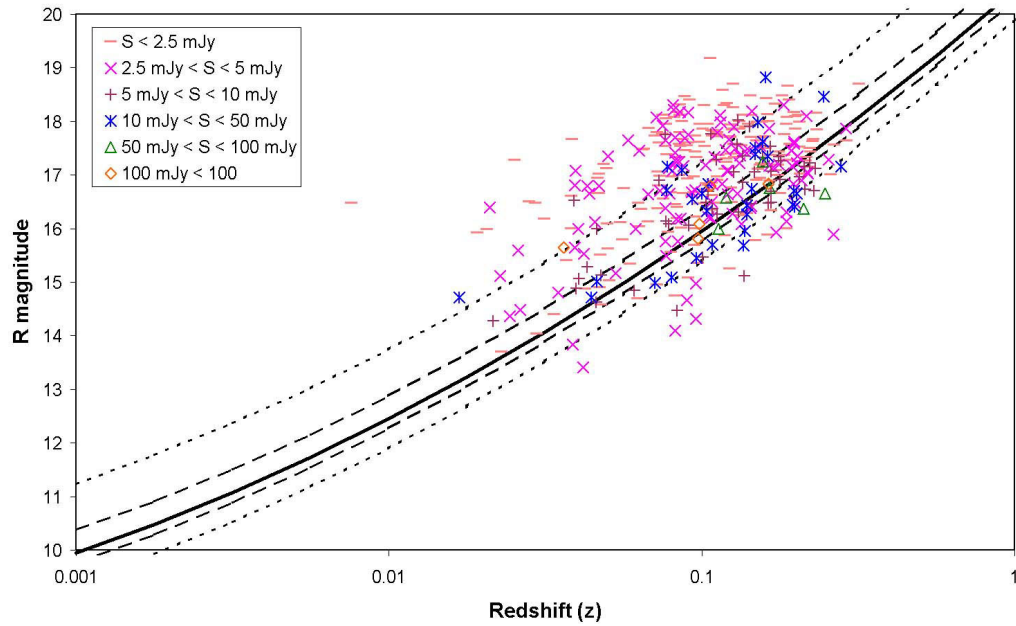
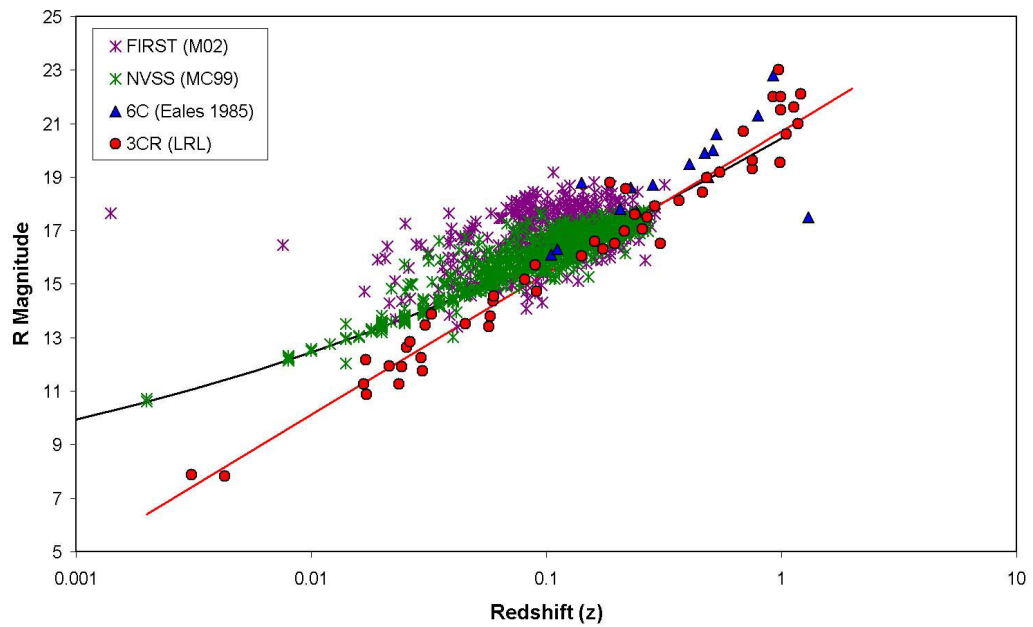


Figure 3-8: Comparison of R mag. vs. redshift for 3CR, 6C, NVSS and FIRST radio sources. The solid black line is the fit from Fig. 3-5, and the red line is from Fig. 3-4.



Sadler et al. (2002) demonstrate that from their total sample of 58,454 2dFGRS galaxies, the number of radio-optical matches becomes that predicted by random chance at separations of ≥ 15 arcsec for NVSS radio sources (see their Figure 1). We have thus adopted a separation cut-off of 15 arcsec for candidate radio sources. Table 3-4 lists all the radio sources within $2 R_{\text{Abell}}$ of each cluster and the photometry for all galaxies within 15 arcsec of them.

The majority of galaxies have $20 < R \text{ mag.} < 22$ (Figure 3-9). This can be explained by the distribution of radio sources with redshift. The radio source population peaks at about $z = 1$ ($R \sim 20.4$ mag). The area-limited nature of our sample will exaggerate this peak because we sample larger volumes at increasing redshifts. The majority of the radio sources we have optically identified within $2 R_{\text{Abell}}$ are consistent with a population of background galaxies. It should also be noted that as we go to lower and lower limiting magnitudes, the probability of mis-identifications increases. Spectra are needed to identify both object redshifts and to confirm that the object type is consistent with a radio galaxy.

Figure 3-9: R – z plot of optical magnitudes of TOC radio sources and cluster redshifts

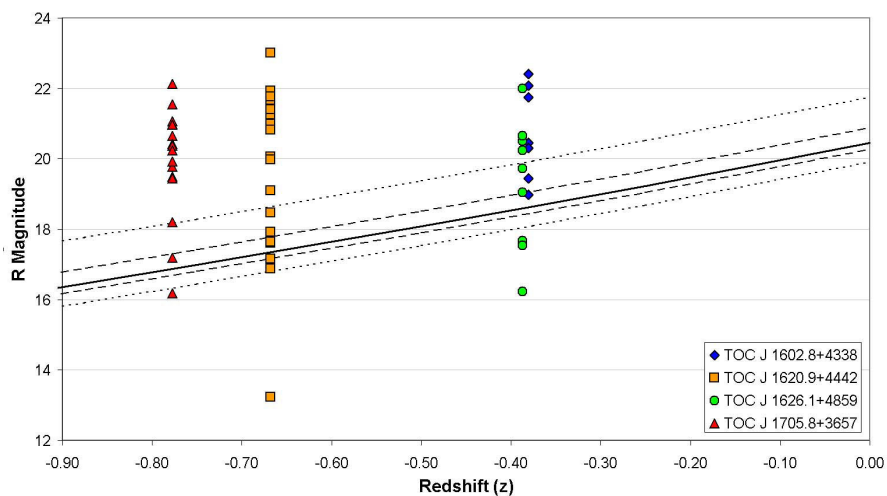


Table 3-4: Radio Sources within 2 R_{Abell} of TOC clusters. A (+) denotes a highly likely cluster member, and a (-) denotes a possible cluster member. The last column of the table indicates if a galaxy's R-magnitude is within 1 or 3 σ of that expected for a radio source at the given cluster's redshift. *Two equally possible optical identifications were found.

TOC 1602.8+4338, $z = 4.16$, $2 R_{\text{Abell}} = 12.6$ arcmin									
Radio Sources				Candidate ID					
ID	RA	DEC	dist. (")	$S_{1.5}$	RA	DEC	R (B-R)	sep. (")	Note
R1(+)	160248.6	433533.5	42.7	9.2	160248.8	433535.9	19.0	3.1	$< 1\sigma$
R2(+)	160259.4	433530.2	89.5	4.2	160259.4	433526.0	19.4	3.0	$< 3\sigma$
	160237.1	433651.9	189	3.6	160237.4	433640.4	22.4	2.2	8
	160249.2	433851.2	228	3.3	160249.6	433842.6	21.7		8
	160240.9	434106.5	380	32.2	160240.9	434105.9	22.1	0.9	1
	160334.9	433440.4	472	3.0					
	160238.0	432417.5	664	6.6	160238.0	432415.7	20.5	0.3	1
	160210.3	432638.7	676	4.3	160210.1	432628.6	20.3	1.5	8
	160333.8	434408.0	711	13.7					
	160144.7	433514.5	726	4.1					
	160242.1	434725.5	747	84.1					

TOC J 1620.9+4442, $z = 0.215$, $R_{\text{Abell}} = 12.7$ arcmin									
Radio Sources				Candidate ID					
ID	RA	DEC	dist. (")	$S_{1.5}$	RA	DEC	R (B-R)	sep. (")	Note
	162106.1	444229.3	84.1	3.7	162105.2	444231.3	21.7	1.1	10
*	1621	1.3444 44 27	147	04	162100.5	444426.3	21.2	1.5	9
					162101.6	444438.9	21.8	2.8	9
	162043.4	444042.7	181	2.8	162043.3	444033.2	23.0	> 23	7
	162040.8	444229.7	191	2.9	162041.0	444234.5	21.4	1.8	4
R1(+)	162040.3	443842.2	278	16.5	162040.3	443844.4	16.9	2.3	$< 3\sigma$

Radio Sources					Candidate ID				
ID	RA	DEC	dist. (")	S _{1.5}	RA	DEC	R (B-R)	sep. (")	Note
	162110.8	444739.2	360	6.4	162111.4	444741.4	21.0	7	
	162047.3	444820.6	396	2.7	162047.8	444808.1	21.9	11	
	162019.6	444342.0	428	3.5	162019.3	444344.3	20.0	3	
	162039.8	443542.4	430	6.1	162040.4	443550.7	13.2	0.9	
	162109.7	445006.8	498	17.0					
	162140.9	444734.7	560	89.0	162141.4	444744.3	20.1	1.1	
	162032.8	443315.7	595	11.5	162033.5	443309.9	21.7	8	
	162138.6	444956.1	637	19.1	162138.8	444960.0	20.1	4	
R2 (+)	162017.6	444957.0	644	10.2	162016.8	444958.7	17.6	1.8	< 1σ
	162141.3	443423.5	647	13.2	162142.0	443418.4	21.0	1.0	
R3 (+)	161960.0	444740.8	710	61.5	162000.5	444740.8	17.6	2.5	< 1σ
	162147.8	443305.9	751	3.3	162147.6	443305.8	19.1	1.5	
	162016.0	442920.2	888	4.7					
	162203.0	445238.3	935	8.3					
	161940.3	443430.1	950	3.3	161941.0	443424.1	20.8	1.4	
	162002.9	445547.1	1015	4.2					
	162203.2	442937.5	1016	45.3	162203.1	442926.5	20.0	1.0	
R4 (-)	162136.8	445803.1	1043	6.4	162137.3	445805.5	18.5	2.5	< 3σ
	162115.2	450018.1	1109	3.7					
	162204.1	442741.8	1110	24.0	162204.0	442732.9	21.8	6	
R5 (-)	162233.3	443348.9	1125	2.6	162232.9	443345.1	17.9	1.0	< 3σ
R6 (+)	161938.9	445427.2	1128	28.5	161938.6	445422.8	17.2	1.8	< 1σ
	162005.1	445925.8	1188	3.4					

TOC 1626.1+4859, $z = 0.410$, $2 R_{\text{Abell}} = 20.1$ arcmin.

Radio Sources					Candidate ID				
ID	RA	DEC	dist. (")	$S_{1.5}$	RA	DEC	R (B-R)	sep. (")	Note
R1(+)	162546.2	490043.5	22.8	14.7	162546.3	490042.1	18.8	2.1	$< 1\sigma$
	162555.6	490042.8	103	3.0	162555.8	490039.0	16.2	1.4	
	162553.6	485855.2	116	4.2	162553.1	485858.7	20.5	1.6	
R2(-)	162559.9	485817.4	187	26.3	162560.0	485816.3	17.7	0.7	$< 3\sigma$
	162549.4	485636.4	226	2.3	162549.5	485632.2	20.2	0.7	
	162604.3	490417.0	301	6.1					
R3(-)	162620.2	490003.0	343	2.8	162620.7	490008.9	19.0	2.1	$< 3\sigma$
R4(-)	162457.6	490039.0	471	4.4	162458.0	490038.5	19.7	1.9	$< 3\sigma$
	162632.0	485652.8	502	26.6	162631.8	485704.1	22.0	0.5	
	162625.0	485451.0	509	3.1	162624.9	485441.7	20.7		
	162636.9	490425.3	562	5.3					
	162615.6	485050.0	642	43.7	162615.7	485049.4	20.7		
	162516.3	491058.1	700	2.7					
R5(-)	162629.7	490936.7	707	7.8	162629.9	490937.8	17.5	2.5	$< 3\sigma$
	162652.5	485555.5	710	4.7	162652.2	485554.4	21.0		
	162433.5	485605.8	752	3.8					

TOC 1705.8+3657, $z = 0.167$, $2 R_{\text{Abell}} = 24.7$

Radio Sources					Candidate ID				
ID	RA	DEC	dist. (")	$S_{1.5}$	RA	DEC	R (B-R)	sep. (")	Note
	170601.0	365755.2	26.2	6.2	170601.4	365758.8	21.5		
	170552.8	365613.6	124	45.9	170552.9	365613.9	20.7	1.0	
	170610.5	365617.1	135	2.8	170610.8	365613.7	>23		
	170545.1	365619.2	203	21.1	170545.4	365617.7	20.4		
	170538.0	365645.4	279	20.2					

Radio Sources					Candidate ID				
ID	RA	DEC	dist. (")	S _{1.5}	RA	DEC	R	(B-R) sep. (")	Note
	170542.2	370046.1	299	13.1					
	170559.4	365047.4	402	6.9	170559.7	365059.6	19.8	1.5	
	170635.0	365143.4	534	4.1	170635.6	365145.2	21.0		
R1(+)	170502.5	365835.2	704	3.6	170502.9	365831.1	16.2	1.9	< 3 σ
	170635.9	364718.9	740	10.0	170635.4	364725.1	21.1		
	170524.4	370809.3	776	10.0					
	170506.7	364830.6	845	3.4	170506.4	364832.9	21.0	0.3	
	170458.3	365042.6	855	59.7	170458.0	365045.6	20.4		
	170506.5	370648.2	859	3.0	170506.7	370702.6	20.2	1.7	
	170610.5	364309.8	867	3.5	170610.4	364304.1	18.2	0.9	
	170555.7	364256.1	875	6.3	170554.7	364251.7	19.9	2.1	
	170448.6	370025.7	886	3.0					
	170600.4	364236.7	892	76.5					
	170642.5	371020.9	918	6.4	170642.2	371018.4	19.5		
	170626.4	371203.2	925	18.4					
	170718.7	365731.9	931	6.3	170718.4	365732.5			
	170714.7	370523.3	1002	3.5					
	170721.3	364704.8	1148	3.1					
	170435.2	370708.7	1179	3.0	170435.9	370657.1	19.5	1.9	
	170645.3	371549.0	1221	4.5					
	170446.4	371123.8	1223	4.3					
	170734.5	370700.0	1256	4.5					
	170420.4	370620.5	1317	2.6	170420.7	370629.1	22.1		
	170410.9	365526.2	1326	3.2					
	170751.5	365409.1	1339	8.9					
	170752.9	365046.3	1401	4.9					
R2(+)	170419.5	370957.0	1427	99.7	170419.2	370954.4	17.2	1.7	< 1 σ
	170760.0	370137.2	1446	17.9					

As can be seen in Figure 3-9, the majority of the optical objects identified have magnitudes $R = 20 - 22$ mag. This can be explained by the physical distribution of radio sources with redshift: the radio source population peaks at a redshift around $z = 1$ ($R \sim 20.4$ mag). The area-limited nature of our sample exaggerates this peak because we sampled larger volumes at increasing redshifts. The majority of the radio sources we optically identified within $2 R_{\text{Abell}}$ are consistent with a population of background galaxies. It should also be noted as we go to lower and lower limiting magnitudes, the probability of mis-identifications increases. Spectra are needed to identify both object redshifts and confirm that the object type is consistent with a radio galaxy.

We consider any source with an R-magnitude within 3σ of expected to be a potential cluster member. To assess if an optical-radio source was a potential cluster member we considered its B-R colors, distance from cluster center, R-magnitude and its $S_{1.5}$. Our assessments of the sources in each TOC cluster are given below. The number of likely radio galaxies found in each cluster is not large and these clusters do not appear to have an unusual amount of radio-activity (Miller & Owen 2001). On average we believe our clusters contain two galaxies associated with radio emission (most likely AGN).

TOC J 1602.8+4338 ($z = 0.416$): There are two radio sources, R1 and R2, within the central region of the cluster that both have magnitudes consistent with the cluster's redshift at the $< 1 \sigma$ level, and have early-type galaxy colors. These radio sources are considered cluster members (see Figure 3-10).

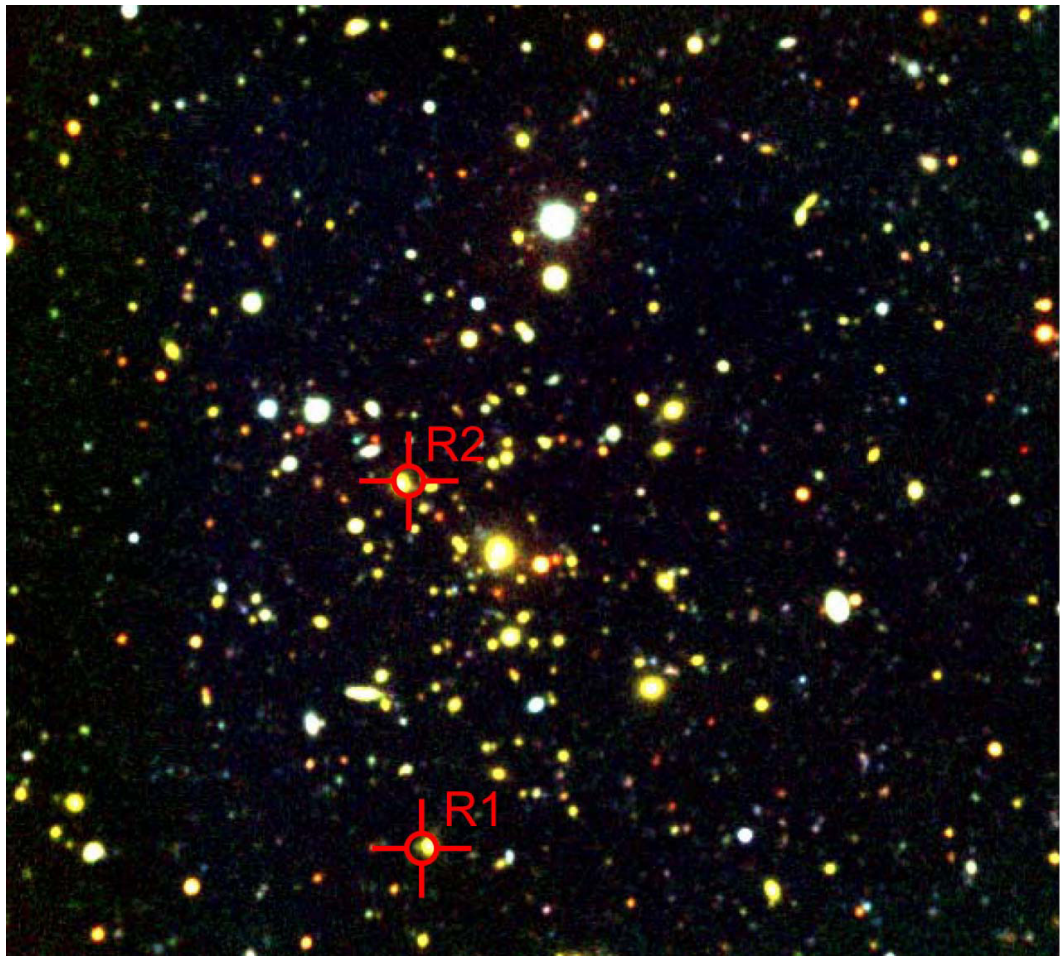


Figure 3-10: Central Region of TOC J 1602+4338 at $z=0.416$. Each red target has a 10 arcsec radius and marks a NVSS radio source location.

TOC J 1620.9+4442 ($z = 0.215$): This system has six potential cluster radio galaxies. R1, is in the center of the cluster (see Figure 3-11) and has early-type color. We accept it as a likely cluster member. Three other sources (R2, R3, R6) have R-magnitudes within 1σ of the expected, and $S > 10$ mJy ($S = 10.2, 61.6, 28.5$ mJy), implying that they are more likely to follow the R-z relationship. Their early-type colors and magnitudes cause us to accept them as cluster members. The remaining two galaxies have indeterminate

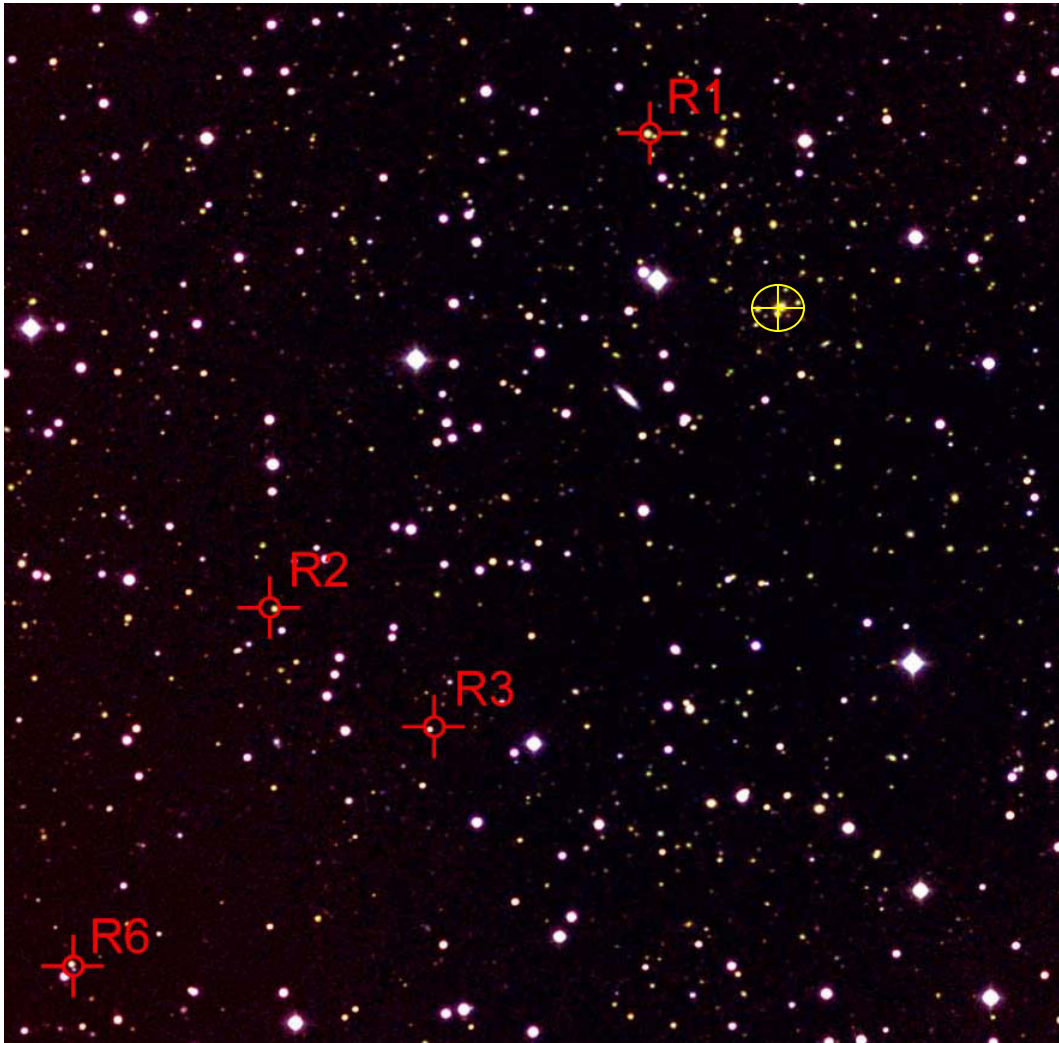


Figure 3-11: Central Region of TOC J 1620.9+4442 at $z = 0.215$. Each red target has a 10 arcsec radius and marks a NVSS radio source location. Cluster center is marked in yellow.

membership. R4 has early-type colors, and may be a member. R5 is very blue, and if it is a cluster member, it is a star bursting system.

TOC J 1626.1+4859 ($z = 0.410$): R1 has a magnitude consistent with expected at the $< 1 \sigma$ level. It has late-type galaxy colors, but is accepted as a probable cluster member. R2 has $S > 10$ mJy, but is extremely blue. If it is a cluster

member, it is undergoing dramatic star formation. The remaining three systems with magnitudes within 3σ of expected are lower power systems. They are located beyond $1 R_{\text{Abell}}$ and have colors consistent with late type galaxies at $z = 0.410$. They are accepted as low probability cluster members.

TOC J 1705.8+3657 ($z = 0.167$): There is one galaxy with a magnitude consistent within 1σ and one within 3σ of expected. R2 has $S_{1.5} = 99.7$ mJy and it is probably at the same redshift as the cluster. R1 is located within $1 R_{\text{Abell}}$, and while it has $S_{1.5} = 3.6$ mJy and is thus harder to pin to the R-z relationship, bright radio sources are rare enough that we believe it is likely to also be at the cluster's redshift.

RICHNESS

As will be shown more clearly in Chapter 4, a cluster's richness plays a large role in the evolution of its member galaxies. In order to correctly compare our clusters to systems in the literature, we need to determine their richness. There are a variety of ways to do this. Most widely known is the Abell Richness, R , which measures all the galaxies brighter than $m_3 + 2$ within $1 R_{\text{Abell}}$ of the cluster center, where m_3 is the magnitude of the third ranked galaxy. Another prevalent richness measure for clusters containing radio sources is $N_{0.5}$, which measures the number of galaxies brighter than $m_1 + 3$ within 0.5 Mpc of the cluster's dominant radio source, where m_1 is the magnitude of the radio galaxy (Hill & Lilly 1991). This richness class has also been defined to instead measure all the galaxies with magnitudes $M = -19 - -25$ mag within 0.5 Mpc of the radio galaxy (Zirbel 1997). Neither of these richness scales is well suited for our

clusters. The Abell richness measurement scheme is designed for large clusters, which our systems are not. The $N_{0.5}$ technique was designed to be utilized in clusters with a powerful dominate radio galaxy, such as those found in the 3CR catalogues, where the radio galaxy is often synonymous with the clusters first ranked galaxy. Our radio galaxies are not this powerful, do not typically lie in the center of the cluster potential wells, and are not the brightest cluster galaxies.

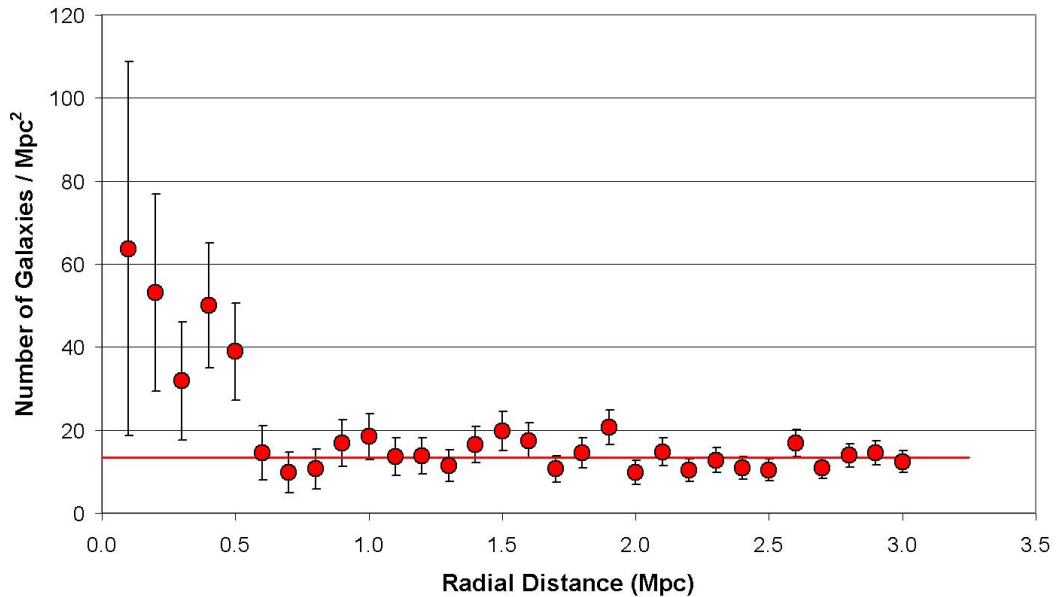
Instead of using either of these richness determination methods, we have instead adopted the N_{30} richness measure of Butcher and Oemler (1985, 1984, 1983, 1978). They wanted to define a richness measure that would provide a consistent richness for clusters with a variety of sizes, morphological distributions, and that are located at a variety of redshifts. Their technique starts by determining the radius R_{30} that contains 30% of the clusters' galaxies, and then it counts the galaxies with $M_V > -20$. R_{30} , unlike a metric radius, measures the same fraction of the total galaxy population in extended giant clusters as it does in small groups. The bright end of cluster luminosity functions are variable and basing the lower magnitude cutoff on the magnitudes of the brightest few galaxies can cause significant variations in the populations counted in different clusters (Butcher and Oemler 1984; Bhavsar 1989; Zirbel 1997). The absolute magnitude

Cluster	Redshift	$N_{\text{Field}} - \text{Simple}$		$N_{\text{Field}} - \text{Fit}$		R_{30}		N_{30}
	z	(# / Mpc ²)	err	b*	(# / Mpc ²)	err	(arcmin) (Mpc)	(#)
TOC J 1602.8+4338	0.416	10.4	3.0-5.1	10.2	1.2	0.71	0.26	21
TOC J 1620.9+4442	0.215	11.71922	2.9-4.8	10.3	1.2	2.82	0.65	42
TOC J 1626.1+4859	0.41	21.1	3.8-4.8	20.7	2.4	0.58	0.21	17
TOC J 1705.8+3657	0.167	10.5	2.9-4.7	11.5	1.3	3.53	0.66	28

Table 3-5: R_{30} , N_{30} and Field galaxy Densities. The simple N_{Field} values are from fits to where the radial galaxy distribution becomes flat. The fit N_{Field} value comes from integrating $N(R)$.

*This is the scaling factor for the local field density: $\log N = 0.39R+b$

Figure 3-12: Radial galaxy density for TOC 1620.9+4442.

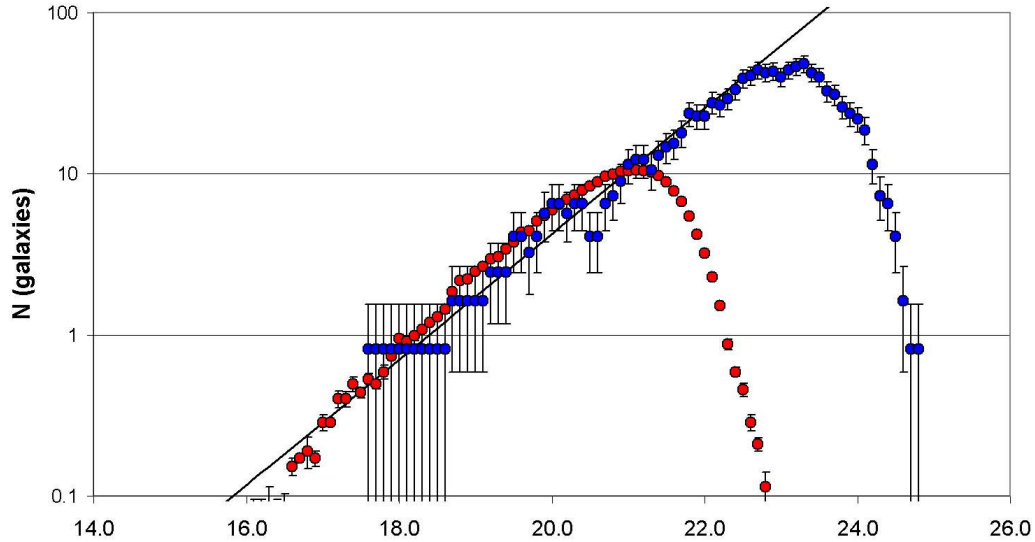


limit of the N_{30} definition should sample similar galaxy populations in clusters with a variety of BCG and radio galaxy characteristics.

To measure the clusters' galaxy populations we needed to statistically correct for foreground and background galaxy populations. We did this in two ways. Our first, simplistic, method was to do radial plots of $N(r)$ and determine where the galaxy counts flattened out. The radius where $N(r)$ became constant was considered R_{100} , the radius containing roughly the entire cluster population. We then fit a line to the galaxy counts beyond R_{100} and considered this value to be the typical field galaxy distribution (see Figure 3-12 and Table 3-5).

To check if this simple counting method accurately accounted for field galaxies across all brightnesses, we also determined $N(R)$ for the field galaxy population (Figure 3-13). We found that the galaxy brightness distribution for galaxies more than $2 R_{Abell}$ from the cluster center had the same slope as Tyson's

Figure 3-13: Number of field galaxies as a function of R-magnitude. The scaling is arbitrary. Red points are galaxies in IGI field of view and blue points are galaxy counts from IGI.



(1988) galaxy counts, however, the overall number density in the direction of our clusters varied from field to field. In general:

$$\log N (\text{galaxies} / 0.5 \text{ Mag} / \text{Mpc}^2) = 0.39 R + b,$$

where b is adjusted to the local density of each region. Integrating this relationship to the R value that corresponds to $M_V = -20$ for each cluster, we calculated the fit value of each clusters field population. We found that the idealized field galaxy population, taking into account a full range of brightnesses, predicted a value well within the errors of our simplistic field determination (see Table 3-5).

To check the reasonableness of our values, we compared them to those found by BO84 for 33 clusters (Figure 3-14). We found that our clusters were completely comparable, and are similar to Abell $R=0$ clusters.

COLOR DISTRIBUTIONS

The statistical nature of our field galaxy correction makes the creation of an accurate color-magnitude diagram impossible. Instead, following Butcher and Oemler (1984) and Metevier et al. (2000) we used our color magnitude diagrams to determine the slope of the color-magnitude effect. This effect causes more luminous E and S0 galaxies to have redder colors than their lower luminosity counterparts. All four of our clusters shared the same correction in the B-R vs. R plane. After correcting all our galaxies, even the late-type and field populations, for this effect, we determined the galaxy color distributions for each cluster (Figure 3-15). The radial color distribution and cluster blue fractions will be discussed in the next chapter. The 4 clusters are compared in rest frame colors in Figure 3-16. The color distribution of these clusters is typical for their densities, with the smallest clusters, TOC J 1602.8+4338 and TOC J 1626.1+4859, having the flattest color distributions, and the richest cluster, TOC J 1705.8+3657 having a distinct early-type galaxy enhancement. The colors of these systems, as compared to their number densities, will be discussed in the next chapter.

SUMMARY

The four clusters we selected for detailed observations are spread across low and moderate redshifts, are all Abell richness class $R = 0$ or less, and are generally non-remarkable systems. Their brightest cluster galaxy magnitudes and spectral redshifts are in good agreement. In each cluster there are several optical galaxies that we believe are associated with radio sources. Without spectra we cannot confirm our identifications, or confirm that the objects belong to the

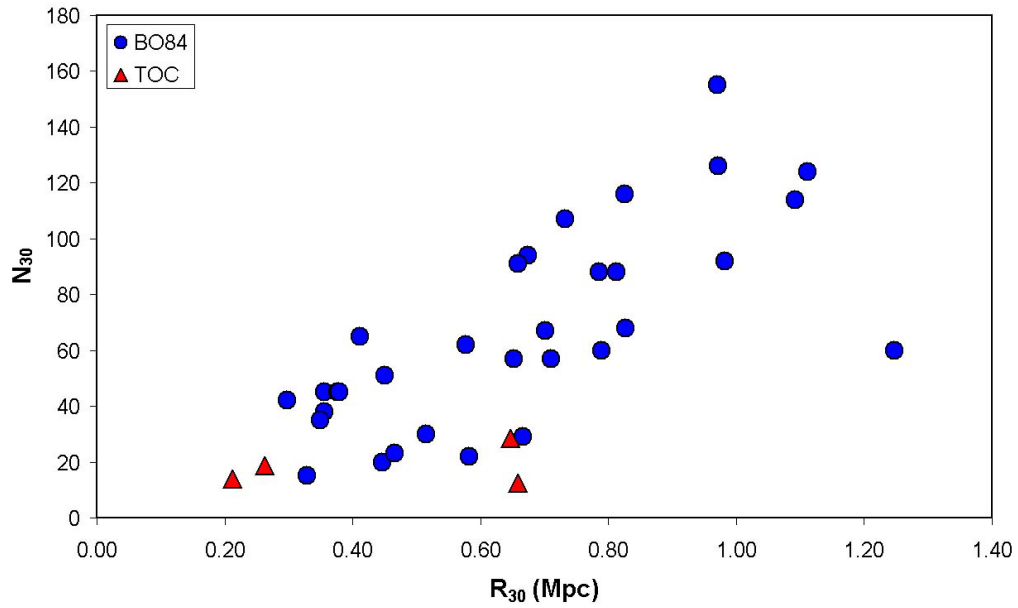


Figure 3-14: R_{30} vs. N_{30} for the 33 clusters from BO84, and the TOC sample. The spread in R_{30} is a reflection of the various cluster concentrations.

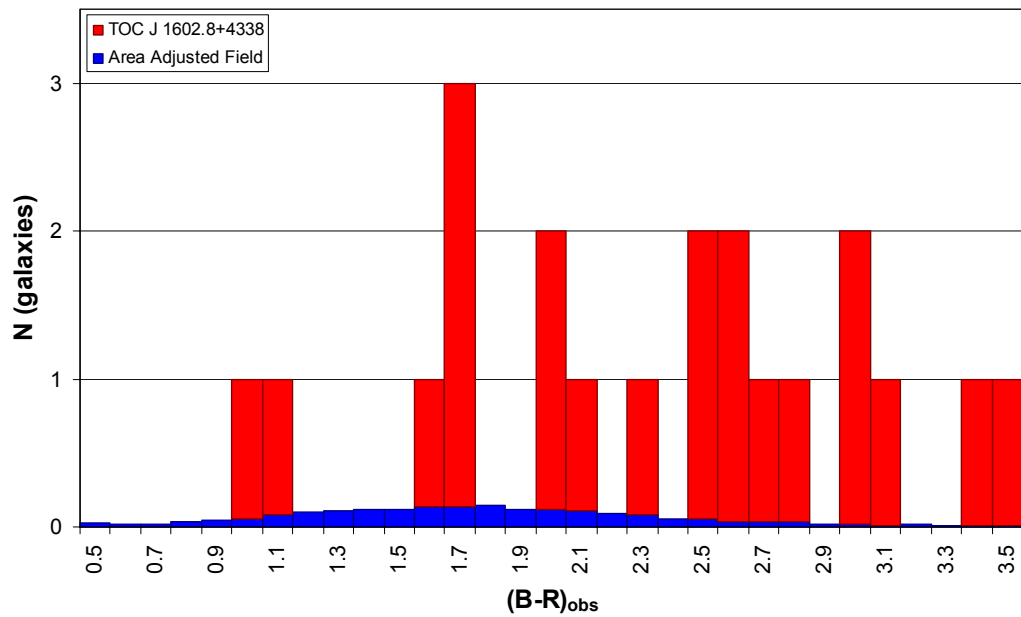


Figure 3-15 Cluster Color Diagrams. a(above) TOC J 1602.8+4338 at $z = 0.416$. For Sab galaxies $B-R = 2.56$.

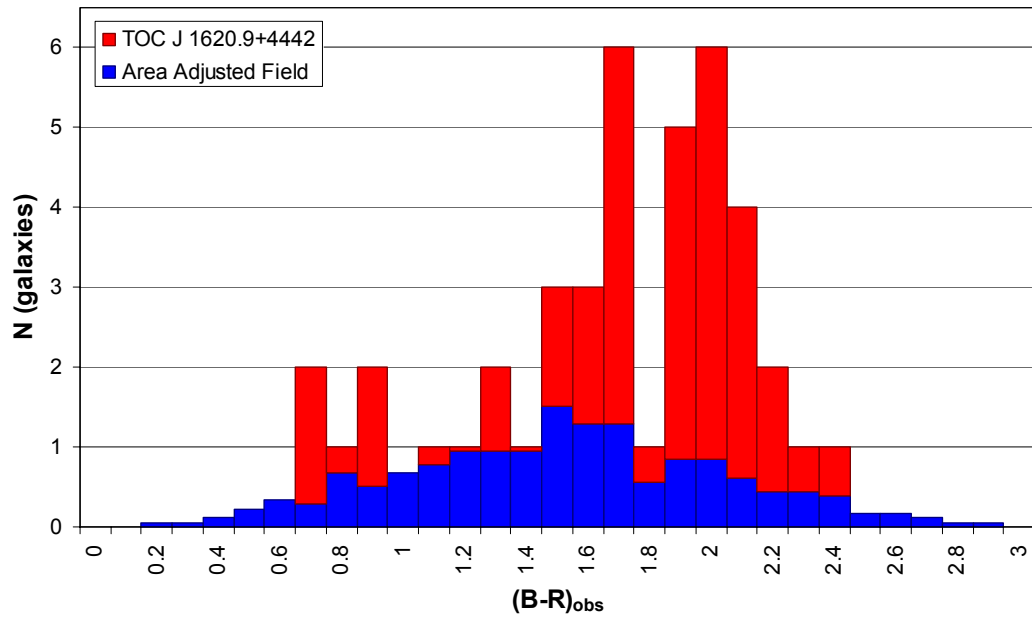
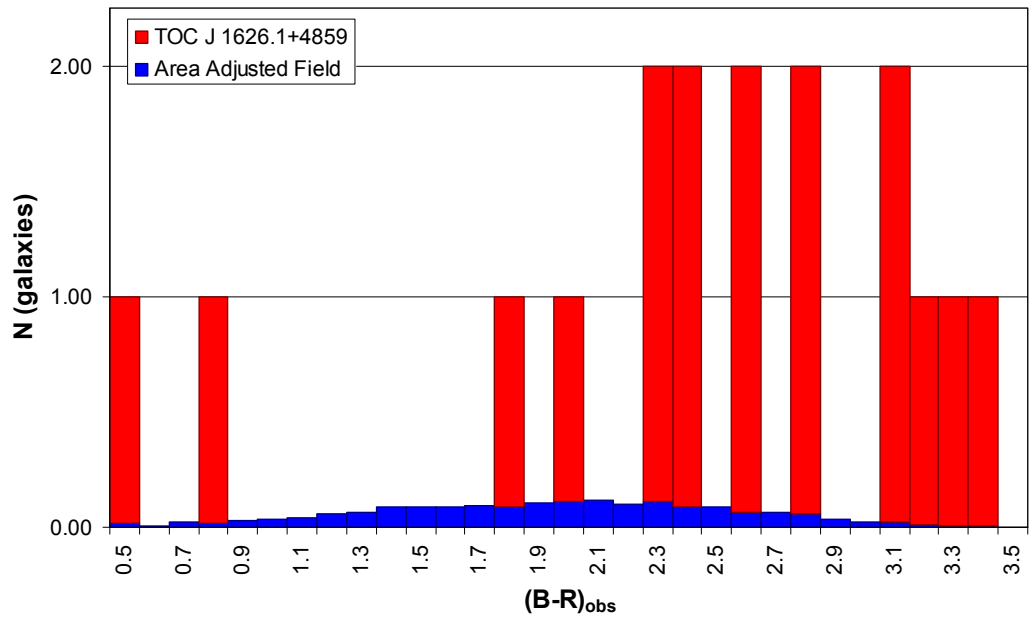


Figure 3-15 (continued.) b (above): TOC J 1620.9+4442 at $z = 0.215$. For Sab galaxies $B-R = 2.01$. c (below): TOC J 1626.1+4859 at $z = 0.410$. For Sab galaxies $B-R = 2.55$.



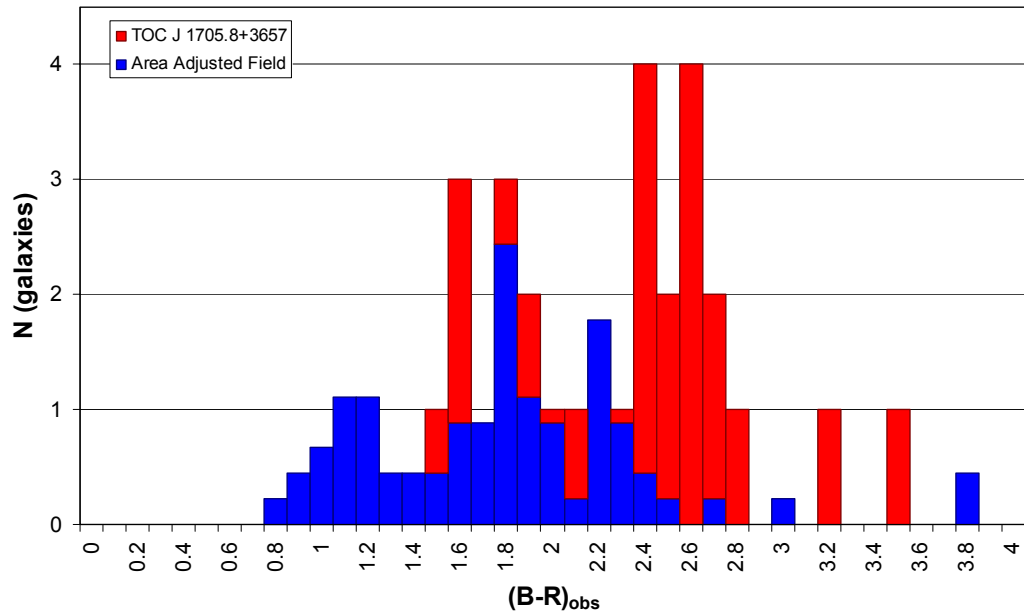


Figure 3-15 (continued.) d; TOC J 1705.8+3657 at $z = 0.167$. For Sab galaxies $B-R = 1.87$.

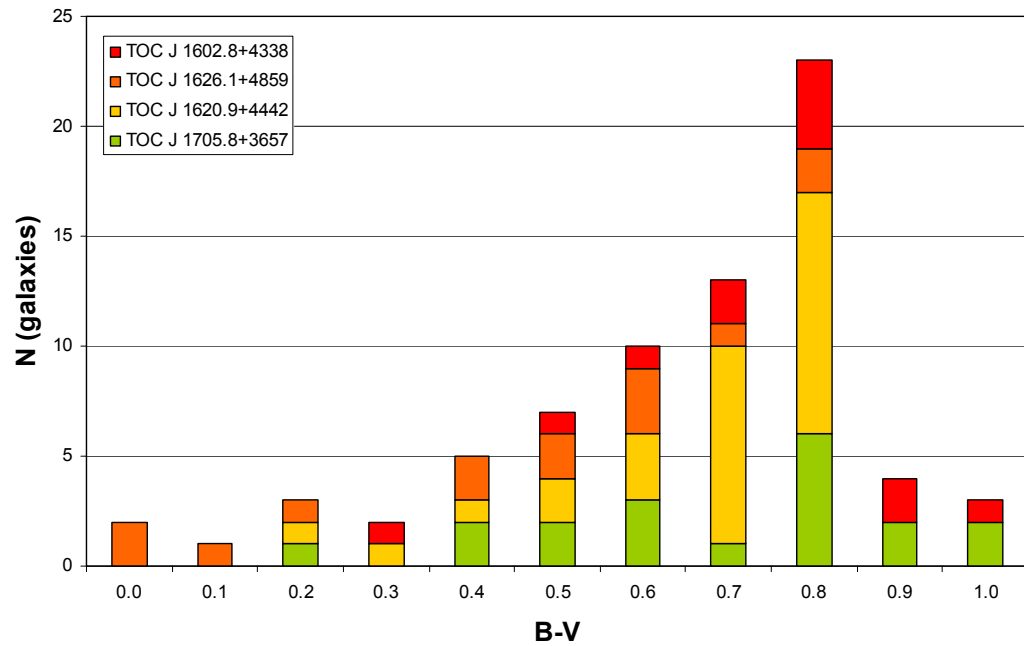


Figure 3-16: Rest frame Color Distribution for all TOC Clusters. Field galaxies have been subtracted. For Sab galaxies, $B-V = 0.78$.

clusters. Using the R-z relationship for radio sources, and taking into account the $S_{1.5}$ for each object, we have tried to assess the probability of objects within $2 R_{\text{Abell}}$ being cluster members. On average we believe our clusters contain two galaxies associated with radio emission (most likely AGN). This does not make our clusters unusual.

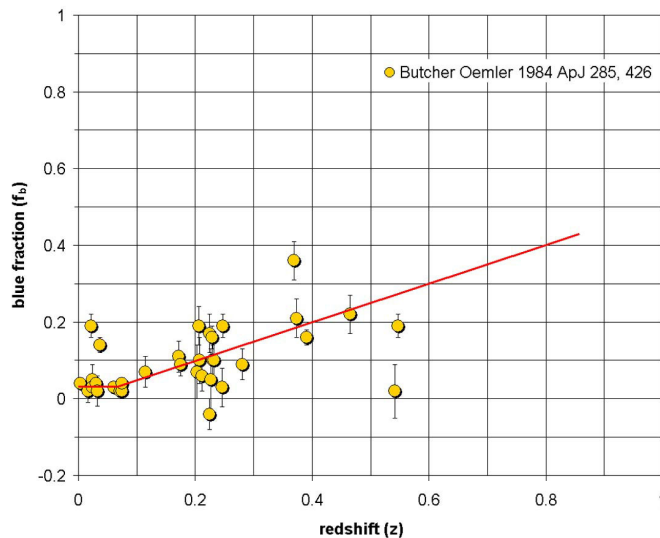
With a sample of only four galaxy clusters it is difficult to draw any conclusions about the types of clusters typically identified by our radio-source overdensity technique. The fact that we found 1 super-positioning of two clusters raises concern that our technique may be particularly prone to finding line of sight alignments. We are encouraged that all 4 of the fields we selected for detailed follow-up were real clusters.

Chapter 4: All the Pretty Colors

In 1957 Zwicky became the first to note that “[f]rom cursory inspection of 100-inch and 200-inch plates, it appears that [the color range of cluster galaxies] is increasing with distance of the clusters. Many interpretations of this observation are possible such as . . . intergalactic obscuration, the Stebbins-Whitford effect, or some systematic evolutionary phenomena.” The change in galaxy morphology/color distribution in clusters was later quantified by Butcher and Oemler (1984 – hereafter BO84). They demonstrated that for a collection of 33 clusters with redshifts between $z = 0.003$ and $z = 0.54$, the fraction of galaxies with B-V colors > 0.2 magnitudes bluer than the red ridge⁹ increases from < 0.1 in the local universe to 0.2 and higher at redshifts of $z > 0.3$ (see Figure 4-1).

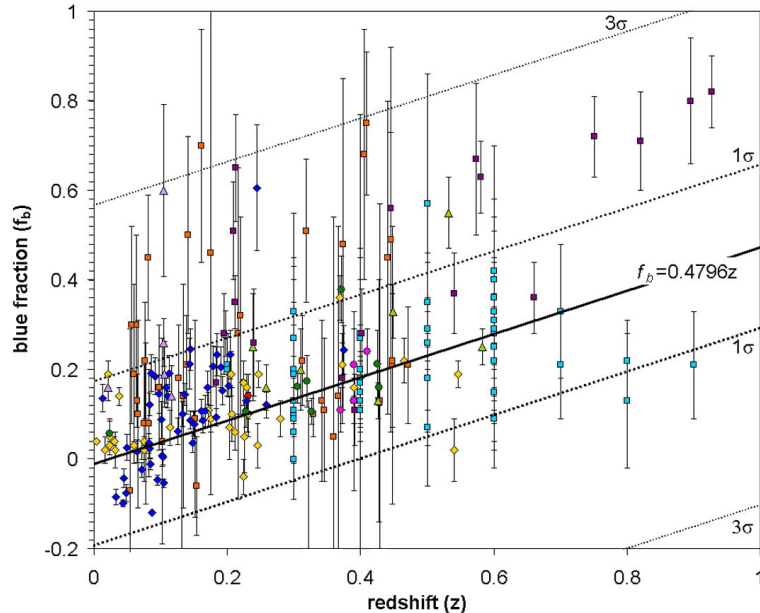
Since Butcher and Oemler’s original work, numerous authors have sought to further refine the relationship between a cluster’s redshift and blue fraction. While it is clear that there is a trend for

Figure 4-1: Plot of points BO84 used to show the B-O effect. The fit is from BO84 as well.



⁹ Red-Ridge: The density ridge created by E and S0 galaxies in cluster color-magnitude diagrams.

Figure 4-2: Collection of published blue fractions from literature. Taken as a whole, f_B values appear almost randomly scattered. To understand the trend described in BO84, another parameter is necessary.



- Abraham, R.G. 1996, ApJ 471 694
- Allington, J.R., Ellis, R.S., Zirbel, E.L. and Oemler, A. 1993. ApJ 404, 521
- Butcher Oemler 1984 ApJ 285, 426
- Fairley, B.W. et al. 2002 MNRAS 330, 755
- Kodama, Tadayuki and Bower, R.G. MNRAS 321, 18
- Lubin, L.M. 1996 AJ 112, 23
- Margoniner, V.E. and R.R. de Carvalho 2000, AJ 119, 1562
- Metevier, A.J.; Romer, A.K. and Ulmer, M.P. 2000, AJ 119, 1090
- Oemler, A.; Dressler, A. and Butcher, H.R. 1997, ApJ 474, 561
- Rakos, K.D. and Schombert, J.M. 1995 439, 47

more clusters to have large blue fractions in the high z universe than there are locally (see Figure 4-2), it is unclear if there is an overall bluing of all clusters with redshift. In this chapter we will describe different techniques for measuring cluster blue fractions, we

will discuss the blue fractions of our four clusters, and we will consider a large sample of clusters taken from the literature that allow us to sample a large range in cluster redshifts and richnesses.

MEASUREMENTS

The original definition of a cluster's blue fraction came from BO84. They defined a cluster's blue fraction, f_B , using only those galaxies inside of R_{30} with $M_V > -20$. Galaxies were separated into blue and red using color diagrams.

Those galaxies 0.2 magnitudes or more blueward of the red-ridge were classified as blue. They defined the blue fraction as:

$$f_B = N_{\text{blue}} / N_{30}.$$

This technique has the advantage of measuring the same physical fraction of cluster galaxies regardless of cluster size or concentration and of measuring down to a similar population of faint galaxies at all redshifts. It has the disadvantage of being sensitive to fluctuations in the color of the red-ridge. The basic premise that the Butcher-Oemler effect blues clusters raises the concern that the red-ridge may not always reflect the exact same cluster morphology population. This blue galaxy definition also requires accurate K-corrections to rest frame for all galaxies.

The largest study of the B-O effect was done by Margoniner et al. (2001 – hereafter M01). They measured f_B for 295 Abell clusters with redshifts $z < 0.4$. They considered all the galaxies within 0.7 Mpc ($H_0 = 67 \text{ km s}^{-1} \text{ Mpc}$) of the cluster centers that had an R magnitude between $M^* - 1$ and $M^* + 2$. They defined their blue galaxies as galaxies with “(g-r) colors 0.2 magnitudes below the linear locus in the CM relation.” This technique has two disadvantages: M^{*10} is not a constant from cluster to cluster and a metric radius of 0.7 Mpc will not sample the same fraction of galaxies in clusters of varying size. This produces two possible problems. In clusters with a fainter M^* , f_B will be artificially high because more blue dwarf galaxies will be sampled. Also, smaller clusters will appear artificially bluer than larger clusters. This is because the cores of clusters

¹⁰ M^* was defined by Schechter (1976) as a characteristic absolute magnitude corresponding to the knee in the galaxy magnitude-number distribution. While the value varies from cluster to cluster, Schechter found that for a sample of 14 Abell clusters a value of $M_{B(0)} = -20.6$ is a good fit.

Table 4-1: f_B for TOC clusters

Field	f_B	err
TOC J 1602.8+4338	0.37	0.14
TOC J 1620.9+4442	0.22	0.09
TOC J 1626.1+4859	0.23	0.12
TOC J 1705.8+3657	0.14	0.09

are red and the field is blue, with the halos of clusters showing a radial color gradient. In large clusters, a metric radius will tend to sample less of the bluer halo and produce a low f_B . In smaller clusters, a metric radius will include more of the blue halo, and possibly even some of the blue field galaxy population, producing a high f_B . As a result, use of a metric radius will make f_B values appear to be a function of cluster richness/size. This was the finding of M01.

Several authors (Kodama et al 2001, Lubin 1996; Fairley et al. 2002) have taken a third approach. They use R_{30} , $M_V < -20$ and a color-cut between blue and red that is based on the expected colors of Sb/Sbc galaxies. This definition has all the advantages of BO84 and places a morphological definition on the division between blue and red galaxies.

In this work we have adopted this third approach. We use our R_{30} values to select galaxies within a uniform fraction of the clusters, and we use $M_V < -20$ and a color cut of $(B-R) = 1.09$ (Fujugita et al. 1995) to select out similar populations of galaxies. The blue fractions for our 4 clusters are given in Table 4-1 and figure 4-3.

THE LITERATURE

We have attempted to glean as large a sample of f_B and richness measurements from the literature as possible. Altogether, we collected information for 238 clusters. These data allow us to study f_B as a function of

Class	m	b	N	σ
R < 0	0.000	0.240	50	0.194
R = 0	0.413	0.018	38	0.105
R = 1	0.348	0.046	60	0.092
R = 2	0.197	0.086	40	0.086
R = 3	0.000	0.112	33	0.102
R = 4, 5	0.000	0.122	17	0.096
all	0.266	0.09	238	0.136

Table 4-2: Fitting parameters for $f_B = m z + b$. N is the number of clusters in each bin, and σ is the standard deviation about the least squares fit.

Abell type. What we find is that we can get a much cleaner fit to each separate Abell Richness then we can for the entire population (see Figure 4-4 and 4-5). More importantly, we find that for clusters with $R < 0$

(groups, and weak clusters), there is a large dispersion in blue fractions (0.194) and no obvious evolution. At the same time, rich clusters ($R = 4$ or 5) show only weak or no evolution, with consistently low f_B values across all redshifts (see Table 4-2). Clusters of intermediate richness show a trend from large evolution for $R = 0$ to low evolution for $R = 3$. In summary, small groups have wide-ranging blue fractions and show no evolution in blue fractions. Clusters with $R = 0$ show large evolution, and the amount of evolution decreases with increasing cluster richness until clusters reach a certain richness ($R \sim 4$) at which point clusters are red, and there is, again, no evolution of f_B . The relationship between cluster size and f_B trends can be looked at in terms of the clusters' velocity dispersions and the change in field galaxy infall rates with time.

As a starting point, let's review what the blue galaxies are. Detailed photometric studies of cluster blue galaxies identify them as primarily multiple or interacting systems and disturbed systems with signs of disruption, such as tidal tails and distorted morphologies (Lavery et al. 1992; Dressler 1994; Couch et al. 1994; Oemler et al. 1997; Conselice and Gallagher 1999), with even the

Figure 4-3: Comparison of our f_B value with those from the literature

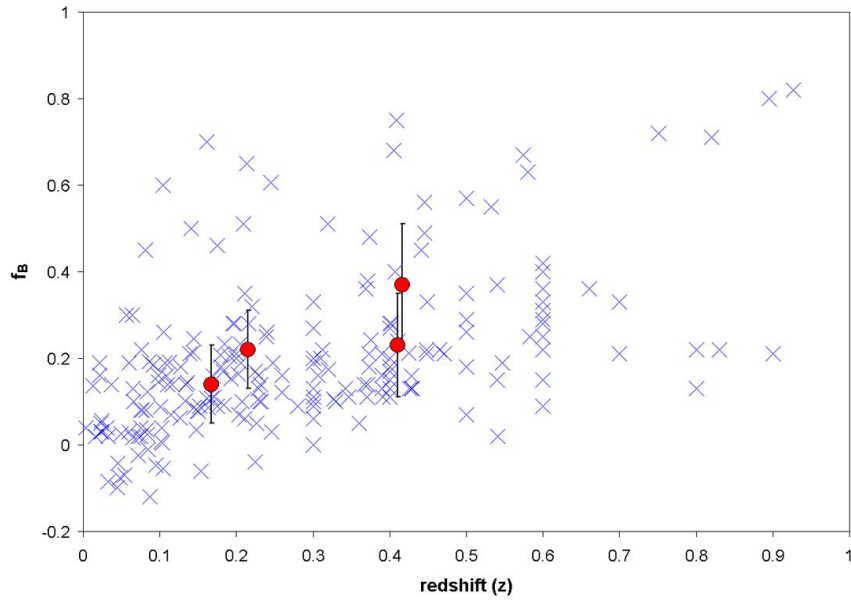


Figure 4-4: Trend of f_B with z for entire cluster data set.
Solid line is a least squares fit, and the dashed lines are $\pm \sigma$.

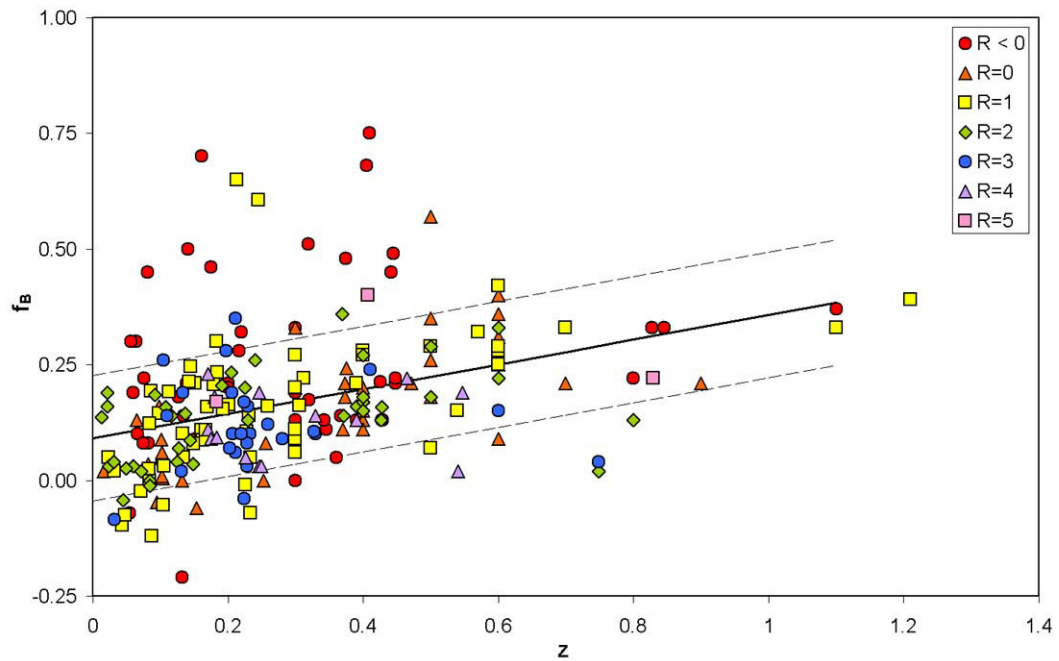


Figure 4-5: f_B trends for various Abell Richnesses.
Solid line is a least squares fit, and the dashed lines are $\pm\sigma$.

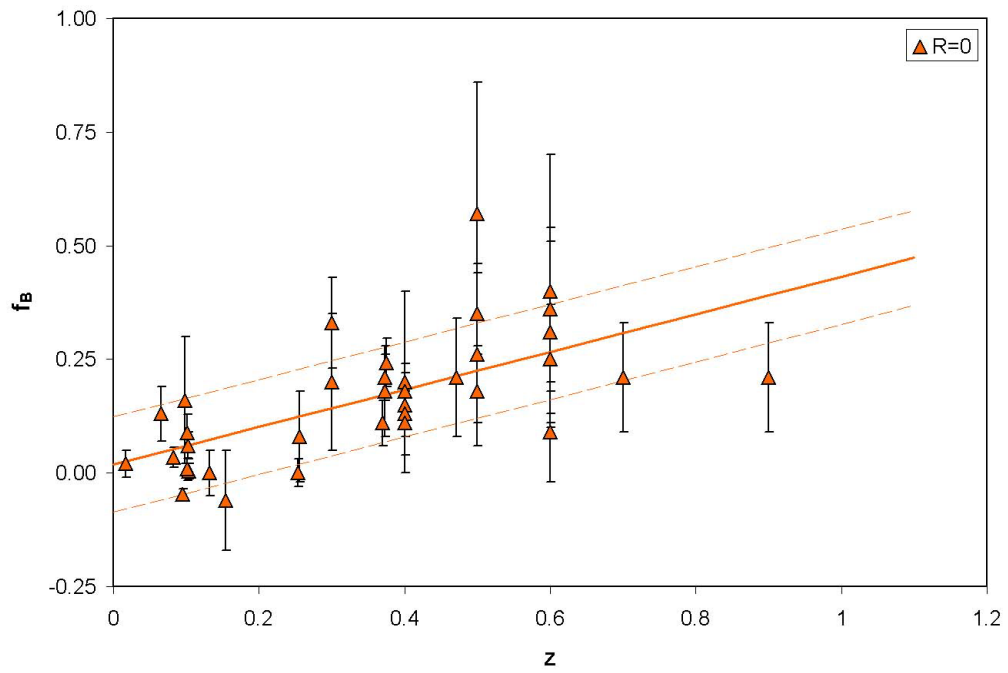
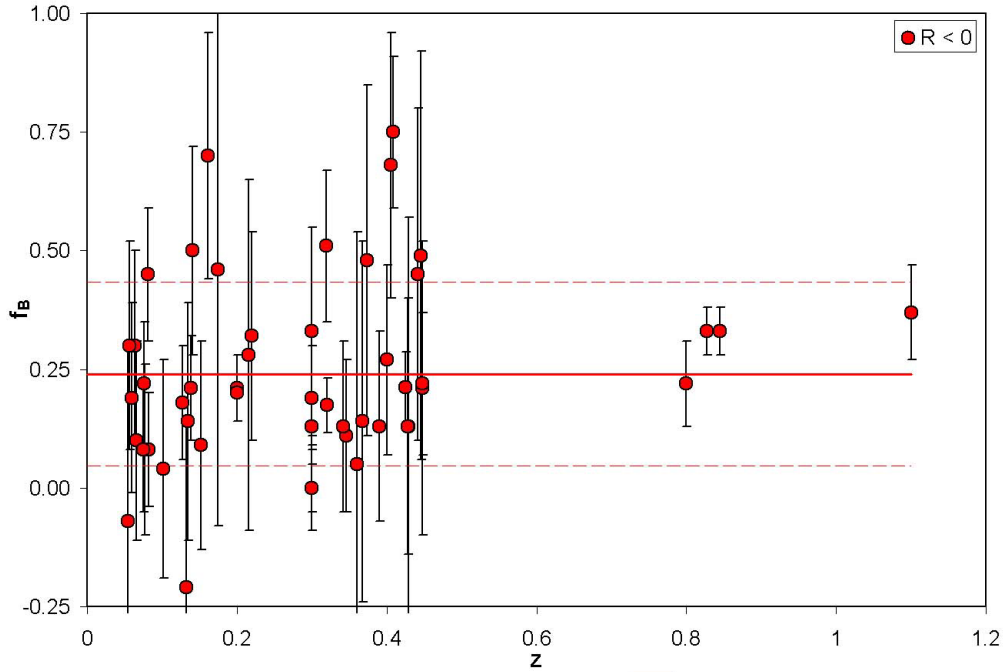


Figure 4-5 (continued...)

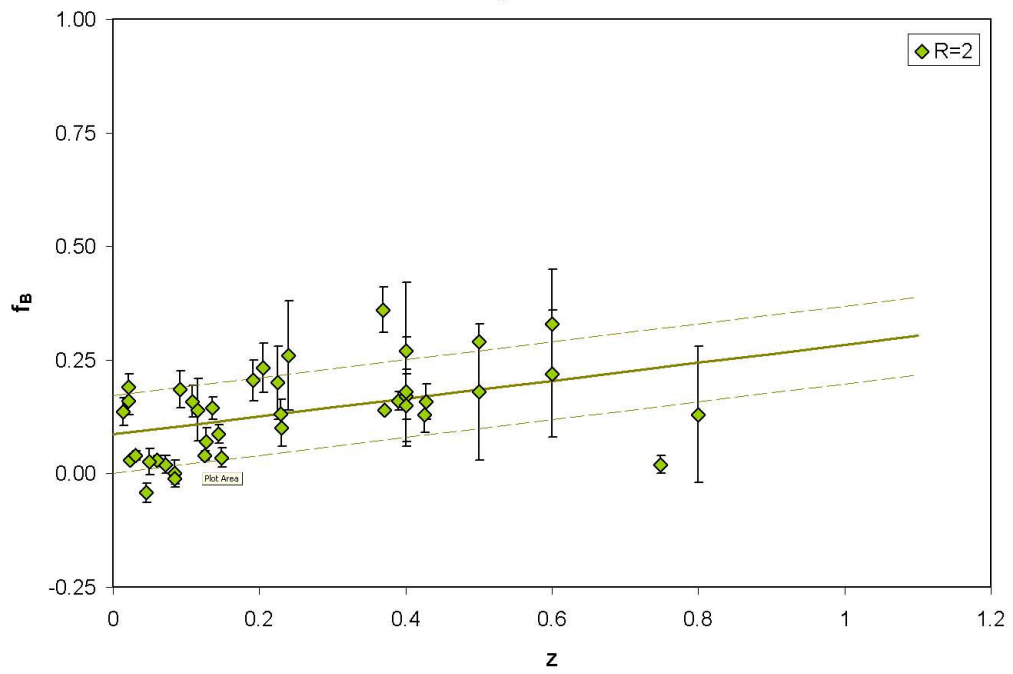
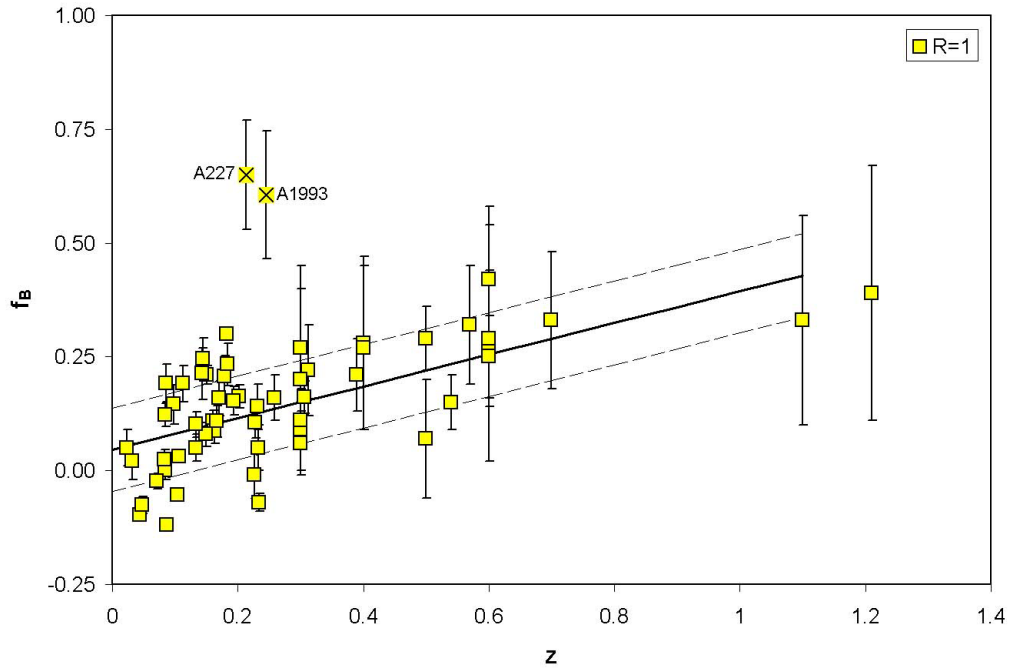
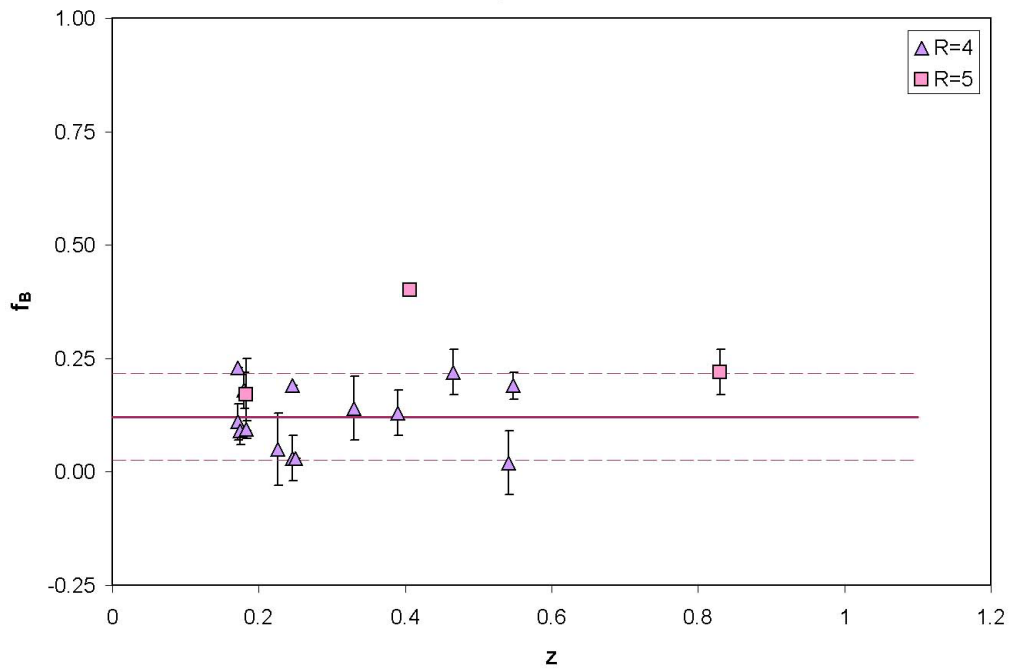
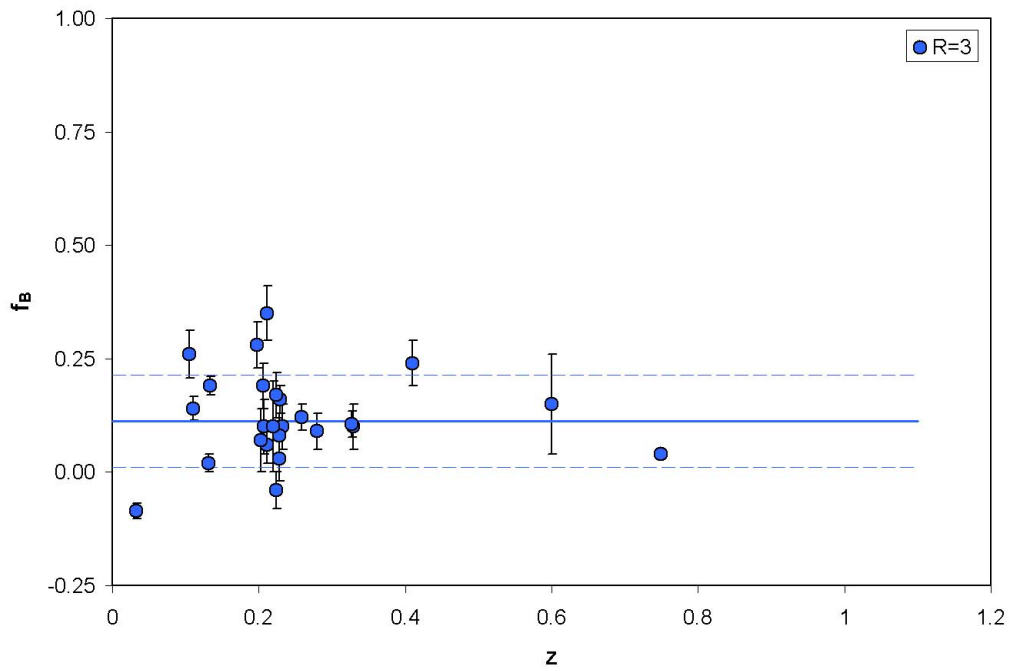


Figure 4-5 (continued...)



“normal” spirals showing unusual star formation patterns such as rings (Oemler et al. 1997). Spectroscopically, these systems are often starbursting or post-starburst galaxies and sometimes even AGNs (Caldwell and Rose 1997; Dressler et al. 1994, Dressler 1997). These galaxies are less centrally concentrated than red cluster galaxies and have a larger velocity dispersion (Carlberg et al. 1996, 1997; Ellington et al. 2001). The red galaxies have a factor of 1.3 smaller rms mean velocity. The CNOC team found that while the number of red galaxies peaks in cluster centers, the population of blue galaxies is negligible in the core and increases to the field value in the outer halo of the cluster. Overall, the number of blue galaxies should be mediated by the rate of field galaxy infall, which was higher in the past (Kaufmann 1995).

As a starting point, let’s review what the blue galaxies are. Detailed photometric studies of cluster blue galaxies identify them as primarily multiple or interacting systems and disturbed systems with signs of disruption, such as tidal tails and distorted morphologies (Lavery et al. 1992; Dressler 1994; Couch et al. 1994; Oemler et al. 1997; Conselice and Gallager 1999), with even the “normal” spirals showing unusual star formation patterns such as rings (Oemler et al. 1997). Spectroscopically, these systems are often starbursting or post-starburst galaxies and sometimes even AGNs (Caldwell and Rose 1997; Dressler et al. 1994, Dressler 1997). These galaxies are less centrally concentrated than red cluster galaxies and have a larger velocity dispersion (Carlberg et al. 1996, 1997; Ellington et al. 2001). The red galaxies have a factor of 1.3 smaller rms mean velocity. The CNOC team found that while the number of red galaxies peaks in

cluster centers, the population of blue galaxies is negligible in the core and increases to the field value in the outer halo of the cluster. Overall, the number of blue galaxies should be mediated by the rate of field galaxy infall, which was higher in the past (Kaufmann 1995).

This morphological and kinematical picture suggests an evolutionary history in which normal spiral galaxies from the field fall into a cluster potential well where they are shocked by the ICM and experience galaxy-galaxy interactions, ram pressure stripping, and galaxy harassment that trigger and truncate episodes of star formation. As the infalling galaxies virialize with the cluster, their starbursts fade and the galaxies redden. The extent to which these mechanisms disrupt an infalling galaxy will depend on the size of the cluster.

At the most simple level, large red clusters cannot have their blue fraction significantly raised by the infall of field galaxies. Ram-pressure stripping can effectively remove 100% of a galaxy's atomic hydrogen in just $10^7 - 10^8$ years, which is a fraction of the crossing time (Quilis, Moore, & Bower 2000, Abadi, Moore & Bower 1999). Given their limited lifetime as blue systems, infalling field galaxies can only create significant blue fractions in small clusters.

The extent to which galaxy-galaxy interactions, ram pressure stripping, and galaxy harassment disrupt an infalling galaxy will depend on the size of the cluster. Low-velocity galaxy-galaxy interactions can trigger the formation of ring galaxies (Icke 1985; Lavery & Henry 1988). These collisions can only be successful in low-velocity-dispersion systems (eg, groups) or in the outermost parts of clusters where the velocity dispersion is low. Similarly, Carlberg et al.

(2001) show that in clusters with high velocity dispersions, where the line of sight velocity dispersion, σ_1 , is $> 150 \text{ km s}^{-1}$, galaxy merger rates are very low, “whereas for $\sigma_1 < 150 \text{ km s}^{-1}$ about 25% of the galaxies will merge in 0.5 Gyr.” They conclude “higher velocity dispersion groups largely act to suppress star formation relative to the less clustered field, leading to ‘embalmed’ galaxies.” This describes a scenario where the ability of galaxy mergers and interactions to trigger star formation decreases with increased cluster size.

The cluster potential well depth can also have a damping effect on star formation. Interactions with the cluster gravitational potential cause tidal triggering of star formation as an infalling galaxy collapses (Gunn & Gott 1972; Dressler & Gunn 1983; Henriksen and Byrd 1996; Abadi et al. 1999). This star formation is then truncated by ram pressure stripping by the cluster’s diffuse gas (Fukita & Nagashima 1999; Abadi et al 1999). Models by Henriksen & Byrd (1996) demonstrate that low-density intracluster gas is more effective at tidally triggering star formation than high-density intracluster gas similar to that seen in local high-mass X-Ray-luminous clusters. At the same time, high-mass systems are more efficient at truncating star formation than lower-mass systems (Abadi et al. 1999). This implies that high-mass clusters will have less tidally triggered star formation and ram-pressure stripping will be more effective at turning off this star formation.

These two facets – high velocity dispersions limiting galaxy interactions and high central potentials limiting star formation – may accentuate the trend we see in the B-O effect varying with cluster richness. For $R = 1-3$, star formation is

triggered at a rate that varies with redshift. This variation with redshift can be explained by the decrease in infall rate with lower redshift (Kaufmann 1995; Nelson et al. 2001; Fairley et al. 2002). At a certain size, around $R = 4$, the cluster's velocity dispersion and ICM collude to prevent the triggering of star formation and remove any gas that may be fueling star formation in infalling galaxies.

We cannot explain the f_B of groups, $R < 0$, with this scenerio. We would propose that in groups, the ICM is simply not rich enough to trigger star formation and that the number of galaxies is sufficiently low that galaxy – galaxy interactions do not play a major roll either. As the groups get smaller and smaller, their velocity dispersions will approach that of galaxy pairs in the field (Carlberg et al. 2001) and the group characteristics will become those of field galaxies. The lower boundary for the B-O effect cannot be defined; however, the large dispersion and lack of f_B enhancement with redshift in our $R < 0$ data indicates that at $N_{Abell} < 30$ the B-O effect disappears.

SUMMARY

The Butcher-Oemler effect is an enigmatic observable. Our literature survey of 238 clusters with published redshifts, a richness and f_B value demonstrates that there is an overall trend for higher redshift clusters to have a higher f_B then lower redshift systems. Our 4 TOC clusters follow this trend and are perfectly normal systems.

In comparing the f_B trends for clusters as a function of cluster richness, we have determined that groups ($R < 0$) show no definitive B-O effect and in general

have a large f_B . We propose that the evolution of galaxies in groups more closely resembles the evolution of field galaxies than that of cluster galaxies. Very rich clusters ($R = 4, 5$) also show no f_B trend with redshift and have a consistently low f_B . Clusters with intermediate redshifts show the B-O effect, with lower richness clusters having a steeper increase in f_B with redshift than higher redshift clusters.

We believe that in clusters, the observed dependence of the B-O effect on both redshift and cluster richness is a reflection of field galaxy infall rates changing with redshift and the ability of the cluster environment to trigger and/or suppress star formation, as well as the cluster's size. A rich red cluster can only minimally be blue enhanced by field galaxy infall. Additionally, the primary mechanisms for triggering star formation – interactions, and tidal effects – work most effectively in systems with a low velocity dispersions and a diffuse ICM; e.g. in lower richness clusters. Ram pressure stripping, which truncates star formation, is most effective in high mass systems. Thus, star formation is most likely to be triggered and last in lower richness clusters, while in high richness clusters, what star formation is able to occur is quickly extinguished. The change in f_B for clusters of similar richnesses at different epochs is explained by the change in field galaxy infall rates with time.

Chapter 5: A Few Brief Words in Closing

Throughout this dissertation, we have described a new technique for finding galaxy clusters, discussed the physical attributes of a small sample of clusters found with this technique, and endeavored to compare our clusters to large samples taken from the literature.

Our ability to say anything with authority is limited by the paucity of our data. Our technique of searching for clusters around radio overdensities is not unreasonable. By looking for clusters in the vicinity of overdensities with 5 radio sources in a 6-arcmin \times 6-arcmin box we find a lower limit success rate of 20% and project a success rate of 35% - 45% percent. The clusters that we found near our radio overdensities were primarily at low redshifts, and it is unclear, due to lack of spectra, if our radio sources are physically associated with the clusters that they are near. Based on our detailed study of 4 clusters found by our technique, we believe that each cluster is associated with an average of only 2 radio sources. At this time, we cannot recommend our technique as being significantly more effective than looking for clusters around individual radio sources.

The four clusters associated with radio overdensities that we studied in detail were in no way unusual. They are low-richness systems with normal BCG magnitudes, typical blue galaxy fractions and no unusual radio properties that we can demonstrate with certainty. We can say that our technique finds low- to moderate-redshift clusters without showing bias towards high mass systems. One concern that we do have is that 1 of our 4 systems was a superposition of clusters,

and our technique may be prone to finding such superpositions. With such a small sample, we have no way of validating this concern.

While comparing our 4 systems to samples from the literature, we stumbled on two trends that are worth emphasis: (1) the radio source R-z relation breaks down with decreasing $S_{1.5}$ values and (2) the B-O effect appears to be a function of both redshift and cluster richness.

The radio source trends (see figures 3-5, 3-6, 3-7, 3-8) show that the brightest radio sources in the sky, as drawn from the 3CR and 6C catalogues, have a different relationship between redshift and R magnitude than their lower flux sources. The lower power ($S_{1.5} < 200$ mJy) sources drawn from the NVSS catalogue show increased scatter in their R-z relationship with decreasing flux (see table 3-3), and the high resolution high sensitivity FIRST catalogue shows only a modest R-z relationship. As a result of these findings, we feel that only sources with $S_{1.5} \geq 10$ mJy can be used with any reliability to constrain the redshift of a radio-optical source.

The observed dependence of the B-O effect on both redshift and cluster richness is a reflection of field-galaxy infall rates and the ability of the cluster environment to trigger and/or suppress star formation. To first order, infalling field galaxies can only significantly affect the blue fraction of small to moderate sized clusters. Cluster dynamics also work to suppress star formation in large clusters, while supporting it in small ones. The primary mechanisms for triggering star formation – interactions and tidal effects – work most effectively in systems with a low velocity dispersions and a diffuse ICM; e.g. in lower richness

clusters. Ram-pressure stripping, which truncates star formation, is most effective in high mass systems. Thus, star formation is most likely to be triggered and to last in lower richness clusters, while in high richness clusters, what star formation can occur is extinguished quickly. Galaxy groups do not follow this trend and may have too low a velocity dispersion and/or too little ICM for their member galaxies' evolution to significantly differ from field galaxy evolution.

This work, like most scientific studies, leaves us longing for a larger, internally consistent data set. Further study into the success of finding clusters around radio source overdensities is probably not justified, but it would be interesting to examine the distribution of radio sources (radio power, optical magnitude, morphology and number) in clusters at different redshifts in more detail. The 2dFGRS and Las Campanas Redshift Survey will be ideal for this. Such a study would help to identify ways to use existing radio surveys to best find new clusters, as well as identify how to tie the radio sources to the clusters without spectra.

What is also needed is a consistent effort by observers to measure cluster richnesses, velocity distributions, and blue fractions. Cluster richnesses are measured using Abell's definition, using N_{20} and by using the inner 0.5 Mpc region. No formula exists to allow one to jump between these three richness criteria. N_{30} measurements, in fact, were found to range from less than one-third to the same as N_{Abell} . Similarly, techniques for measuring f_B ranged from that defined by BO84's paper, to measurements that utilized a region defined by a telescope's field of view and galaxies with spectroscopically confirmed

memberships that were limited in number by observing constraints. In order to tightly define the B-O effect as a function of redshift and cluster size, accurate measurements are needed. These measurements should become easier as large-area surveys begin to probe the high- z universe.

Our suggestions for future study point to the necessity of large surveys. The works that we have utilized the most – the CNOC survey, the Las Campanas Redshift Survey, and the 2dFGRS – are all large collaborations that significantly draw upon the resources of major facilities. The world of extra-galactic astronomy is quickly becoming one in which it is difficult for small collaborations without dedicated observing time to remain observationally competitive. This observer would suggest that perhaps more is to be found in mining the data of the larger groups, than by trying to compete with lesser resources. In many cases, these large surveys find interesting objects that are worthy of detailed follow-up observations, and these observations are likely to yield fruitful discoveries with less observational overhead.

And as a final word to the wise: don't try and observe during monsoon season, no matter how promising your objects may seem.



Appendix 1: Region 1

$16:00:00 \leq \text{RA} \leq 17:00:00, 35:00:00 \leq \text{DEC} \leq 50:00:00$

Total Area: 164.7 square degrees

Figure A1-1: Map of Region 1. All known clusters are listed in table A1-2.

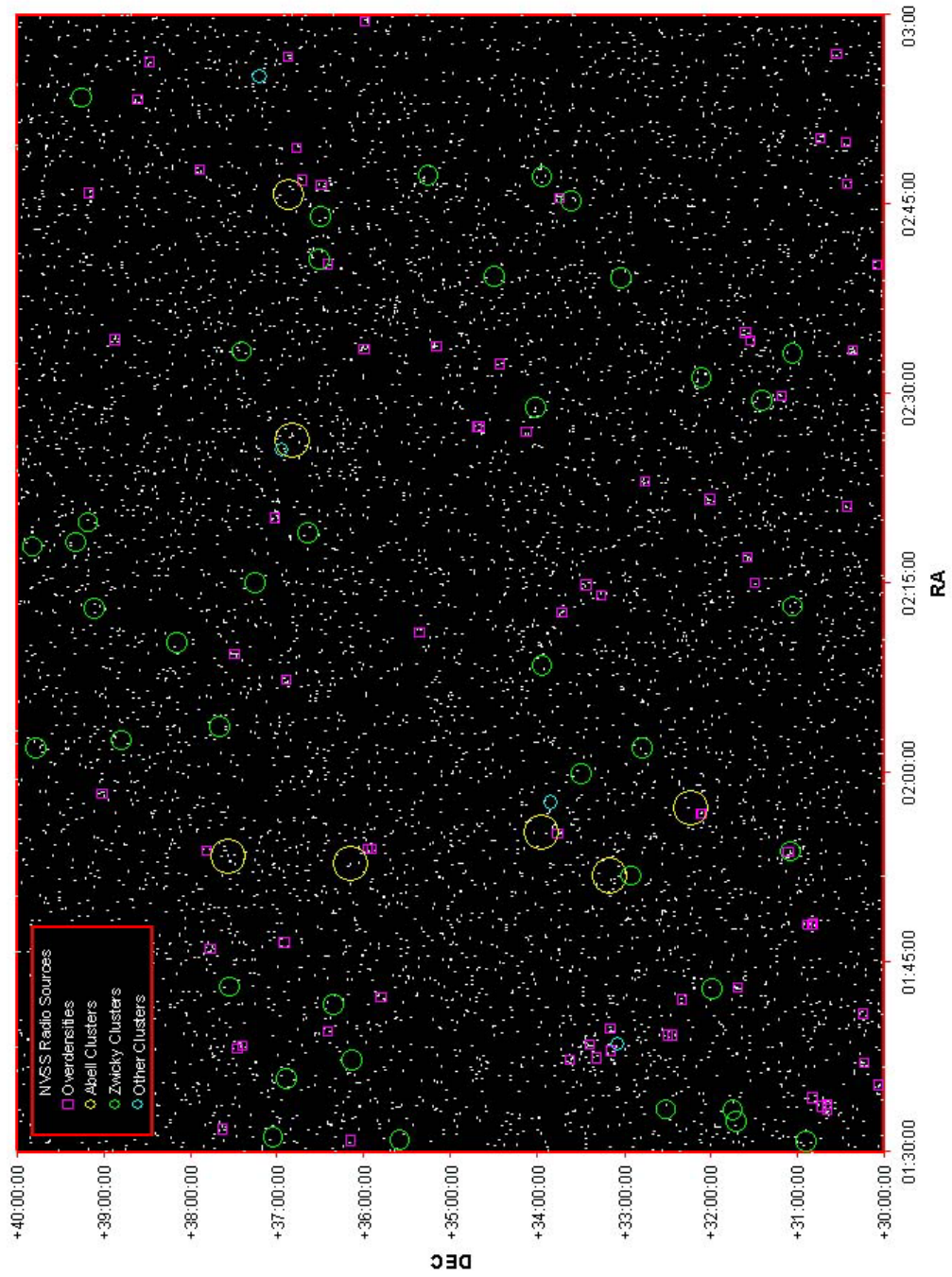


Table A1-1: Complete list of Region 1 overdensities

Name	NVSS Sources	NVSS RA	NVSS DEC	S _{1.5} (mJy)	Data Filt.	Exp
TOCC 0130.9 +3609 Candidate	5	1: 01:30:45	+12:09:14	9.7	B	0
		2: 01:30:46	+12:07:53	30.8	R	1800
		3: 01:30:52	+12:11:31	16.9	I	1800
		4: 01:30:54	+12:05:39	37.7		
		5: 01:31:03	+12:11:27	3.5		
TOCC 0131.4 +4007	6	1: 01:31:12	+16:06:23	4.4		
		2: 01:31:14	+16:08:08	12.3		
		3: 01:31:18	+16:06:04	7.1		
		4: 01:31:27	+16:05:00	2.6		
		5: 01:31:35	+16:07:16	3		
		6: 01:31:37	+16:06:09	26.2		
TOCC 0131.9 +3737	5	1: 01:31:37	+13:34:37	26.5		
		2: 01:31:45	+13:39:41	3.5		
		3: 01:31:52	+13:35:53	3.7		
		4: 01:32:05	+13:35:21	3.6		
		5: 01:32:06	+13:37:06	14.4		
TOCC 0133.4 +3039	6	1: 01:33:10	+06:39:27	3.9		
		2: 01:33:13	+06:38:45	3.9		
		3: 01:33:29	+06:40:27	6		
		4: 01:33:34	+06:41:34	25.8		
		5: 01:33:36	+06:36:29	3.7		
		6: 01:33:37	+06:39:38	3.5		
TOCC 0133.6 +3043	5	1: 01:33:29	+06:40:27	3.9		
		2: 01:33:29	+06:45:38	8.6		
		3: 01:33:34	+06:41:34	25.8		
		4: 01:33:37	+06:39:38	3.5		
		5: 01:33:44	+06:44:38	3.1		
TOCC 0133.8 +3039	6	1: 01:33:34	+06:41:34	3.9		
		2: 01:33:36	+06:36:29	12.4		
		3: 01:33:37	+06:39:38	3.9		
		4: 01:33:51	+06:39:34	3.7		
		5: 01:34:00	+06:40:44	3.4		
		6: 01:34:02	+06:38:29	3.5		

Table A1-1 (continued)

Name	NVSS Sources	NVSS RA	NVSS DEC	S _{1.5} (mJy)	Data Filt.	Exp
TOCC 0134.3 +3049	5	1: 01:34:05	+06:47:17	8.6		
		2: 01:34:13	+06:48:27	2.3		
		3: 01:34:16	+06:51:57	6.1		
		4: 01:34:30	+06:50:43	5.9		
		5: 01:34:33	+06:47:01	71.2		
TOCC 0135.3 +3004	5	1: 01:35:04	+06:04:36	9		
		2: 01:35:11	+06:03:58	5.6		
		3: 01:35:15	+06:05:48	4.2		
		4: 01:35:21	+06:02:07	5.1		
		5: 01:35:30	+06:03:47	32		
TOCC 0137.0 +3013	5	1: 01:36:54	+06:14:32	27.8		
		2: 01:36:55	+06:11:45	27.8		
		3: 01:37:04	+06:14:01	6.2		
		4: 01:37:05	+06:12:24	3.4		
		5: 01:37:07	+06:14:53	10.8		
TOCC 0137.3 +3338 Candidate	6	1: 01:37:09	+09:36:49	4.9	B	0
		2: 01:37:14	+09:38:43	3.2	R	1800
		3: 01:37:23	+09:35:50	8.8	I	0
		4: 01:37:23	+09:39:58	3.2		
		5: 01:37:28	+09:35:25	2.6		
		6: 01:37:29	+09:39:59	37.3		
TOCC 0137.4 +3319 Cluster	5	1: 01:37:17	+09:18:19	8.3	B	0
		2: 01:37:29	+09:21:11	3.5	R	4950
		3: 01:37:33	+09:20:27	3.7	I	2700
		4: 01:37:35	+09:15:53	4.2		
		5: 01:37:36	+09:18:02	4.7		
TOCC 0138.1 +3309	6	1: 01:37:49	+09:10:23	3.3		
		2: 01:37:55	+09:07:50	3.3		
		3: 01:37:59	+09:05:42	3.3		
		4: 01:38:04	+09:07:17	3		
		5: 01:38:10	+09:11:28	28.1		
		6: 01:38:17	+09:10:29	3		

Table A1-1 (continued)

Name	NVSS Sources	NVSS RA	NVSS DEC	S _{1.5} (mJy)	Data Filt.	Exp
TOCC 0138.2 +3727	5	1: 01:37:58	+13:28:51	7.3		
		2: 01:38:15	+13:29:42	7.3		
		3: 01:38:16	+13:23:57	142.2		
		4: 01:38:18	+13:27:47	4.8		
		5: 01:38:25	+13:24:44	7		
TOCC 0138.5 +3323	5	1: 01:38:25	+09:25:37	3.3	B	0
		2: 01:38:26	+09:22:35	5.7	R	4650
		3: 01:38:26	+09:24:14	3.7	I	2700
		4: 01:38:27	+09:20:54	5.7		
		5: 01:38:39	+09:25:57	4.6		
TOCC 0138.5 +3723	5	1: 01:38:16	+13:23:57	142.2	B	0
		2: 01:38:24	+13:21:24	142.2	R	900
		3: 01:38:25	+13:24:44	7	I	0
		4: 01:38:41	+13:24:40	37.2		
		5: 01:38:44	+13:25:20	28.6		
TOCC 0139.3 +3229	5	1: 01:39:09	+08:28:49	3.1		
		2: 01:39:09	+08:26:42	10.3		
		3: 01:39:13	+08:31:39	2.7		
		4: 01:39:14	+08:26:26	14.7		
		5: 01:39:31	+08:28:39	25.7		
TOCC 0139.3 +3226 Candidate	5	1: 01:39:09	+08:28:49	3.1	B	0
		2: 01:39:09	+08:26:42	3.8	R	900
		3: 01:39:14	+08:26:26	14.7	I	0
		4: 01:39:19	+08:24:04	3.6		
		5: 01:39:31	+08:28:39	25.7		
TOCC 0139.5 +3625	5	1: 01:39:17	+12:23:58	6.1		
		2: 01:39:28	+12:22:02	6.1		
		3: 01:39:32	+12:23:04	5.8		
		4: 01:39:40	+12:27:27	31.1		
		5: 01:39:46	+12:27:02	4.3		

Table A1-1 (continued)

Name	NVSS Sources	NVSS RA	NVSS DEC	S _{1.5} (mJy)	Data Filt.	Exp
TOCC 0139.8 +3309	5	1: 01:39:33	+09:11:11	6.2		
		2: 01:39:35	+09:07:01	6.2		
		3: 01:39:35	+09:08:07	6.2		
		4: 01:39:37	+09:09:13	4.2		
		5: 01:39:59	+09:09:16	3.8		
TOCC 0141.0 +3015	5	1: 01:40:46	+06:12:40	3.8	B	0
		2: 01:40:51	+06:11:50	3.8	R	1800
		3: 01:40:56	+06:16:03	3.1	I	0
		4: 01:41:03	+06:17:11	3.3		
		5: 01:41:08	+06:14:46	2.3		
TOCC 0142.1 +3219	5	1: 01:41:52	+08:20:13	9.9	B	0
		2: 01:41:53	+08:22:06	9.9	R	1800
		3: 01:42:13	+08:20:09	5.2	I	0
		4: 01:42:20	+08:18:42	9.3		
		5: 01:42:20	+08:16:40	4.6		
TOCC 0142.3 +3548	5	1: 01:42:09	+11:44:49	4.8		
		2: 01:42:11	+11:45:40	4.8		
		3: 01:42:14	+11:46:39	6.8		
		4: 01:42:27	+11:49:30	2.9		
		5: 01:42:27	+11:50:44	4.1		
TOCC 0143.0 +3140	5	1: 01:42:56	+07:39:14	97.9		
		2: 01:42:58	+07:41:40	2.7		
		3: 01:43:03	+07:37:53	115.2		
		4: 01:43:05	+07:42:56	16.2		
		5: 01:43:05	+07:41:33	4.1		
TOCC 0146.1 +3746	5	1: 01:45:55	+13:46:59	3.2	B	0
		2: 01:45:58	+13:45:01	3.8	R	1800
		3: 01:46:09	+13:43:18	6.5	I	0
		4: 01:46:16	+13:44:18	10.4		
		5: 01:46:16	+13:49:05	25.5		

Table A1-1 (continued)

Name	NVSS Sources	NVSS RA	NVSS DEC	S _{1.5} (mJy)	Data Filt.	Exp
TOCC 0146.6 +3654	5	1: 01:46:18	+12:52:30	3.8		
		2: 01:46:19	+12:51:29	3.8		
		3: 01:46:22	+12:56:51	3.8		
		4: 01:46:26	+12:52:18	2.9		
		5: 01:46:48	+12:52:18	7.2		
TOCC 0148.0 +3050	5	1: 01:47:53	+06:50:42	4.1		
		2: 01:47:55	+06:48:00	5.2		
		3: 01:47:59	+06:47:12	8		
		4: 01:48:00	+06:53:08	4.7		
		5: 01:48:05	+06:50:53	3		
TOCC 0148.1 +3048 Candidate	6	1: 01:47:53	+06:50:42	4.1	B	0
		2: 01:47:54	+06:47:07	6.3	R	900
		3: 01:47:55	+06:48:00	5.2	I	0
		4: 01:47:59	+06:47:12	8		
		5: 01:48:05	+06:50:53	3		
		6: 01:48:15	+06:45:37	3.6		
TOCC 0148.0 +3053	5	1: 01:47:53	+06:50:42	4.1		
		2: 01:48:00	+06:53:08	4.7		
		3: 01:48:00	+06:54:51	7.5		
		4: 01:48:05	+06:50:53	3		
		5: 01:48:08	+06:55:20	5.4		
TOCC 0153.7 +4034	5	1: 01:53:25	+16:31:38	70.9		
		2: 01:53:28	+16:35:52	13.2		
		3: 01:53:31	+16:32:55	68.9		
		4: 01:53:42	+16:33:03	103.1		
		5: 01:53:54	+16:36:57	13.8		
TOCC 0153.7 +3106	5	1: 01:53:32	+07:06:14	11.2		
		2: 01:53:39	+07:03:54	11.9		
		3: 01:53:41	+07:07:35	18.8		
		4: 01:53:48	+07:04:39	7.5		
		5: 01:53:53	+07:05:30	3.6		

Table A1-1 (continued)

Name	NVSS Sources	NVSS RA	NVSS DEC	S _{1.5} (mJy)	Data Filt.	Exp	
TOCC 0154.0+3554	5	1:	01:53:46	+11:55:38	3.7		
		2:	01:53:52	+11:55:50	3.4		
		3:	01:53:53	+11:51:27	3		
		4:	01:54:02	+11:57:00	3.5		
		5:	01:54:12	+11:54:57	2.9		
TOCC 0153.9+3748	5	1:	01:53:40	+13:47:57	15.2		
		2:	01:53:57	+13:46:00	4.2		
		3:	01:53:59	+13:50:07	24.7		
		4:	01:54:00	+13:47:25	6.7		
		5:	01:54:03	+13:50:46	32.7		
TOCC 0153.8+4035	5	1:	01:53:42	+16:33:03	70.9		
		2:	01:53:52	+16:32:20	70.9		
		3:	01:53:54	+16:36:57	70.9		
		4:	01:53:55	+16:37:59	70.9		
		5:	01:54:00	+16:35:19	26.8		
TOCC 0154.0+3557	6	1:	01:53:46	+11:55:38	3.7	B	0
		2:	01:53:49	+11:59:35	3.7	R	1800
		3:	01:53:52	+11:55:50	3.7	I	0
		4:	01:54:02	+11:57:00	3.5		
		5:	01:54:12	+11:54:57	2.9		
		6:	01:54:13	+11:58:09	4.2		
TOCC 0155.2+3345	5	1:	01:55:07	+09:47:06	15.7	B	0
		2:	01:55:09	+09:44:04	2.8	R	1800
		3:	01:55:10	+09:46:32	19.5	I	0
		4:	01:55:18	+09:43:19	30.6		
		5:	01:55:20	+09:44:54	15.9		
TOCC 0156.8+3205	5	1:	01:56:41	+08:04:34	7.3		
		2:	01:56:43	+08:04:35	21.1		
		3:	01:56:44	+08:04:36	12.3		
		4:	01:56:46	+08:06:13	12.7		
		5:	01:56:51	+08:05:29	23.6		

Table A1-1 (continued)

Name	NVSS Sources	NVSS RA	NVSS DEC	S _{1.5} (mJy)	Data Filt.	Exp
TOCC 0156.8 +3207	6	1: 01:56:41	+08:04:34	7.3		
		2: 01:56:43	+08:04:35	7.3		
		3: 01:56:44	+08:04:36	7.3		
		4: 01:56:46	+08:06:13	12.7		
		5: 01:56:51	+08:05:29	23.6		
		6: 01:56:53	+08:09:40	63.1		
TOCC 0158.4 +3901	5	1: 01:58:12	+14:58:49	12.8		
		2: 01:58:20	+15:02:24	4.4		
		3: 01:58:32	+14:59:41	37		
		4: 01:58:34	+15:00:51	6.4		
		5: 01:58:36	+15:01:56	5.4		
TOCC 0200.1 +4051	5	1: 01:59:58	+16:50:38	25.7		
		2: 01:59:59	+16:52:58	10.2		
		3: 02:00:05	+16:51:28	49.7		
		4: 02:00:07	+16:49:11	51.6		
		5: 02:00:12	+16:50:18	52.9		
TOCC 0201.2 +4048	5	1: 02:00:54	+16:47:28	11.9		
		2: 02:00:55	+16:45:42	11.9		
		3: 02:01:17	+16:48:08	3.3		
		4: 02:01:20	+16:50:14	11.8		
		5: 02:01:26	+16:48:48	7		
TOCC 0207.4 +3653	5	1: 02:07:11	+12:53:25	64.4	B	0
		2: 02:07:15	+12:52:23	7	R	1800
		3: 02:07:23	+12:55:16	17.2	I	0
		4: 02:07:28	+12:54:26	22.2		
		5: 02:07:33	+12:50:21	9.1		
TOCC 0209.4 +3729	6	1: 02:09:14	+13:27:59	20.2	B	0
		2: 02:09:22	+13:29:07	3	R	4950
		3: 02:09:22	+13:31:26	7.3	I	4500
		4: 02:09:29	+13:26:50	2.6		
		5: 02:09:30	+13:31:06	30.9		
		6: 02:09:30	+13:29:56	31		

Table A1-1 (continued)

Name	NVSS Sources	NVSS RA	NVSS DEC	S _{1.5} (mJy)	Data Filt.	Exp
TOCC 0211.2 +3521	5	1: 02:10:55	+11:22:20	18.7		
		2: 02:11:12	+11:22:12	7.5		
		3: 02:11:16	+11:19:00	3.5		
		4: 02:11:22	+11:20:17	4.1		
		5: 02:11:23	+11:22:26	8.1		
TOCC 0212.7 +3342	5	1: 02:12:34	+09:43:37	5.2	B	0
		2: 02:12:41	+09:42:28	9.4	R	900
		3: 02:12:47	+09:43:52	3.5	I	0
		4: 02:12:49	+09:40:39	7.2		
		5: 02:12:55	+09:41:38	35.2		
TOCC 0214.0 +3316	5	1: 02:13:50	+09:17:33	4.4		
		2: 02:13:56	+09:13:06	8.4		
		3: 02:13:58	+09:15:46	2.3		
		4: 02:14:08	+09:18:54	23.8		
		5: 02:14:14	+09:15:34	14.5		
TOCC 0214.9 +3326	5	1: 02:14:38	+09:28:23	15.7		
		2: 02:14:49	+09:26:52	7.9		
		3: 02:14:59	+09:28:03	14.6		
		4: 02:15:02	+09:23:31	3.8		
		5: 02:15:05	+09:26:40	3.9		
TOCC 0215.0 +3129	5	1: 02:14:50	+07:28:23	7.9		
		2: 02:14:57	+07:28:18	14.9		
		3: 02:15:00	+07:27:19	11.7		
		4: 02:15:03	+07:26:21	5.8		
		5: 02:15:13	+07:31:50	11.1		
TOCC 0217.1 +3134	5	1: 02:16:58	+07:34:23	42.4	B	0
		2: 02:16:58	+07:31:59	23.6	R	1800
		3: 02:17:07	+07:34:48	3.9	I	1800
		4: 02:17:07	+07:33:23	8.9		
		5: 02:17:19	+07:35:57	2.9		

Table A1-1 (continued)

Name	NVSS Sources	NVSS RA	NVSS DEC	S _{1.5} (mJy)	Data Filt.	Exp
TOCC 0220.2 +3701	5	1: 02:19:59	+12:59:12	43.5		
		2: 02:20:05	+13:03:13	15.9		
		3: 02:20:09	+13:02:15	11.2		
		4: 02:20:10	+12:58:49	368.6		
		5: 02:20:23	+12:59:40	102.1		
TOCC 0221.1 +3025	5	1: 02:20:54	+06:22:20	3.2	B	0
		2: 02:21:06	+06:25:23	26.1	R	900
		3: 02:21:08	+06:26:19	47.9	I	0
		4: 02:21:15	+06:26:47	23.2		
		5: 02:21:16	+06:28:17	6.2		
TOCC 0221.7 +3200	5	1: 02:21:28	+08:01:17	4.1	B	0
		2: 02:21:32	+07:57:10	4.1	R	1200
		3: 02:21:36	+08:00:12	28.8	I	0
		4: 02:21:41	+08:01:37	7.7		
		5: 02:21:51	+08:03:02	13.2		
TOCC 0223.1 +3245	5	1: 02:22:55	+08:45:37	59		
		2: 02:23:02	+08:45:34	3.4		
		3: 02:23:03	+08:42:47	15.2		
		4: 02:23:04	+08:47:05	4.1		
		5: 02:23:16	+08:46:07	10.2		
TOCC 0223.0 +4004	5	1: 02:22:48	+16:01:21	2.9		
		2: 02:22:51	+16:07:12	3		
		3: 02:22:56	+16:06:13	3		
		4: 02:22:58	+16:04:22	7.9		
		5: 02:23:13	+16:01:58	8.1		
TOCC 0223.9 +4044	6	1: 02:23:35	+16:45:44	3.1		
		2: 02:23:37	+16:42:03	3.1		
		3: 02:23:53	+16:45:28	17.3		
		4: 02:23:54	+16:41:17	2.9		
		5: 02:23:57	+16:44:06	3.2		
		6: 02:24:07	+16:43:16	3.9		

Table A1-1 (continued)

Name	NVSS Sources	NVSS RA	NVSS DEC	S _{1.5} (mJy)	Data Filt.	Exp
TOCC 0227.0 +3407	5	1: 02:26:48	+10:05:57	3.4		
		2: 02:26:49	+10:07:41	3.4		
		3: 02:26:55	+10:04:56	118.4		
		4: 02:27:07	+10:08:47	2.3		
		5: 02:27:10	+10:08:08	4.4		
TOCC 0227.4 +3440	5	1: 02:27:11	+10:39:39	7.6	B	0
		2: 02:27:21	+10:38:13	5	R	2100
		3: 02:27:28	+10:42:41	3	I	0
		4: 02:27:30	+10:36:56	3.9		
		5: 02:27:37	+10:39:25	8.2		
TOCC 0227.4 +3441	5	1: 02:27:11	+10:39:39	7.6		
		2: 02:27:16	+10:43:46	7.6		
		3: 02:27:21	+10:38:13	7.6		
		4: 02:27:28	+10:42:41	3		
		5: 02:27:37	+10:39:25	8.2		
TOCC 0229.8 +3111 Cluster	5	1: 02:29:35	+07:08:02	4.6	B	0
		2: 02:29:46	+07:09:23	7.5	R	900
		3: 02:29:47	+07:13:08	2.3	I	900
		4: 02:29:49	+07:11:18	11.9		
		5: 02:30:00	+07:11:41	20		
TOCC 0232.4 +3425 Cluster	5	1: 02:32:13	+10:25:33	8.1	B	0
		2: 02:32:16	+10:26:58	12.3	R	900
		3: 02:32:29	+10:24:06	2601.1	I	6600
		4: 02:32:29	+10:23:31	237.7		
		5: 02:32:29	+10:23:08	81.7		
TOCC 0233.4 +3021 Candidate	6	1: 02:33:14	+06:19:37	5.5	B	0
		2: 02:33:18	+06:22:39	9.9	R	4800
		3: 02:33:24	+06:21:57	8.7	I	9300
		4: 02:33:25	+06:20:10	6.2		
		5: 02:33:31	+06:22:34	33.5		
		6: 02:33:39	+06:20:51	6.2		

Table A1-1 (continued)

Name	NVSS Sources	NVSS RA	NVSS DEC	S _{1.5} (mJy)	Data Filt.	Exp
TOCC 0233.6 +3560	6	1: 02:33:27	+12:01:33	9.3	B	0
		2: 02:33:31	+11:58:00	15.7	R	900
		3: 02:33:36	+12:00:52	3.5	I	6600
		4: 02:33:39	+11:58:47	2.6		
		5: 02:33:40	+11:57:33	4.1		
		6: 02:33:41	+11:59:56	3.2		
TOCC 0233.4 +4015	5	1: 02:33:16	+16:18:02	2.6		
		2: 02:33:23	+16:12:37	8		
		3: 02:33:29	+16:13:35	8		
		4: 02:33:32	+16:12:16	8		
		5: 02:33:34	+16:16:21	14.6		
TOCC 0233.8 +3510	5	1: 02:33:41	+11:11:41	8.2	B	0
		2: 02:33:44	+11:10:39	21.1	R	1500
		3: 02:33:48	+11:09:41	2.8	I	0
		4: 02:33:52	+11:07:44	2.5		
		5: 02:33:58	+11:11:04	3.8		
TOCC 0234.2 +3132	5	1: 02:34:06	+07:29:10	51.2		
		2: 02:34:10	+07:29:28	51.2		
		3: 02:34:17	+07:29:40	7.7		
		4: 02:34:22	+07:29:46	86.6		
		5: 02:34:24	+07:34:19	957		
TOCC 0234.3 +3852	5	1: 02:34:05	+14:49:51	8.3	B	0
		2: 02:34:06	+14:54:10	8.3	R	900
		3: 02:34:20	+14:49:00	8.3	I	0
		4: 02:34:21	+14:51:47	49.7		
		5: 02:34:34	+14:51:30	3.6		
TOCC 0234.9 +3136	5	1: 02:34:43	+07:38:25	65.7		
		2: 02:34:43	+07:36:44	3.5		
		3: 02:34:53	+07:33:27	2.9		
		4: 02:35:03	+07:36:02	3.4		
		5: 02:35:05	+07:37:29	4.4		

Table A1-1 (continued)

Name			NVSS Sources	NVSS RA	NVSS DEC	S _{1.5} (mJy)	Data Filt.	Exp
TOCC	0246.9	+3642	5	1: 02:46:47	+12:44:54	12.3		
				2: 02:46:52	+12:39:14	28.7		
				3: 02:46:52	+12:45:01	12.3		
				4: 02:46:58	+12:42:57	7.8		
				5: 02:47:05	+12:43:54	27.7		
TOCC	0247.8	+3753	5	1: 02:47:31	+13:52:31	8.3		
				2: 02:47:32	+13:54:51	8.3		
				3: 02:47:53	+13:55:33	8.3		
				4: 02:47:55	+13:54:19	2.6		
				5: 02:48:00	+13:50:07	2.7		
TOCC	0249.4	+3647	5	1: 02:49:13	+12:46:56	10.9	B	0
	Candidate			2: 02:49:27	+12:45:10	14	R	900
				3: 02:49:37	+12:49:20	16.2	I	0
				4: 02:49:38	+12:45:21	8.5		
				5: 02:49:40	+12:43:51	2.7		
TOCC	0249.9	+3026	5	1: 02:49:40	+06:28:54	10.3		
				2: 02:49:42	+06:23:00	14.9		
				3: 02:49:44	+06:26:45	10.3		
				4: 02:49:45	+06:24:51	61.4		
				5: 02:50:07	+06:23:22	4.5		
TOCC	0250.2	+3043	5	1: 02:50:02	+06:40:28	40.7	B	0
	Candidate			2: 02:50:04	+06:43:57	4.1	R	1800
				3: 02:50:05	+06:46:03	3.8	I	0
				4: 02:50:23	+06:41:59	6		
				5: 02:50:24	+06:43:39	4.9		
TOCC	0253.3	+3836	5	1: 02:53:03	+14:38:18	3.1		
				2: 02:53:09	+14:35:26	663.2		
				3: 02:53:10	+14:37:15	10.7		
				4: 02:53:27	+14:33:29	18.3		
				5: 02:53:33	+14:34:11	3.3		

Table A1-1 (continued)

Name	NVSS Sources	NVSS RA	NVSS DEC	S _{1.5} (mJy)	Data Filt.	Exp	
TOCC 0255.5 +4056	5	1:	02:55:20	+16:55:19	2.4		
		2:	02:55:28	+16:56:10	12.1		
		3:	02:55:29	+16:54:27	12		
		4:	02:55:32	+16:53:09	9.2		
		5:	02:55:35	+16:57:59	6.5		
TOCC 0256.3 +3828	5	1:	02:56:01	+14:28:36	5.6		
		2:	02:56:09	+14:27:11	5.6		
		3:	02:56:13	+14:26:25	5.8		
		4:	02:56:30	+14:28:39	3.3		
		5:	02:56:31	+14:29:55	6.6		
TOCC 0256.7 +3652	8	1:	02:56:29	+12:50:45	2.4	B	0
		2:	02:56:31	+12:49:30	2.4	R	6000
		3:	02:56:33	+12:55:05	2.4	I	3900
		4:	02:56:45	+12:49:41	2.4		
		5:	02:56:46	+12:50:35	2.4		
		6:	02:56:47	+12:52:00	10.2		
		7:	02:56:53	+12:51:34	7.8		
		8:	02:56:54	+12:49:40	3		
TOCC 0256.8 +3032 Cluster	5	1:	02:56:38	+06:30:02	21.5	B	7200
		2:	02:56:49	+06:32:31	31.6	R	2700
		3:	02:56:51	+06:35:10	5.8	I	3600
		4:	02:57:01	+06:29:37	8.1		
		5:	02:57:02	+06:34:18	4.6		
TOCC 0259.5 +3559	5	1:	02:59:18	+12:00:54	18.4		
		2:	02:59:21	+11:56:36	54.2		
		3:	02:59:32	+11:56:30	32.3		
		4:	02:59:38	+11:58:30	8.3		
		5:	02:59:38	+11:57:18	92.8		

Table A1-2: List of all known clusters in Region 1

Name	RA	DEC	z	Reference
ZwCl 0128.1+3038	01:30:55	+30:53:27	...	Zwicky & Kowal 1968
ZwCl 0128.1+3519	01:30:58	+35:34:27	...	Zwicky & Kowal 1968
ZwCl 0128.4+3647	01:31:17	+37:02:26	...	Zwicky & Kowal 1968
ZwCl 0129.7+3127	01:32:32	+31:42:24	...	Zwicky & Kowal 1968
ZwCl 0130.5+3129	01:33:20	+31:44:23	...	Zwicky & Kowal 1968
ZwCl 0130.6+3215	01:33:26	+32:30:22	...	Zwicky & Kowal 1968
ZwCl 0132.9+3638	01:35:48	+36:53:18	...	Zwicky & Kowal 1968
ZwCl 0134.4+3553	01:37:17	+36:08:16	...	Zwicky & Kowal 1968
HST J013835+33043	01:38:36	+33:04:21	...	Ostander et al. 1998
ZwCl 0138.8+3605	01:41:42	+36:20:08	...	Zwicky & Kowal 1968
ZwCl 0140.1+3144	01:42:58	+31:59:05	...	Zwicky & Kowal 1968
ZwCl 0140.2+3718	01:43:08	+37:33:05	...	Zwicky & Kowal 1968
ZwCl 0149.0+3240	01:51:54	+32:54:48	...	Zwicky & Kowal 1968
ABELL 0260	01:51:54	+33:09:48	0.04	Stuble & Rood 1999
ABELL 0262	01:52:50	+36:08:46	0.02	Stuble & Rood 1999
RXC J0152.9+3732	01:52:59	+37:32:07	0.30	Bohringer et al. 2000
ABELL 0263	01:53:22	+37:33:45	...	Abell & Olowin 1989
ZwCl 0150.9+3050	01:53:47	+31:04:44	...	Zwicky & Kowal 1968
1RXS J015505.4+335452	01:55:06	+33:55:12	0.09	Wei et al. 1999
V Zw 139	01:55:07	+33:53:41	...	Zwicky 1971
ABELL 0272	01:55:19	+33:56:41	0.09	Stuble & Rood 1999
ABELL 0278	01:57:18	+32:13:37	0.09	Stuble & Rood 1999
SCL 036	01:57:43	+33:50:36	...	Einasto et al 1997
ZwCl 0157.0+3315	01:59:55	+33:29:31	...	Zwicky & Kowal 1968
ZwCl 0159.1+3232	02:02:01	+32:46:27	...	Zwicky & Kowal 1968
ZwCl 0159.0+3932	02:02:01	+39:46:27	...	Zwicky & Kowal 1968
ZwCl 0159.6+3833	02:02:37	+38:47:25	...	Zwicky & Kowal 1968
ZwCl 0200.7+3725	02:03:42	+37:39:23	...	Zwicky & Kowal 1968
ZwCl 0205.5+3342	02:08:27	+33:56:12	...	Zwicky & Kowal 1968
ZwCl 0207.3+3755	02:10:20	+38:09:08	...	Zwicky & Kowal 1968
ZwCl 0210.0+3852	02:13:03	+39:06:01	...	Zwicky & Kowal 1968
ZwCl 0210.3+3049	02:13:14	+31:03:01	...	Zwicky & Kowal 1968
ZwCl 0212.0+3701	02:15:02	+37:14:57	...	Zwicky & Kowal 1968
ZwCl 0214.9+3935	02:17:59	+39:48:50	...	Zwicky & Kowal 1968
ZwCl 0215.2+3905	02:18:16	+39:18:49	...	Zwicky & Kowal 1968
ZwCl 0216.0+3625	02:19:02	+36:38:47	...	Zwicky & Kowal 1968
ZwCl 0216.8+3857	02:19:52	+39:10:45	...	Zwicky & Kowal 1968
CID 15	02:25:36	+36:57:00	0.04	Wegner et al. 1996
ABELL 0349	02:26:21	+36:49:29	...	Abell & Olowin 1989
ZwCl 0225.8+3347	02:28:54	+34:00:20	0.19	Zwicky & Kowal 1968
ZwCl 0226.5+3111	02:29:28	+31:24:20	...	Zwicky & Kowal 1968

Table A1-2 (continued)

Name	RA	DEC	z	Reference
ZwCl 0228.3+3153	02:31:17	+32:06:16	...	Zwicky & Kowal 1968
ZwCl 0230.2+3050	02:33:10	+31:03:10...		Zwicky & Kowal 1968
ZwCl 0230.3+3711	02:33:23	+37:24:10...		Zwicky & Kowal 1968
ZwCl 0236.2+3249	02:39:13	+33:01:54...		Zwicky & Kowal 1968
ZwCl 0236.2+3417	02:39:15	+34:29:54...		Zwicky & Kowal 1968
ZwCl 0237.6+3618	02:40:41	+36:30:50...		Zwicky & Kowal 1968
ZwCl 0241.0+3617	02:44:06	+36:29:40...		Zwicky & Kowal 1968
ZwCl 0242.2+3323	02:45:15	+33:35:37...		Zwicky & Kowal 1968
ABELL 0376	02:45:48	+36:51:36	0.05	Abell & Olowin 1989
RXC J0246.0+3653	02:46:03	+36:53:16	0.05	Bohringer et al. 2000
ZwCl 0244.2+3344	02:47:15	+33:56:31...		Zwicky & Kowal 1968
ZwCl 0244.2+3503	02:47:17	+35:15:31...		Zwicky & Kowal 1968
ZwCl 0250.3+3903	02:53:29	+39:15:13...		Zwicky & Kowal 1968
SCL 044	02:55:08	+37:12:08...		Einasto et al 1997

Appendix 2: Region 2

$1:30:00 \leq \text{RA} \leq 3:00:00, 30:00:00 \leq \text{DEC} \leq 40:00:00$

Total Area: 183.6 square degrees

Figure A2-1: Map of Region 1. All known clusters are listed in table A1-2.

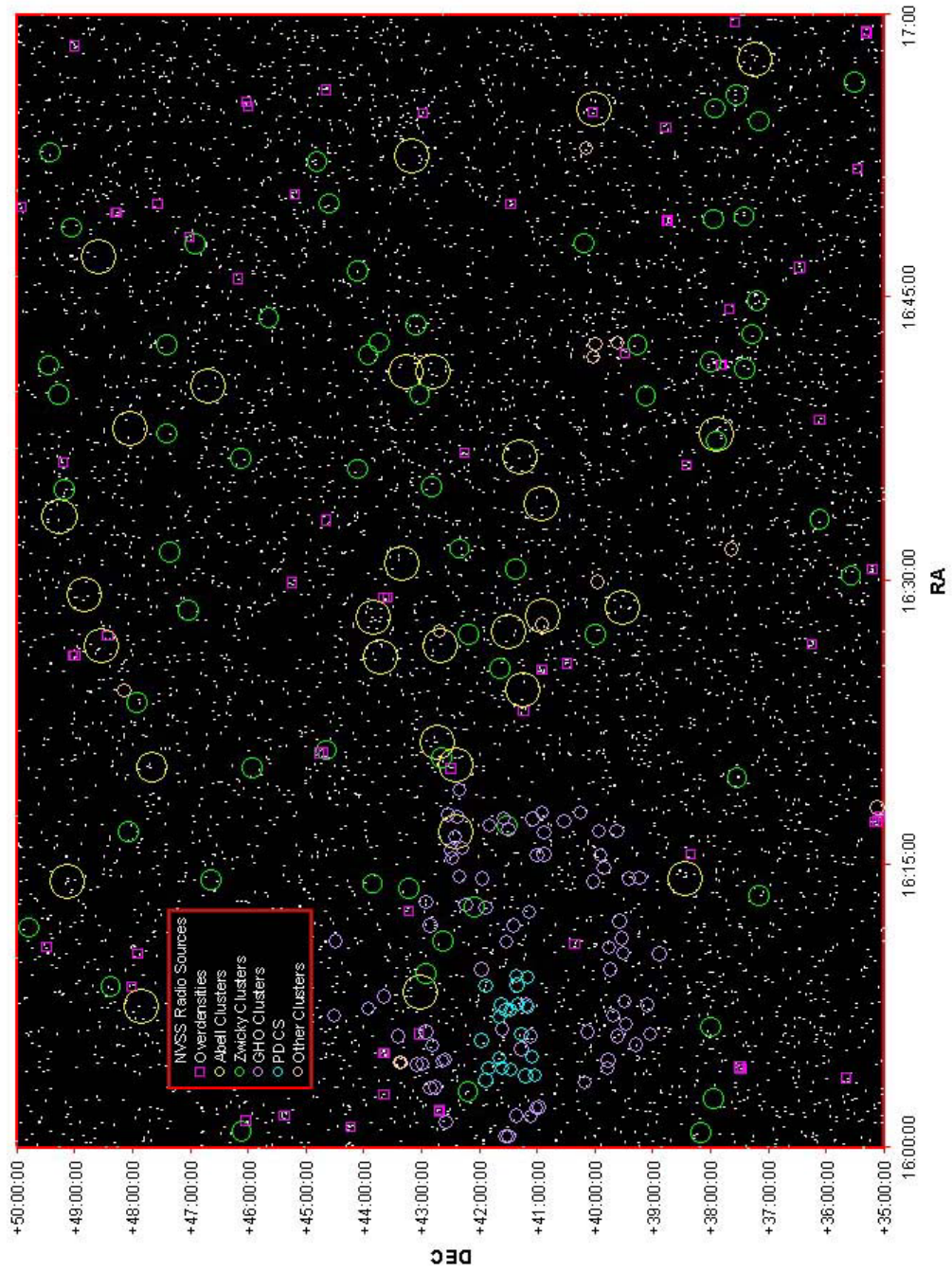


Table A2-1: Complete list of Region 2 overdensities

Name	NVSS Sources	NVSS RA	NVSS DEC	S _{1.5} (mJy)	Data Filt.	Exp
TOCC 1601.1 +4413 Candidate	6				B	0
e		1: 16:00:55	+44:12:15	31.3	R	3000
		2: 16:00:59	+44:15:25	4.8	I	3000
		3: 16:01:05	+44:11:56	3.7		
		4: 16:01:07	+44:14:23	37.9		
		5: 16:01:12	+44:10:36	29.9		
TOCC 1601.5 +4602	5					
		1: 16:01:21	+46:02:08	106.7		
		2: 16:01:22	+46:00:42	13.7		
		3: 16:01:22	+45:59:18	90.5		
		4: 16:01:29	+46:04:54	2.3		
		5: 16:01:33	+45:59:53	4.8		
TOCC 1601.7 +4522	5					
		1: 16:01:34	+45:22:12	5.5		
		2: 16:01:40	+45:23:52	3.6		
		3: 16:01:49	+45:24:12	11.2		
		4: 16:01:50	+45:19:19	17.8		
		5: 16:01:54	+45:21:07	2.3		
TOCC 1602.0 +4242	5					
		1: 16:01:46	+42:43:56	4		
		2: 16:01:47	+42:40:01	3.1		
		3: 16:02:00	+42:42:38	10		
		4: 16:02:03	+42:40:35	47.6		
		5: 16:02:09	+42:43:07	5.7		
TOCC 1602.0 +4240	5					
		1: 16:01:47	+42:40:01	3.1		
		2: 16:01:59	+42:37:36	3.1		
		3: 16:02:00	+42:42:38	4		
		4: 16:02:03	+42:40:35	47.6		
		5: 16:02:09	+42:43:07	5.7		
TOCC 1602.8 +4338 Cluster	5				B	10000
		1: 16:02:37	+43:36:52	3.6	R	2400
		2: 16:02:41	+43:41:06	32.2	I	5900
		3: 16:02:49	+43:35:34	9.2		
		4: 16:02:49	+43:38:51	3.3		
		5: 16:02:59	+43:35:30	4.2		

Table A2-1 (continued)

Name		NVSS Sources	NVSS RA	NVSS DEC	S _{1.5} (mJy)	Data Filt.	Exp
TOCC	1603.7 +3539	5				B	0
	Candidat						
	e		1: 16:03:31	+35:41:40	3.9	R	2700
			2: 16:03:32	+35:36:28	2.6	I	3000
			3: 16:03:38	+35:38:50	10		
			4: 16:03:42	+35:37:10	4.4		
			5: 16:03:50	+35:40:43	8.1		
TOCC	1604.2 +3726	5					
			1: 16:03:58	+37:29:19	2.7		
			2: 16:04:11	+37:27:33	6.6		
			3: 16:04:16	+37:25:42	17.7		
			4: 16:04:16	+37:23:20	45.1		
			5: 16:04:28	+37:26:42	10.8		
TOCC	1604.2 +3730	6					
			1: 16:03:58	+37:29:19	2.7		
			2: 16:04:11	+37:27:33	2.7		
			3: 16:04:17	+37:32:28	46.5		
			4: 16:04:20	+37:31:16	7.4		
			5: 16:04:23	+37:30:08	68.8		
			6: 16:04:28	+37:26:42	10.8		
TOCC	1604.3 +3730	5					
			1: 16:04:11	+37:27:33	2.7		
			2: 16:04:17	+37:32:28	46.5		
			3: 16:04:20	+37:31:16	2.7		
			4: 16:04:23	+37:30:08	68.8		
			5: 16:04:28	+37:26:42	10.8		
TOCC	1604.3 +3728	5					
			1: 16:04:11	+37:27:33	2.7		
			2: 16:04:16	+37:25:42	2.7		
			3: 16:04:20	+37:31:16	2.7		
			4: 16:04:23	+37:30:08	2.7		
			5: 16:04:28	+37:26:42	10.8		
TOCC	1605.0 +4339	5					
			1: 16:04:53	+43:37:07	5.2		
			2: 16:04:58	+43:37:46	6.2		
			3: 16:05:02	+43:41:45	84.7		
			4: 16:05:05	+43:38:18	4.3		
			5: 16:05:10	+43:38:52	11.2		

Table A2-1 (continued)

Name	NVSS Sources	NVSS RA	NVSS DEC	S _{1.5} (mJy)	Data Filt. Exp
TOCC 1605.0 +4337	5	1: 16:04:53	+43:37:07	5.2	
		2: 16:04:54	+43:35:07	5	
		3: 16:04:58	+43:37:46	6.2	
		4: 16:05:05	+43:38:18	4.3	
		5: 16:05:10	+43:38:52	11.2	
TOCC 1606.1 +4303	6	1: 16:05:50	+43:04:48	9.7	
		2: 16:05:50	+43:02:47	9.7	
		3: 16:05:58	+43:00:43	2.9	
		4: 16:06:04	+43:01:11	9.8	
		5: 16:06:16	+43:02:34	22.9	
		6: 16:06:16	+43:00:48	4.5	
TOCC 1608.6 +4801	5	1: 16:08:28	+48:00:45	5.6	
		2: 16:08:29	+48:00:11	15.7	
		3: 16:08:29	+47:59:54	8.2	
		4: 16:08:35	+48:02:44	5.5	
		5: 16:08:38	+47:58:48	9.7	
TOCC 1610.3 +4754	5	1: 16:10:03	+47:53:23	38.6	
		2: 16:10:05	+47:55:35	10.4	
		3: 16:10:06	+47:56:58	6.2	
		4: 16:10:13	+47:51:37	19.9	
		5: 16:10:30	+47:52:38	11.4	
TOCC 1610.7 +4929	5	1: 16:10:25	+49:27:45	3.3	
		2: 16:10:38	+49:28:30	4	
		3: 16:10:49	+49:30:15	3.7	
		4: 16:10:54	+49:28:08	6.5	
		5: 16:10:57	+49:29:02	12.6	
TOCC 1610.8 +4021	5	1: 16:10:32	+40:22:25	2.3	
		2: 16:10:40	+40:20:19	43.9	
		3: 16:10:45	+40:18:49	14.9	
		4: 16:10:49	+40:19:38	4.4	
		5: 16:11:00	+40:18:40	16.6	

Table A2-1 (continued)

Name	NVSS Sources	NVSS RA	NVSS DEC	S _{1.5} (mJy)	Data Filt. Exp
TOCC 1612.6 +4313	5	1: 16:12:20	+43:10:44	5.6	
		2: 16:12:23	+43:12:13	2.6	
		3: 16:12:33	+43:15:02	53.5	
		4: 16:12:41	+43:13:21	6.8	
		5: 16:12:48	+43:12:11	65.8	
TOCC 1615.56 +3820	5	1: 16:15:19	+38:17:47	2.8	
		2: 16:15:26	+38:22:04	2.8	
		3: 16:15:34	+38:19:56	11.2	
		4: 16:15:46	+38:21:30	41.7	
		5: 16:15:48	+38:17:58	14	
TOCC 1617.3 +3510	5	1: 16:17:09	+35:07:42	12	
		2: 16:17:16	+35:08:46	132.2	
		3: 16:17:17	+35:10:10	10.9	
		4: 16:17:17	+35:11:46	44.1	
		5: 16:17:23	+35:07:16	95	
TOCC 1617.3 +3506	5	1: 16:17:09	+35:07:42	12	
		2: 16:17:16	+35:08:46	12	
		3: 16:17:23	+35:07:16	12	
		4: 16:17:25	+35:04:54	96.8	
		5: 16:17:28	+35:04:09	121	
TOCC 1617.6 +3503	5	1: 16:17:25	+35:04:54	12	
		2: 16:17:28	+35:04:09	121	
		3: 16:17:32	+35:02:26	938.3	
		4: 16:17:39	+35:00:48	774	
		5: 16:17:43	+35:03:07	13.8	
TOCC 1620.1 +4229	5	1: 16:19:54	+42:26:29	5.1	
		2: 16:20:08	+42:28:31	165	
		3: 16:20:09	+42:30:02	9.8	
		4: 16:20:09	+42:27:33	2.8	
		5: 16:20:15	+42:30:44	4.1	

Table A2-1 (continued)

Name	NVSS Sources	NVSS RA	NVSS DEC	S _{1.5} (mJy)	Data Filt.	Exp
TOCC 1620.9 +4442	5	1:	16:20:41 +44:38:42	16.5	B	4500
		2:	16:20:41 +44:42:30	2.9	R	6200
		3:	16:20:43 +44:40:43	2.8	I	1500
		4:	16:21:01 +44:44:27	4.3		
		5:	16:21:06 +44:42:29	3.7		
TOCC 1620.9 +4445	5	1:	16:20:41 +44:42:30	16.5		
		2:	16:20:47 +44:48:21	2.7		
		3:	16:21:01 +44:44:27	4.3		
		4:	16:21:06 +44:42:29	3.7		
		5:	16:21:11 +44:47:39	6.4		
TOCC 1623.1 +4114	5	1:	16:22:56 +41:14:32	2.6		
		2:	16:22:59 +41:16:19	14.5		
		3:	16:23:13 +41:12:05	16.4		
		4:	16:23:17 +41:15:20	2.8		
		5:	16:23:20 +41:16:48	2.3		
TOCC 1625.3 +4055	5	1:	16:25:10 +40:53:34	163.5	B	0
		2:	16:25:13 +40:57:15	47.7	R	1200
		3:	16:25:15 +40:52:31	5.3	I	0
		4:	16:25:18 +40:55:18	8		
		5:	16:25:27 +40:56:07	5		
TOCC 1625.7 +4029	5	1:	16:25:26 +40:26:19	3.9		
		2:	16:25:39 +40:30:52	28.5		
		3:	16:25:44 +40:28:35	5.3		
		4:	16:25:50 +40:29:21	32.4		
		5:	16:25:54 +40:28:23	68.2		
TOCC 1626.1 +4859 Cluster	6	1:	16:25:46 +49:00:42	14.7	B	7000
		2:	16:25:49 +48:56:36	14.7	R	4800
		3:	16:25:54 +48:58:55	4.2	I	3900
		4:	16:25:56 +49:00:43	3		
		5:	16:26:00 +48:58:17	26.3		
		6:	16:26:20 +49:00:03	2.8		

Table A2-1 (continued)

Name	NVSS Sources	NVSS RA	NVSS DEC	S _{1.5} (mJy)	Data Filt.	Exp
TOCC 1626.1 +4901	6	1: 16:25:46	+49:00:42	14.7		
		2: 16:25:54	+48:58:55	14.7		
		3: 16:25:56	+49:00:43	3		
		4: 16:26:00	+48:58:17	26.3		
		5: 16:26:04	+49:04:17	6.1		
		6: 16:26:20	+49:00:03	2.8		
TOCC 1626.7 +3615	5	1: 16:26:32	+36:17:23	40.6		
		2: 16:26:37	+36:14:55	30.4		
		3: 16:26:43	+36:12:20	92.1		
		4: 16:26:49	+36:14:27	2.9		
		5: 16:26:50	+36:13:14	4		
TOCC 1627.1 +4826	5	1: 16:26:48	+48:24:40	14.2		
		2: 16:26:54	+48:27:38	37.1		
		3: 16:26:54	+48:23:35	4.8		
		4: 16:27:02	+48:23:17	7.1		
		5: 16:27:22	+48:28:19	13		
TOCC 1629.1 +4338	5	1: 16:28:58	+43:37:30	11.7		
		2: 16:29:06	+43:37:37	14		
		3: 16:29:07	+43:40:50	2.7		
		4: 16:29:12	+43:36:35	3.8		
		5: 16:29:18	+43:35:31	3.7		
TOCC 1629.1 +4335	5	1: 16:28:58	+43:37:30	11.7		
		2: 16:29:06	+43:37:37	11.7		
		3: 16:29:08	+43:31:58	6.6		
		4: 16:29:12	+43:36:35	11.7		
		5: 16:29:18	+43:35:31	3.7		
TOCC 1629.9 +4514 Cluster	5	1: 16:29:50	+45:12:42	9.2	B	1000
		2: 16:29:53	+45:13:34	11.7	R	3600
		3: 16:29:55	+45:16:09	26.4	I	4200
		4: 16:29:57	+45:11:22	3.3		
		5: 16:30:03	+45:12:13	7.3		

Table A2-1 (continued)

Name		NVSS Sources	NVSS RA	NVSS DEC	S _{1.5} (mJy)	Data Filt. Exp
TOCC	1630.6 +3512	5				
			1: 16:30:27	+35:13:08	3.8	
			2: 16:30:32	+35:13:23	3	
			3: 16:30:33	+35:10:57	3.4	
			4: 16:30:42	+35:12:07	3.3	
			5: 16:30:49	+35:11:57	15.9	
TOCC	1633.2 +4438	5				
			1: 16:33:02	+44:36:50	3.2	
			2: 16:33:06	+44:35:12	3.2	
			3: 16:33:08	+44:41:08	3.2	
			4: 16:33:12	+44:38:44	2.8	
			5: 16:33:26	+44:40:52	3.5	
TOCC	1636.3 +4912	5				
			1: 16:36:00	+49:10:44	13	
			2: 16:36:04	+49:09:57	13	
			3: 16:36:16	+49:12:25	260.3	
			4: 16:36:22	+49:13:26	22.1	
			5: 16:36:32	+49:14:23	111.4	
TOCC	1636.1 +3824	5				
			1: 16:35:56	+38:21:03	2.3	
			2: 16:35:59	+38:21:55	2.3	
			3: 16:36:10	+38:25:25	2.3	
			4: 16:36:11	+38:26:46	2.3	
			5: 16:36:17	+38:21:59	97.6	
TOCC	1636.8 +4215	5				
			1: 16:36:37	+42:16:56	4.5	
			2: 16:36:44	+42:12:58	7.4	
			3: 16:36:44	+42:17:29	6.1	
			4: 16:36:49	+42:16:08	4	
			5: 16:37:03	+42:13:02	3.3	
TOCC	1638.6 +3607	5				
			1: 16:38:22	+36:06:56	6.9	
			2: 16:38:27	+36:06:54	17.5	
			3: 16:38:35	+36:08:27	9.3	
			4: 16:38:38	+36:04:51	28.2	
			5: 16:38:45	+36:06:32	5.9	

Table A2-1 (continued)

Name		NVSS Sources	NVSS RA	NVSS DEC	S _{1.5} (mJy)	Data Filt.	Exp
TOCC	1641.5 +3749	5					
			1: 16:41:13	+37:51:56	7.1		
			2: 16:41:19	+37:49:33	2.9		
			3: 16:41:19	+37:47:02	13.1		
			4: 16:41:37	+37:47:35	8.2		
			5: 16:41:42	+37:48:45	2.3		
TOCC	1641.5 +3748	5					
			1: 16:41:19	+37:49:33	7.1		
			2: 16:41:19	+37:47:02	13.1		
			3: 16:41:37	+37:47:35	8.2		
			4: 16:41:38	+37:46:21	18		
			5: 16:41:42	+37:48:45	2.3		
TOCC	1642.1 +3928	5					
			1: 16:41:53	+39:30:11	4		
			2: 16:41:55	+39:25:44	18.9		
			3: 16:42:07	+39:28:39	3.3		
			4: 16:42:07	+39:27:24	4.1		
			5: 16:42:17	+39:30:45	3.6		
TOCC	1644.4 +3739	5					
	Candidat e		1: 16:44:10	+37:38:29	9.5		
			2: 16:44:27	+37:39:09	64.5		
			3: 16:44:27	+37:41:56	3.7		
			4: 16:44:36	+37:36:49	2.3		
			5: 16:44:40	+37:39:05	11.6		
TOCC	1646.0 +4610	5					
			1: 16:45:46	+46:07:04	22.2		
			2: 16:46:01	+46:10:00	40.9		
			3: 16:46:08	+46:08:49	25.3		
			4: 16:46:15	+46:12:06	10.5		
			5: 16:46:17	+46:10:57	2.7		
TOCC	1646.6 +3626	5				B	5500
	Candidat e		1: 16:46:26	+36:24:34	2.9	R	2400
			2: 16:46:32	+36:28:22	7.2	I	3900
			3: 16:46:39	+36:27:02	20.8		
			4: 16:46:43	+36:28:08	21.7		
			5: 16:46:47	+36:26:56	15.7		

Table A2-1 (continued)

Name	NVSS Sources	NVSS RA	NVSS DEC	S _{1.5} (mJy)	Data Filt.	Exp
TOCC 1648.2 +4701	6	1: 16:48:03	+46:58:54	13.5	B	2500
		2: 16:48:12	+47:03:44	4.4	R	4200
		3: 16:48:15	+47:02:07	3	I	3000
		4: 16:48:15	+46:58:33	8.5		
		5: 16:48:26	+46:59:28	11.2		
		6: 16:48:26	+46:58:06	2.9		
TOCC 1649.1 +3846	7	1: 16:48:49	+38:48:14	264.8	B	0
		2: 16:48:52	+38:46:11	264.8	R	1800
		3: 16:48:54	+38:44:41	3.9	I	0
		4: 16:49:00	+38:43:13	4.3		
		5: 16:49:06	+38:43:58	10.3		
		6: 16:49:15	+38:42:49	4.4		
		7: 16:49:20	+38:44:28	3.2		
TOCC 1649.5 +4817	5	1: 16:49:19	+48:16:22	3.1		
		2: 16:49:23	+48:14:28	4.1		
		3: 16:49:33	+48:19:46	48		
		4: 16:49:34	+48:14:52	7.5		
		5: 16:49:42	+48:17:45	11.5		
TOCC 1649.5 +4815	5	1: 16:49:19	+48:16:22	3.1		
		2: 16:49:23	+48:14:28	4.1		
		3: 16:49:34	+48:14:52	7.5		
		4: 16:49:37	+48:12:53	4.2		
		5: 16:49:42	+48:17:45	11.5		
TOCC 1649.8 +4955	5	1: 16:49:33	+49:52:58	5.6		
		2: 16:49:42	+49:55:47	4.5		
		3: 16:49:45	+49:54:23	9.8		
		4: 16:50:01	+49:56:25	4.2		
		5: 16:50:04	+49:53:49	10.7		
TOCC 1649.9 +4734	5	1: 16:49:38	+47:33:31	2.5		
		2: 16:49:47	+47:31:39	5.8		
		3: 16:49:49	+47:36:32	4.3		
		4: 16:50:06	+47:31:00	17.5		
		5: 16:50:12	+47:31:24	2.4		

Table A2-1 (continued)

Name	NVSS Sources	NVSS RA	NVSS DEC	S _{1.5} (mJy)	Data Filt. Exp
TOCC 1649.9 +4127	5	1: 16:49:43	+41:26:01	14.5	
		2: 16:49:52	+41:27:12	2.8	
		3: 16:50:00	+41:26:18	5.9	
		4: 16:50:06	+41:26:48	10.7	
		5: 16:50:08	+41:28:17	3.6	
TOCC 1650.5 +4511	6	1: 16:50:21	+45:12:48	8.7	
		2: 16:50:21	+45:13:20	24.5	
		3: 16:50:21	+45:13:40	12.6	
		4: 16:50:30	+45:08:09	11.7	
		5: 16:50:34	+45:13:34	138.8	
		6: 16:50:36	+45:09:23	16.5	
TOCC 1651.8 +3527	5	1: 16:51:39	+35:23:59	2.9	
		2: 16:51:40	+35:28:41	2.9	
		3: 16:51:45	+35:25:42	3.9	
		4: 16:51:53	+35:29:33	7.2	
		5: 16:51:56	+35:24:12	6.2	
TOCC 1654.0 +3846	5	1: 16:53:49	+38:46:04	3.8	
		2: 16:53:49	+38:47:20	9	
		3: 16:53:56	+38:43:58	38.1	
		4: 16:54:08	+38:46:49	18.5	
		5: 16:54:13	+38:44:40	6.7	
TOCC 1654.8 +4002	5	1: 16:54:38	+40:00:36	4.5	
		2: 16:54:43	+40:02:47	81.5	
		3: 16:54:48	+40:01:23	2.5	
		4: 16:54:51	+40:03:27	2.9	
		5: 16:55:03	+40:00:20	2.6	
TOCC 1654.8 +4258	5	1: 16:54:29	+42:56:08	4.3	
		2: 16:54:37	+43:00:18	4.3	
		3: 16:54:49	+42:58:25	14.9	
		4: 16:54:52	+42:59:39	5	
		5: 16:55:01	+42:55:09	4.5	

Table A2-1 (continued)

Name	NVSS Sources	NVSS RA	NVSS DEC	S _{1.5} (mJy)	Data Filt. Exp
TOCC 1655.1 +4600	5	1: 16:54:57	+45:58:13	3.6	
		2: 16:55:09	+46:01:28	6.7	
		3: 16:55:11	+46:02:12	8.3	
		4: 16:55:15	+46:00:48	10.8	
		5: 16:55:18	+46:02:26	12.7	
TOCC 1655.4 +4601	5	1: 16:55:09	+46:01:28	3.6	
		2: 16:55:11	+46:02:12	3.6	
		3: 16:55:15	+46:00:48	10.8	
		4: 16:55:18	+46:02:26	12.7	
		5: 16:55:36	+45:59:15	30.3	
TOCC 1656.0 +4438	5	1: 16:55:48	+44:35:01	3.3	
		2: 16:56:03	+44:37:53	6.8	
		3: 16:56:05	+44:36:58	8.8	
		4: 16:56:06	+44:40:51	20.1	
		5: 16:56:17	+44:39:49	11.7	
TOCC 1658.33 +4900	5	1: 16:58:04	+48:58:49	7.6	
		2: 16:58:13	+48:59:37	3.3	
		3: 16:58:16	+48:58:02	23.5	
		4: 16:58:23	+49:00:00	5.1	
		5: 16:58:35	+49:02:02	10.3	
TOCC 1659.0 +3518	5	1: 16:58:46	+35:15:37	14.3	
		2: 16:58:55	+35:16:00	11.1	
		3: 16:58:57	+35:19:53	5.2	
		4: 16:58:58	+35:17:05	45.6	
		5: 16:59:13	+35:17:41	10.1	
TOCC 1659.1 +3518	5	1: 16:58:55	+35:16:00	14.3	
		2: 16:58:57	+35:19:53	14.3	
		3: 16:58:58	+35:17:05	45.6	
		4: 16:59:13	+35:17:41	10.1	
		5: 16:59:20	+35:16:04	8.2	

Table A2-1 (continued)

Name	NVSS Sources	NVSS RA	NVSS DEC	S _{1.5} (mJy)	Data Filt. Exp
TOCC 1659.6 +3734	5	1: 16:59:19	+37:35:59	3.5	
		2: 16:59:32	+37:35:28	20.3	
		3: 16:59:43	+37:34:10	4.2	
		4: 16:59:48	+37:36:13	2.8	
		5: 16:59:49	+37:31:54	109.8	

Table A2-2: List of all known clusters in Region 2

Name	RA	DEC	z	Reference
GHO 1558+4140	16:00:35	+41:32:02	0.39	Gunn et al. 1986
GHO 1558+4137	16:00:36	+41:28:44	...	Gunn et al. 1986
ZwCl 1559.0+3819	16:00:48	+38:10:39	...	Zwicky & Kowal 1968
ZwCl 1559.3+4615	16:00:51	+46:06:39	...	Zwicky & Kowal 1968
GHO 1559+4242	16:01:22	+42:34:35	...	Gunn et al. 1986
GHO 1559+4114	16:01:40	+41:05:54	0.30	Gunn et al. 1986
GHO 1600+4129	16:01:44	+41:21:12	0.43	Gunn et al. 1986
GHO 1600+4109	16:02:06	+41:01:23	0.54	Gunn et al. 1986
GHO 1600+4105	16:02:10	+40:57:26	...	Gunn et al. 1986
ZwCl 1600.8+3804	16:02:36	+37:55:46	...	Zwicky & Kowal 1968
ZwCl 1601.3+4220	16:02:59	+42:11:47	...	Zwicky & Kowal 1968
GHO 1601+4259	16:03:11	+42:50:54	0.54	Gunn et al. 1986
GHO 1601+4253	16:03:14	+42:45:36	0.54	Gunn et al. 1986
GHO 1601+4017	16:03:28	+40:09:25	...	Gunn et al. 1986
PDCS 028S	16:03:35	+41:52:34	1.00	Postman et al. 1996
PDCS 067	16:03:49	+41:11:13	0.50	Postman et al. 1996
PDCS 065	16:03:52	+41:01:53	0.40	Postman et al. 1996
PDCS 071	16:04:07	+41:27:18	0.70	Postman et al. 1996
PDCS 076	16:04:11	+41:50:00	0.30	Postman et al. 1996
GHO 1602+3954	16:04:12	+39:46:34	...	Gunn et al. 1986
PDCS 027S	16:04:13	+41:35:53	0.70	Postman et al. 1996
GHO 1602+4312	16:04:25	+43:04:53	0.90	Gunn et al. 1986
GHO 1602+4305	16:04:29	+42:57:47	...	Gunn et al. 1986
GHO 1602+4329	16:04:31	+43:21:17	0.92	Gunn et al. 1986
[AEC93] 1603+4329 S	16:04:32	+43:21:13	...	Aragon-Salamanca et al. 1993
[AEC93] 1603+4329 N	16:04:32	+43:21:39	...	Aragon-Salamanca et al. 1993
GHO 1602+4245	16:04:37	+42:37:05	...	Gunn et al. 1986
GHO 1602+3953	16:04:40	+39:45:35	...	Gunn et al. 1986
GHO 1603+4244	16:04:41	+42:35:54	...	Gunn et al. 1986
PDCS 074	16:04:46	+41:38:50	0.30	Postman et al. 1996
PDCS 066	16:04:49	+41:05:06	0.90	Postman et al. 1996
GHO 1603+4124	16:05:14	+41:16:02	...	Gunn et al. 1986

Table A2-2 (continued)

Name	RA	DEC	z	Reference
GHO 1603+4256	16:05:24	+42:48:50	...	Gunn et al. 1986
GHO 1603+3924	16:05:30	+39:16:21	...	Gunn et al. 1986
PDCS 079	16:05:41	+41:57:33	0.40	Postman et al. 1996
GHO 1604+4114	16:05:53	+41:06:34	...	Gunn et al. 1986
GHO 1604+3944	16:05:54	+39:36:04	...	Gunn et al. 1986
GHO 1604+4331	16:05:55	+43:23:28	...	Gunn et al. 1986
GHO 1604+3910	16:06:02	+39:02:47	...	Gunn et al. 1986
PDCS 068	16:06:03	+41:15:37	0.50	Postman et al. 1996
GHO 1604+4015	16:06:07	+40:07:41	...	Gunn et al. 1986
GHO 1604+4303	16:06:08	+42:54:59	0.90	Gunn et al. 1986
GHO 1604+4144	16:06:20	+41:35:54	0.30	Gunn et al. 1986
ZwCl 1604.6+3807	16:06:24	+37:59:00	...	Zwicky & Kowal 1968
GHO 1604+3935	16:06:33	+39:27:49	...	Gunn et al. 1986
PDCS 075	16:06:53	+41:39:09	0.90	Postman et al. 1996
GHO 1605+3948	16:07:01	+39:40:02	...	Gunn et al. 1986
GHO 1605+4438	16:07:02	+44:30:21	...	Gunn et al. 1986
PDCS 072	16:07:17	+41:27:01	0.60	Postman et al. 1996
PDCS 025S	16:07:18	+41:32:16	0.60	Postman et al. 1996
GHO 1605+4403	16:07:26	+43:55:16	...	Gunn et al. 1986
PDCS 023S	16:07:28	+41:09:26	0.60	Postman et al. 1996
ABELL 2157	16:07:29	+47:51:05	...	Abell & Olowin 1989
GHO 1605+4119	16:07:33	+41:11:11	...	Gunn et al. 1986
GHO 1605+3913	16:07:34	+39:05:11	...	Gunn et al. 1986
PDCS 026S	16:07:36	+41:36:36	1.10	Postman et al. 1996
PDCS 069	16:07:39	+41:19:17	0.30	Postman et al. 1996
GHO 1605+3936	16:07:43	+39:28:29	...	Gunn et al. 1986
GHO 1606+4346	16:07:59	+43:38:18	...	Gunn et al. 1986
ABELL 2158	16:08:15	+43:00:07	0.13	Stuble & Rood 1999
ZwCl 1607.1+4830	16:08:33	+48:22:09	...	Zwicky & Kowal 1968
PDCS 077	16:08:35	+41:52:43	0.20	Postman et al. 1996
PDCS 078	16:08:38	+41:20:08	1.00	Postman et al. 1996
PDCS 024S	16:09:02	+41:09:25	1.10	Postman et al. 1996
PDCS 070	16:09:07	+41:21:32	0.20	Postman et al. 1996
ZwCl 1607.6+4303	16:09:15	+42:55:11	...	Zwicky & Kowal 1968
GHO 1607+3952	16:09:26	+39:44:12	...	Gunn et al. 1986
GHO 1607+4204	16:09:26	+41:57:00	...	Gunn et al. 1986
GHO 1608+3900	16:10:16	+38:52:51	...	Gunn et al. 1986
GHO 1608+3937	16:10:22	+39:30:09	...	Gunn et al. 1986
GHO 1608+3952	16:10:37	+39:44:22	...	Gunn et al. 1986
GHO 1609+4139	16:10:52	+41:31:35	...	Gunn et al. 1986
GHO 1609+4436	16:10:56	+44:28:30	...	Gunn et al. 1986
ZwCl 1609.3+4245	16:10:57	+42:37:18	...	Zwicky & Kowal 1968

Table A2-2 (continued)

Name	RA	DEC	z	Reference
GHO 1609+3939	16:11:07	+39:31:42	...	Gunn et al. 1986
ZwCl 1610.3+4955	16:11:41	+49:47:21	...	Zwicky & Kowal 1968
GHO 1610+4258	16:11:46	+42:51:03	...	Gunn et al. 1986
GHO 1610+4131	16:11:47	+41:23:27	...	Gunn et al. 1986
GHO 1610+3941	16:12:02	+39:33:52	...	Gunn et al. 1986
GHO 1610+4114	16:12:31	+41:06:54	...	Gunn et al. 1986
GHO 1611+4200	16:12:43	+41:52:49	...	Gunn et al. 1986
ZwCl 1611.1+4213	16:12:46	+42:05:25	...	Zwicky & Kowal 1968
GHO 1611+4221	16:12:52	+42:13:43	...	Gunn et al. 1986
GHO 1611+4302	16:13:01	+42:54:50	...	Gunn et al. 1986
ZwCl 1611.6+3717	16:13:25	+37:09:27	...	Zwicky & Kowal 1968
ZwCl 1612.1+4320	16:13:44	+43:12:29	...	Zwicky & Kowal 1968
ZwCl 1612.4+4358	16:14:00	+43:50:30	...	Zwicky & Kowal 1968
GHO 1612+4008	16:14:04	+40:01:12	...	Gunn et al. 1986
ABELL 2169	16:14:07	+49:07:31	0.06	Stubble & Rood 1999
ZwCl 1612.7+4645	16:14:12	+46:37:31	...	Zwicky & Kowal 1968
GHO 1612+3932	16:14:16	+39:24:31	...	Gunn et al. 1986
ABELL 2167	16:14:16	+38:25:31	...	Abell & Olowin 1989
GHO 1612+4203	16:14:17	+41:56:07	0.29	Gunn et al. 1986
GHO 1612+3920	16:14:19	+39:13:25	...	Gunn et al. 1986
GHO 1612+4227	16:14:22	+42:20:25	...	Gunn et al. 1986
GHO 1613+3957	16:14:48	+39:50:15	...	Gunn et al. 1986
GHO 1613+4235	16:15:22	+42:27:53	0.45	Gunn et al. 1986
GHO 1613+4106	16:15:30	+40:59:29	...	Gunn et al. 1986
GHO 1613+4000	16:15:31	+39:52:59	...	Gunn et al. 1986
GHO 1613+4100	16:15:31	+40:52:42	...	Gunn et al. 1986
GHO 1614+4236	16:15:45	+42:29:19	...	Gunn et al. 1986
GHO 1614+4223	16:15:52	+42:16:31	...	Gunn et al. 1986
GHO 1614+4232	16:16:29	+42:25:03	...	Gunn et al. 1986
GHO 1615+4059	16:16:42	+40:51:40	...	Gunn et al. 1986
ABELL 2172	16:16:45	+42:23:41	0.14	Stubble & Rood 1999
ZwCl 1615.3+4811	16:16:45	+48:03:41	...	Zwicky & Kowal 1968
GHO 1615+4003	16:16:46	+39:55:46	...	Gunn et al. 1986
GHO 1615+3944	16:16:47	+39:36:52	...	Gunn et al. 1986
GHO 1615+4136	16:16:54	+41:28:53	...	Gunn et al. 1986
GHO 1615+4156	16:17:04	+41:48:42	...	Gunn et al. 1986
ZwCl 1615.4+4137	16:17:04	+41:29:42	...	Zwicky & Kowal 1968
GHO 1615+4038	16:17:18	+40:31:19	...	Gunn et al. 1986
GHO 1615+4110	16:17:25	+41:03:37	...	Gunn et al. 1986
GHO 1615+4141	16:17:29	+41:34:07	...	Gunn et al. 1986
GHO 1615+4229	16:17:33	+42:22:26	...	Gunn et al. 1986
GHO 1616+4239	16:17:38	+42:32:20	...	Gunn et al. 1986

Table A2-2 (continued)

Name	RA	DEC	z	Reference
GHO 1616+4021	16:17:45	+40:14:26	...	Gunn et al. 1986
GHO 1616+4101	16:17:46	+40:53:56	...	Gunn et al. 1986
CID 64	16:18:00	+35:06:00	0.03	Wegner et al. 1996
GHO 1617+4227	16:18:57	+42:20:13	...	Gunn et al. 1986
ZwCl 1617.8+3739	16:19:35	+37:31:51	...	Zwicky & Kowal 1968
ZwCl 1618.6+4603	16:20:07	+45:55:54	...	Zwicky & Kowal 1968
ABELL 2180	16:20:09	+47:39:54	...	Abell & Olowin 1989
ABELL 2179	16:20:14	+42:24:54	0.14	Stuble & Rood 1999
ZwCl 1619.0+4246	16:20:38	+42:38:56	...	Zwicky & Kowal 1968
ZwCl 1619.5+4445	16:21:04	+44:37:58	...	Zwicky & Kowal 1968
ABELL 2183	16:21:32	+42:42:59	0.14	Stuble & Rood 1999
ZwCl 1622.1+4802	16:23:32	+47:55:08	...	Zwicky & Kowal 1968
HST J162413+48077	16:24:13	+48:07:47	...	Ostander et al. 1998
HST J162413+48078	16:24:14	+48:07:49	...	Ostander et al. 1998
ABELL 2187	16:24:16	+41:15:10	0.18	Stuble & Rood 1999
ZwCl 1623.7+4145	16:25:21	+41:38:15	...	Zwicky & Kowal 1968
ABELL 2190	16:25:59	+43:41:17	...	Abell & Olowin 1989
ABELL 2195	16:26:36	+48:32:20	...	Abell & Olowin 1989
ABELL 2192	16:26:37	+42:40:20	0.19	Stuble & Rood 1999
ZwCl 1625.5+4006	16:27:12	+39:59:22	...	Zwicky & Kowal 1968
ZwCl 1625.6+4217	16:27:14	+42:10:22	...	Zwicky & Kowal 1968
ABELL 2196	16:27:21	+41:29:23	0.13	Stuble & Rood 1999
RXC J1627.3+4240	16:27:24	+42:40:42	0.03	Bohringer et al. 2000
RXC J1627.6+4055	16:27:42	+40:54:40	0.03	Bohringer et al. 2000
ABELL 2198	16:28:05	+43:49:26	0.08	Stuble & Rood 1999
ABELL 2197	16:28:10	+40:54:26	0.03	Stuble & Rood 1999
ZwCl 1627.0+4708	16:28:28	+47:01:27	...	Zwicky & Kowal 1968
ABELL 2199	16:28:37	+39:31:28	0.03	Stuble & Rood 1999
ABELL 2202	16:29:17	+48:49:31	...	Abell & Olowin 1989
CAN 166	16:29:57	+39:56:36	0.06	Wegner et al. 1996
ZwCl 1628.5+3540	16:30:20	+35:33:34	...	Zwicky & Kowal 1968
ZwCl 1629.0+4128	16:30:39	+41:21:36	...	Zwicky & Kowal 1968
ABELL 2206	16:30:59	+43:19:37	...	Abell & Olowin 1989
ZwCl 1630.1+4728	16:31:32	+47:21:40	...	Zwicky & Kowal 1968
HST J163141+37375	16:31:42	+37:37:35	...	Ostander et al. 1998
ZwCl 1630.1+4227	16:31:43	+42:20:40	...	Zwicky & Kowal 1968
ZwCl 1631.5+3613	16:33:19	+36:06:46	...	Zwicky & Kowal 1968
ABELL 2212	16:33:28	+49:15:48	0.19	Stuble & Rood 1999
ABELL 2211	16:34:04	+40:55:50	0.14	Stuble & Rood 1999
ZwCl 1633.5+4916	16:34:52	+49:09:54	...	Zwicky & Kowal 1968
ZwCl 1633.4+4256	16:35:00	+42:49:54	...	Zwicky & Kowal 1968
ZwCl 1634.4+4412	16:35:57	+44:05:58	...	Zwicky & Kowal 1968

Table A2-2 (continued)

Name	RA	DEC	z	Reference
ZwCl 1635.0+4613	16:36:29	+46:07:00	...	Zwicky & Kowal 1968
ABELL 2213	16:36:33	+41:17:00	0.16	Stuble & Rood 1999
ZwCl 1635.7+3800	16:37:27	+37:54:03	...	Zwicky & Kowal 1968
ABELL 2214	16:37:45	+37:54:05	0.16	Stuble & Rood 1999
ZwCl 1636.4+4729	16:37:50	+47:23:06	...	Zwicky & Kowal 1968
ABELL 2215	16:38:06	+48:03:07	...	Abell & Olowin 1989
ZwCl 1638.1+3913	16:39:49	+39:07:13	...	Zwicky & Kowal 1968
ZwCl 1638.5+4922	16:39:51	+49:16:14	...	Zwicky & Kowal 1968
ZwCl 1638.3+4307	16:39:53	+43:01:14	...	Zwicky & Kowal 1968
ABELL 2219	16:40:21	+46:41:16	0.23	Stuble & Rood 1999
ABELL 2221	16:41:05	+43:15:19	0.10	Stuble & Rood 1999
ABELL 2222	16:41:05	+42:47:19	...	Abell & Olowin 1989
ZwCl 1639.5+3729	16:41:16	+37:23:19	...	Zwicky & Kowal 1968
ZwCl 1640.1+4932	16:41:26	+49:26:21	...	Zwicky & Kowal 1968
ZwCl 1639.9+3805	16:41:39	+37:59:21	...	Zwicky & Kowal 1968
[VMF98] 184	16:41:52	+40:01:29	0.51	Vikhlinin et al. 1998
ZwCl 1640.4+4400	16:41:57	+43:54:22	...	Zwicky & Kowal 1968
ZwCl 1640.8+3921	16:42:30	+39:15:24	...	Zwicky & Kowal 1968
ZwCl 1641.1+4729	16:42:31	+47:23:25	...	Zwicky & Kowal 1968
[VMF98] 185	16:42:33	+39:59:05	...	Vikhlinin et al. 1998
[VMF98] 186	16:42:39	+39:35:53	0.47	Vikhlinin et al. 1998
ZwCl 1641.1+4349	16:42:39	+43:43:25	...	Zwicky & Kowal 1968
ZwCl 1641.3+3723	16:43:04	+37:17:26	...	Zwicky & Kowal 1968
ZwCl 1642.0+4310	16:43:35	+43:04:29	...	Zwicky & Kowal 1968
ZwCl 1642.5+4544	16:43:59	+45:38:31	...	Zwicky & Kowal 1968
ZwCl 1643.1+3717	16:44:52	+37:11:34	...	Zwicky & Kowal 1968
ZwCl 1644.9+4411	16:46:26	+44:05:41	...	Zwicky & Kowal 1968
ABELL 2230	16:47:10	+48:35:44	0.14	Stuble & Rood 1999
ZwCl 1646.4+4659	16:47:50	+46:53:47	...	Zwicky & Kowal 1968
ZwCl 1646.2+4016	16:47:52	+40:10:46	...	Zwicky & Kowal 1968
ZwCl 1647.4+4908	16:48:44	+49:02:51	...	Zwicky & Kowal 1968
ZwCl 1647.4+3801	16:49:08	+37:55:52	...	Zwicky & Kowal 1968
ZwCl 1647.6+3730	16:49:21	+37:24:52	...	Zwicky & Kowal 1968
ZwCl 1648.5+4440	16:50:01	+44:34:56	...	Zwicky & Kowal 1968
ZwCl 1650.7+4453	16:52:12	+44:48:05	0.18	Zwicky & Kowal 1968
ABELL 2233	16:52:28	+43:10:06	...	Abell & Olowin 1989
ZwCl 1651.4+4930	16:52:43	+49:25:07	...	Zwicky & Kowal 1968
RX J1652.6+4011	16:52:56	+40:09:13	0.15	Bohringer et al. 2000
ZwCl 1652.6+3714	16:54:21	+37:09:13	...	Zwicky & Kowal 1968
ABELL 2235	16:54:58	+40:01:16	0.15	Stuble & Rood 1999
ZwCl 1653.3+3800	16:55:02	+37:55:16	...	Zwicky & Kowal 1968
ZwCl 1654.0+3738	16:55:44	+37:33:19	...	Zwicky & Kowal 1968
ZwCl 1654.6+3535	16:56:24	+35:30:22	...	Zwicky & Kowal 1968
ABELL 2238	16:57:39	+37:13:27	...	Abell & Olowin 1989

Appendix 3: TOC J1602.8 + 4338

Table A3-1: Basic Data

z	0.416 ± 0.004
f_B	0.37 ± 0.14
R_{30}	0.71 arcmin
N_{30}	18.8 ± 4

Table A3-2: Standard Star Corrections

	PFC Final Co-add	IGI Final Co-add (Cluster)	IGI Final Co-add (Comparison)
b1	-2.362 ± 0.06	-4.842 ± 0.10	-4.865 ± 0.11
b2	-0.111 ± 0.02	-0.140 ± 0.01	-0.140 ± 0.01
r1	-3.104 ± 0.04	-4.957 ± 0.18	-4.887 ± 0.10
r2	0.025 ± 0.06		
i1	-2.970 ± 0.04	-4.275 ± 0.16	-4.332 ± 0.09
i2	-0.071 ± 0.06		

Table A3-3: Image characteristics. “fil” is filter, “exp” is exposure time and “elip” is ellipticity.

PFC Images				IGI Images (Cluster)				IGI Images (Comparison)			
Date	fil	exp	seeing elip	Date	fil	exp	seeing elip	Date	fil	exp	seeing elip
4/22/2001	B	600	3.06 0.02	5/28/2001	B	500	3.13 0.03	5/27/2001	B	500	3.32 0.06
4/22/2001	B	600	3.20 0.02	5/28/2001	B	500	3.04 0.06	5/27/2001	B	500	3.17 0.05
4/22/2001	B	600	3.20 0.02	5/28/2001	B	500	2.90 0.06	5/27/2001	B	500	3.04 0.03
4/22/2001	B	600	3.04 0.02	5/12/1999	B	500	3.22 0.02	5/27/2001	B	500	3.13 0.05
4/22/2001	B	600	3.13 0.04	5/12/1999	B	500	3.23 0.03	5/27/2001	B	500	3.04 0.07
4/22/2001	B	600	2.92 0.12	5/12/1999	B	500	3.34 0.02	5/27/2001	B	500	3.04 0.05
4/22/2001	B	600	3.20 0.15	5/12/1999	B	500	4.43 0.09	5/29/2001	B	500	3.58 0.05
4/22/2001	B	600	2.83 0.07	5/12/1999	B	500	4.31 0.11	5/29/2001	B	500	3.51 0.06
4/23/2001	B	300	3.18 0.06	6/27/2001	B	500	3.01 0.08	5/29/2001	B	500	3.49 0.07
4/24/2001	B	450	2.33 0.05	6/27/2001	B	500	2.90 0.07	5/29/2001	B	500	4.19 0.07
4/24/2001	B	450	2.21 0.10	6/27/2001	B	500	2.92 0.05	5/29/2001	B	500	3.74 0.09
5/23/2001	B	300	2.03 0.16	4/28/2001	B	500	2.78 0.08	5/29/2001	B	500	3.23 0.06
5/24/2001	B	900	2.07 0.27	4/28/2001	B	500	2.78 0.08	6/27/2001	B	500	2.75 0.06
5/24/2001	B	900	2.10 0.26	4/28/2001	B	500	2.87 0.08	6/27/2001	B	500	2.78 0.05
5/24/2001	B	900	2.19 0.19	4/28/2001	B	500	2.83 0.05	6/27/2001	B	500	2.86 0.06
5/24/2001	B	900	2.07 0.20	4/28/2001	B	500	2.90 0.06	5/27/2001	R	300	2.86 0.05
5/24/2001	B	900	2.17 0.29	4/28/2001	B	500	3.06 0.05	5/27/2001	R	300	3.04 0.03
5/25/2001	B	900	2.19 0.09	4/28/2001	B	500	2.93 0.08	5/27/2001	R	300	3.12 0.05
5/25/2001	B	900	2.19 0.06	4/28/2001	B	500	2.74 0.06	5/27/2001	R	300	3.16 0.03
5/25/2001	B	900	2.45 0.03	4/28/2001	B	500	2.66 0.05	5/27/2001	R	300	2.85 0.06
5/25/2001	B	900	2.14 0.08	5/12/1999	R	300	3.58 0.04	5/27/2001	R	300	3.10 0.04
4/22/2001	R	600	2.59 0.06	5/12/1999	R	300	4.18 0.04	5/27/2001	R	300	2.83 0.04
4/22/2001	R	600	2.83 0.17	5/12/1999	R	300	3.58 0.03	5/27/2001	R	300	3.18 0.03
4/22/2001	R	600	2.59 0.04	5/12/1999	R	300	3.08 0.07	5/28/2001	R	500	2.61 0.06
4/22/2001	R	600	2.85 0.03	5/12/1999	R	300	4.66 0.01	5/28/2001	R	500	2.83 0.07
4/22/2001	R	600	3.56 0.06	5/12/1999	R	300	4.64 0.03	5/28/2001	R	500	2.68 0.05
4/22/2001	R	600	3.30 0.02	5/28/2001	R	300	2.61 0.06	5/28/2001	R	500	3.04 0.05
4/22/2001	R	600	3.39 0.04	5/28/2001	R	300	2.57 0.08	5/28/2001	R	500	2.79 0.07
4/22/2001	R	600	3.20 0.02	6/27/2001	R	300	2.46 0.06	5/28/2001	R	500	2.65 0.13
4/22/2001	R	600	3.37 0.02	6/27/2001	R	300	2.38 0.06	6/25/2001	I	300	2.85 0.15
4/22/2001	R	600	3.49 0.02	6/27/2001	R	300	3.43 0.05	6/25/2001	I	300	2.86 0.07
4/22/2001	R	600	3.34 0.03	6/27/2001	R	300	2.58 0.06	6/25/2001	I	300	2.58 0.08
4/23/2001	R	600	3.63 0.03	5/15/1999	I	300	2.22 0.10	6/25/2001	I	300	2.80 0.11
4/24/2001	R	300	1.92 0.07	5/15/1999	I	300	2.21 0.06	6/25/2001	I	300	2.78 0.09
4/25/2001	R	600	2.03 0.06	5/15/1999	I	300	2.17 0.14	6/25/2001	I	300	2.96 0.09
4/25/2001	R	600	2.00 0.09	5/15/1999	I	300	2.22 0.12	6/25/2001	I	300	2.45 0.09
4/25/2001	R	600	2.14 0.05	5/15/1999	I	300	2.26 0.16	6/25/2001	I	300	2.54 0.05
5/24/2001	R	600	2.03 0.18	5/15/1999	I	300	2.80 0.08	6/25/2001	I	300	2.57 0.07
5/23/2001	I	300	2.12 0.13	5/15/1999	I	300	2.94 0.06	6/25/2001	I	300	2.48 0.07
4/24/2001	I	450	2.35 0.12	5/15/1999	I	300	2.92 0.12	6/25/2001	I	300	2.64 0.08
4/24/2001	I	450	2.38 0.07	6/24/2001	I	300	2.75 0.15	6/25/2001	I	300	3.27 0.10
4/23/2001	I	450	2.64 0.04	6/24/2001	I	300	2.78 0.19				
6/2/2001	I	300	2.64 0.14	6/25/2001	I	300	2.28 0.13				
6/2/2001	I	300	2.73 0.09	6/25/2001	I	300	2.29 0.15				
6/2/2001	I	600	2.78 0.15	6/25/2001	I	300	2.29 0.12				
6/2/2001	I	600	2.78 0.15	6/25/2001	I	500	2.85 0.04				
6/2/2001	I	600	3.20 0.14	6/25/2001	I	500	2.80 0.05				
6/2/2001	I	600	3.30 0.10	6/25/2001	I	500	2.87 0.07				
				6/25/2001	I	500	2.86 0.07				

Appendix 4: TOC J1620.9 + 4442

Table A4-1: Basic Data

z	0.215 ± 0.001
f_B	0.22 ± 0.09
R_{30}	2.82 arcmin
N_{30}	28.5 ± 5

Table A4-2: Standard Star Corrections

	PFC Final Co-add	IGI Final Co-add (Cluster)	IGI Final Co-add (Comparison)
b1	-1.576 ± 0.07	-4.250 ± 0.14	-3.241 ± 0.15
b2	-0.111 ± 0.02	-0.140 ± 0.01	-0.140 ± 0.01
r1	-2.491 ± 0.04	-4.619 ± 0.10	-4.699 ± 0.10
r2	0.025 ± 0.02		
i1	-2.929 ± 0.06	-3.584 ± 0.17	-3.584 ± 0.23
i2	-0.071 ± 0.06		

Table A4-3: Image characteristics. “fil” is filter, “exp” is exposure time and “elip” is ellipticity.

PFC Images				IGI Images (Cluster)				IGI Images (Comparison)			
Date	fil	Exp	seeing elip	Date	fil	Exp	seeing elip	Date	fil	Exp	seeing elip
4/23/2001	B	300	3.86 0.10	5/10/2000	B	500	3.32 0.10	6/23/2001	B	500	3.23 0.12
4/23/2001	B	450	3.86 0.06	5/10/2000	B	500	3.08 0.04	6/23/2001	B	500	3.31 0.11
4/24/2001	B	450	2.19 0.09	5/10/2000	B	500	3.01 0.04	6/23/2001	B	500	3.27 0.11
5/23/2001	B	300	2.00 0.21	4/29/2001	B	500	3.67 0.08	6/23/2001	B	500	3.31 0.10
5/25/2001	B	900	2.26 0.19	4/29/2001	B	500	3.54 0.09	6/23/2001	B	500	3.16 0.09
5/25/2001	B	900	2.14 0.11	4/29/2001	B	500	3.58 0.04	6/23/2001	B	500	3.21 0.09
4/23/2001	R	300	3.70 0.03	4/29/2001	B	500	3.40 0.05	6/26/2001	B	300	3.11 0.03
4/24/2001	R	300	2.10 0.09	5/27/2001	B	500	3.25 0.04	6/26/2001	B	300	3.08 0.04
4/25/2001	R	600	2.26 0.08	5/27/2001	B	500	3.53 0.04	6/26/2001	B	300	3.27 0.02
4/25/2001	R	600	2.10 0.06	5/27/2001	B	500	3.24 0.04	6/26/2001	B	300	3.03 0.04
4/25/2001	R	600	2.17 0.07	5/27/2001	B	500	3.73 0.03	6/26/2001	B	300	3.27 0.04
4/26/2001	R	600	2.10 0.15	6/28/2001	B	500	2.71 0.07	6/26/2001	B	300	3.41 0.03
4/26/2001	R	600	2.59 0.34	6/28/2001	B	500	2.59 0.08	6/26/2001	B	300	3.46 0.02
4/26/2001	R	600	2.15 0.18	6/28/2001	B	500	3.05 0.08	6/26/2001	B	300	3.37 0.05
4/26/2001	R	600	2.03 0.12	5/8/2000	R	300	3.07 0.03	6/26/2001	B	300	3.57 0.04
5/23/2001	R	300	1.88 0.14	5/8/2000	R	300	2.73 0.05	6/26/2001	B	300	3.14 0.09
5/25/2001	R	600	2.03 0.11	5/8/2000	R	300	2.84 0.03	6/26/2001	B	300	3.16 0.06
4/23/2001	I	300	3.70 0.03	5/8/2000	R	300	3.34 0.03	6/26/2001	B	300	3.20 0.08
4/24/2001	I	450	2.23 0.08	5/10/2000	R	300	2.80 0.10	6/26/2001	B	300	3.06 0.09
5/23/2001	I	300	2.04 0.13	5/10/2000	R	300	2.87 0.13	6/26/2001	B	300	3.51 0.07
6/3/2001	I	600	4.42 0.10	5/10/2000	R	300	2.76 0.08	4/29/2001	R	300	4.29 0.11
6/3/2001	I	600	4.66 0.07	4/29/2001	R	300	3.27 0.09	4/29/2001	R	300	3.84 0.14
6/3/2001	I	600	4.38 0.12	4/29/2001	R	300	3.25 0.10	4/29/2001	R	300	3.77 0.13
				4/29/2001	R	300	3.14 0.07	4/29/2001	R	300	3.58 0.12
				5/27/2001	R	300	3.60 0.04	4/29/2001	R	300	3.58 0.15
				5/27/2001	R	300	3.46 0.03	4/29/2001	R	300	3.81 0.14
				5/27/2001	R	300	3.43 0.04	6/28/2001	R	300	2.38 0.11
				5/27/2001	R	300	3.47 0.04	6/28/2001	R	300	2.43 0.11
				5/27/2001	R	300	3.63 0.04	6/28/2001	R	300	2.41 0.10
				5/28/2001	R	500	2.73 0.15				
				5/28/2001	R	500	2.46 0.06				
				5/28/2001	R	500	2.54 0.06				
				5/28/2001	R	500	2.52 0.07				
				5/28/2001	R	500	2.68 0.09				
				5/28/2001	R	500	2.45 0.13				
				5/28/2001	R	500	3.04 0.07				
				5/28/2001	R	500	3.25 0.09				
				5/10/2000	I	300	3.56 0.07				
				5/10/2000	I	300	3.30 0.05				
				5/10/2000	I	300	3.57 0.10				
				5/10/2000	I	300	4.57 0.07				
				5/10/2000	I	300	3.86 0.08				
				5/10/2000	I	300	3.65 0.07				

Appendix 5: TOC J1626.1 + 4859

Table A5-1: Basic Data

z	0.410 ± 0.01
f_B	0.23 ± 0.12
R_{30}	0.58 arcmin
N_{30}	14.06 ± 4

Table A5-2: Standard Star Corrections

	PFC Final Co-add	IGI Final Co-add (Cluster)	IGI Final Co-add (Comparison)
b1	-1.889 ± 0.11	-4.547 ± 0.11	-3.858 ± 0.50
b2	-0.111 ± 0.02	-0.140 ± 0.01	-0.140 ± 0.01
r1	-2.404 ± 0.05	-4.541 ± 0.13	-4.152 ± 0.50
r2	0.025 ± 0.02		
i1	-2.891 ± 0.05	-4.113 ± 0.14	-4.113 ± 0.50
i2	-0.071 ± 0.06		

Table A5-3: Image characteristics. “fil” is filter, “exp” is exposure time and “elip” is ellipticity.

PFC Images				IGI Images (Cluster)				IGI Images (Comparison)			
Date	fil	Exp	seeing elip	Date	fil	Exp	seeing elip	Date	fil	Exp	seeing elip
4/24/2001	B	450	2.24 0.07	5/9/2000	B	500	2.73 0.03	6/23/2001	B	500	3.32 0.07
5/23/2001	B	300	2.05 0.13	5/9/2000	B	500	3.10 0.04	6/23/2001	B	500	3.06 0.07
5/23/2001	B	900	2.31 0.20	5/9/2000	B	500	2.73 0.04	6/23/2001	B	500	3.11 0.06
5/24/2001	B	900	2.35 0.23	5/9/2000	B	500	2.55 0.03	6/23/2001	B	500	2.86 0.07
5/24/2001	B	900	2.24 0.27	5/9/2000	B	500	2.50 0.04	6/23/2001	B	500	3.01 0.11
5/24/2001	B	900	2.35 0.31	5/10/2000	B	500	3.30 0.05	6/23/2001	B	500	3.08 0.10
5/24/2001	B	900	2.43 0.23	5/10/2000	B	500	3.32 0.04	6/23/2001	B	500	2.79 0.11
5/24/2001	B	900	2.03 0.13	5/10/2000	B	500	3.27 0.05	6/23/2001	B	500	3.17 0.09
5/25/2001	B	900	2.47 0.28	5/10/2000	B	500	3.03 0.06	6/23/2001	B	500	3.19 0.14
5/25/2001	B	900	2.03 0.06	5/10/2000	B	500	3.25 0.05	6/28/2001	B	500	2.61 0.08
5/26/2001	B	900	2.21 0.05	6/28/2001	B	500	2.77 0.08	6/28/2001	B	500	2.48 0.09
5/26/2001	B	900	2.03 0.06	6/28/2001	B	500	2.68 0.05	6/28/2001	B	500	2.74 0.08
5/26/2001	B	900	2.05 0.05	6/28/2001	B	500	2.64 0.07	6/23/2001	R	300	2.24 0.04
4/24/2001	R	300	2.12 0.06	6/28/2001	B	500	2.61 0.06	6/23/2001	R	300	2.24 0.07
5/23/2001	R	300	2.00 0.09	5/10/2000	R	300	2.90 0.05	6/23/2001	R	300	2.35 0.08
5/23/2001	R	600	2.21 0.20	5/10/2000	R	300	3.30 0.09	6/23/2001	R	300	2.37 0.06
5/23/2001	R	600	1.88 0.08	5/10/2000	R	300	3.34 0.06	6/23/2001	R	300	2.52 0.06
5/24/2001	R	600	1.86 0.21	6/23/2001	R	300	2.33 0.06	6/23/2001	R	300	2.47 0.05
5/24/2001	R	600	1.95 0.28	6/23/2001	R	300	2.79 0.08	6/23/2001	R	300	2.59 0.09
5/25/2001	R	600	1.88 0.08	6/23/2001	R	300	2.47 0.08	6/23/2001	R	300	2.63 0.05
5/25/2001	R	600	2.07 0.12	6/23/2001	R	300	2.52 0.08	6/23/2001	R	300	2.68 0.05
5/26/2001	R	600	2.07 0.06	6/23/2001	R	300	2.47 0.10	6/28/2001	R	300	2.15 0.07
5/26/2001	R	600	1.95 0.12	6/27/2001	R	300	2.71 0.04	6/28/2001	R	300	2.17 0.07
5/26/2001	R	600	1.98 0.10	6/27/2001	R	300	2.67 0.06	6/28/2001	R	300	2.24 0.10
4/24/2001	I	450	2.21 0.05	6/27/2001	R	300	2.58 0.06	6/25/2001	I	300	3.32 0.07
5/23/2001	I	300	2.10 0.16	6/28/2001	R	300	2.58 0.10	6/25/2001	I	300	3.20 0.10
6/3/2001	I	600	4.22 0.14	6/28/2001	R	300	2.80 0.08	6/25/2001	I	300	2.87 0.07
6/3/2001	I	600	4.51 0.22	6/28/2001	R	300	3.05 0.05	6/25/2001	I	300	2.94 0.08
6/3/2001	I	600	4.31 0.12	6/28/2001	R	300	3.23 0.07	6/25/2001	I	300	2.71 0.12
6/3/2001	I	600	4.85 0.10	6/28/2001	R	300	2.90 0.06	6/25/2001	I	300	2.73 0.11
				5/7/2000	I	300	3.65 0.07	6/25/2001	I	300	3.53 0.10
				5/7/2000	I	300	2.64 0.13	6/25/2001	I	300	3.37 0.08
				5/7/2000	I	300	2.76 0.05	6/25/2001	I	300	3.21 0.07
				5/7/2000	I	300	2.53 0.06	6/25/2001	I	300	2.78 0.07
				5/7/2000	I	300	2.33 0.06	6/25/2001	I	300	3.76 0.08
				5/7/2000	I	300	2.17 0.11	6/25/2001	I	300	3.64 0.09
				5/7/2000	I	300	2.22 0.08				
				5/7/2000	I	300	2.22 0.09				
				5/7/2000	I	300	2.24 0.07				
				6/25/2001	I	300	3.11 0.14				
				6/25/2001	I	300	3.06 0.13				
				6/25/2001	I	300	2.92 0.11				
				6/25/2001	I	300	3.19 0.09				

Appendix 6: TOC J1705.8 + 3657

Table A5-1: Basic Data

z	0.167 ± 0.01
f_B	0.14 ± 0.09
R_{30}	3.53 arcmin
N_{30}	12.36 ± 3

Table A5-2: Standard Star Corrections

	PFC Final Co-add	IGI Final Co-add (Cluster)	IGI Final Co-add (Comparison)
b1	-0.612 ± 0.16	-4.624 ± 0.13	-4.461 ± 0.19
b2	-0.111 ± 0.02	-0.140 ± 0.01	-0.140 ± 0.01
r1	-2.470 ± 0.06	-4.210 ± 0.13	-4.494 ± 0.12
r2	0.025 ± 0.02		
i1	-1.885 ± 0.05	-3.408 ± 0.14	-3.422 ± 0.11
i2	-0.071 ± 0.06		

Table A6-3: Image characteristics. “fil” is filter, “exp” is exposure time and “elip” is ellipticity.

PFC Images				IGI Images (Cluster)				IGI Images (Comparison)			
Date	fil	exp	seeing elip	Date	fil	exp	seeing elip	Date	fil	exp	seeing elip
4/23/2001	B	150	3.60 0.07	6/23/2001	B	500	3.32 0.07	5/28/2001	B	500	3.56 0.06
4/24/2001	B	450	3.39 0.08	6/23/2001	B	500	3.06 0.07	5/28/2001	B	500	3.61 0.11
5/23/2001	B	600	1.86 0.11	6/23/2001	B	500	3.11 0.06	5/28/2001	B	500	3.77 0.05
5/23/2001	B	600	2.14 0.16	6/23/2001	B	500	2.86 0.07	5/28/2001	B	500	3.64 0.08
5/23/2001	B	600	2.05 0.17	6/23/2001	B	500	3.01 0.11	5/28/2001	B	500	3.51 0.07
5/24/2001	B	900	2.00 0.21	6/23/2001	B	500	3.08 0.10	5/28/2001	B	500	3.59 0.17
5/24/2001	B	900	2.07 0.20	6/23/2001	B	500	2.79 0.11	5/28/2001	B	500	3.32 0.23
5/24/2001	B	900	2.10 0.20	6/23/2001	B	500	3.17 0.09	5/28/2001	B	500	3.30 0.25
5/26/2001	B	900	2.03 0.16	6/23/2001	B	500	3.19 0.14	5/29/2001	B	500	4.43 0.15
5/26/2001	B	900	2.05 0.17	6/28/2001	B	500	2.61 0.08	5/29/2001	B	500	3.86 0.05
5/26/2001	B	900	2.00 0.14	6/28/2001	B	500	2.48 0.09	5/29/2001	B	500	3.57 0.06
5/26/2001	B	900	2.03 0.14	6/28/2001	B	500	2.74 0.08	5/29/2001	B	500	3.69 0.06
5/26/2001	B	900	2.17 0.21	6/23/2001	R	300	2.24 0.04	6/23/2001	B	500	4.44 0.04
4/23/2001	R	150	3.23 0.08	6/23/2001	R	300	2.24 0.07	6/23/2001	B	500	4.27 0.05
4/24/2001	R	300	2.68 0.07	6/23/2001	R	300	2.35 0.08	6/26/2001	B	300	3.60 0.05
4/25/2001	R	600	2.33 0.11	6/23/2001	R	300	2.37 0.06	6/26/2001	B	300	3.77 0.05
4/25/2001	R	600	2.52 0.20	6/23/2001	R	300	2.52 0.06	6/26/2001	B	300	4.07 0.05
4/25/2001	R	600	2.26 0.11	6/23/2001	R	300	2.47 0.05	6/26/2001	B	300	3.79 0.06
4/25/2001	R	600	2.24 0.09	6/23/2001	R	300	2.59 0.09	6/26/2001	B	300	3.67 0.06
4/25/2001	R	600	2.05 0.05	6/23/2001	R	300	2.63 0.05	6/26/2001	B	300	3.60 0.07
4/25/2001	R	600	2.08 0.06	6/23/2001	R	300	2.68 0.05	6/28/2001	B	500	3.39 0.07
4/25/2001	R	600	2.10 0.05	6/28/2001	R	300	2.15 0.07	6/28/2001	B	500	3.30 0.08
4/25/2001	R	600	2.00 0.07	6/28/2001	R	300	2.17 0.07	6/28/2001	B	500	3.30 0.07
4/25/2001	R	600	2.03 0.09	6/28/2001	R	300	2.24 0.10	6/25/2001	I	300	3.34 0.06
5/23/2001	R	300	2.05 0.15	6/25/2001	I	300	3.32 0.07	6/25/2001	I	300	3.81 0.22
5/24/2001	R	600	1.88 0.22	6/25/2001	I	300	3.20 0.10	6/25/2001	I	300	3.56 0.14
5/24/2001	R	600	2.33 0.22	6/25/2001	I	300	2.87 0.07	6/25/2001	I	300	3.60 0.14
5/25/2001	R	600	2.14 0.18	6/25/2001	I	300	2.94 0.08	6/25/2001	I	300	3.30 0.13
5/25/2001	R	600	2.10 0.08	6/25/2001	I	300	2.71 0.12	6/25/2001	I	300	2.94 0.18
4/23/2001	I	150	3.64 0.08	6/25/2001	I	300	2.73 0.11	6/25/2001	I	300	3.84 0.11
4/24/2001	I	450	3.18 0.08	6/25/2001	I	300	3.53 0.10	6/25/2001	I	300	3.86 0.11
5/23/2001	I	300	2.10 0.16	6/25/2001	I	300	3.37 0.08	6/25/2001	I	300	3.87 0.13
6/3/2001	I	600	4.19 0.11	6/25/2001	I	300	3.21 0.07	6/25/2001	I	300	3.71 0.14
6/3/2001	I	600	4.45 0.10	6/25/2001	I	300	2.78 0.07	6/25/2001	I	300	3.69 0.17
6/3/2001	I	600	2.38 0.17	6/25/2001	I	300	3.76 0.08	6/25/2001	I	300	4.03 0.16
6/3/2001	I	600	4.49 0.09	6/25/2001	I	300	3.64 0.09	6/25/2001	I	300	3.50 0.13
6/3/2001	I	600	4.73 0.08					5/28/2001	R	300	3.46 0.28
6/3/2001	I	600	5.04 0.10					5/28/2001	R	300	2.85 0.22
								5/28/2001	R	300	3.11 0.25
								5/28/2001	R	300	2.73 0.12
								5/29/2001	R	300	3.43 0.08
								5/29/2001	R	300	3.39 0.07
								5/29/2001	R	300	3.34 0.07
								5/29/2001	R	300	3.08 0.07
								5/29/2001	R	300	3.25 0.06
								5/29/2001	R	300	3.11 0.09
								6/28/2001	R	500	3.25 0.13
								6/28/2001	R	300	3.01 0.05
								6/28/2001	R	300	2.87 0.04
								6/28/2001	R	300	3.04 0.06

Special Acknowledgements

We would like to thank Harald Ebeling for kindly checking his ROSAT data for any possible serendipitous cluster observations.

This research has made use of the NASA/IPAC Extragalactic Database (NED), which is operated by the Jet Propulsion Laboratory, California Institute of Technology, under contract with the National Aeronautics and Space Administration.

This material is based in part upon work supported by the Texas Advanced Research Program under Grant No. 009658-0710-1999.

The author was generously supported through funds provided by the Curtis T. Vaughan, Jr. Centennial Chair in Astronomy.

The author would like to acknowledge the invaluable help provided by Kelley Knight and Matthew Dunn who proofread this manuscript.

Bibliography

- Abadi, M.G., Moore, B. and Bower, R.G. 1999. MNRAS 308, 947
- Abell, G.O., 1958, ApJ, 3, 211
- Allen, S.W.; Schmidt, R.W. and Fabian, A.C. 2002. MNRAS 334, 11
- Allington-Smith, J.R., et al. 1993 ApJ 404, 521
- Andreon, S and Ettori, S. 1999. ApJ 516, 647
- Bahcall, N. A. 2000. Phys. Scripta T85, 32
- Bahcall, N.A. 1988. ARA&A 26, 631
- Bahcall, N.A. and Fan, X. 1998 ApJ 504, 1
Bender, R and Ziegler, B. Bruzual, G. 1996. ApJL 463, L51
- Becker, R.H.; White, R.L. and Helfand, D.J. 1995, ApJ 450, 559
- Benn, C.R.; Rowan-Robinson, M.; McMahon, R.G.; Broadhurst, T.J. and Lawrence, A. 1993. MNRAS 263, 98
- Bergmann, M. 2000 private communication
- Bhavsar, S.P. 1989. ApJ 338, 718
- Blake, C. & Wall, J. 2002, MNRAS 329, L37
- Blanton, E.L. et al. 2001. AJ 121, 291
- Bruzual, A. G. and Charlot, S. 1993. ApJ 405, 538
- Burns, J. et al. 1994. ApJ 423, 94
- Butcher, H. and Oemler, A., Jr. 1985. ApJS 57, 665
- Butcher, H. and Oemler, A., Jr. 1984. ApJ 285, 426

Butcher, H.; Wells, D.C. and Oemler, A. Jr. 1983. ApJS 52, 183

Butcher, H. and Oemler, A. Jr. 1978 ApJ 226, 559

Caldwell, N. and Rose, J.A. 1997. 113, 492

Carlberg, R.G. et al 1997. ApJL 476, 7

Carlberg, R.G., et al. 1996. ApJ 462, 32

Carlberg, R.G. et al. 2001. ApJ 563, 736

Claver, C.F. "The Age of the Milky way Galaxy from White Dwarf Chronometry" (1995: University of Texas, Austin)

Cognoni, I et al 2001. ApJ 560, 86

Colless, M. et al. "Looking Deep in the Southern Sky, Proceedings of the ESO/Australia Workshop held at Sydney, Australia, 10-12 December 1997." Edited by Faffaella Morganti and Warrick J. Couch. (Berlin: Springer-Verlag, 1999). p. 9

Conselice, C.J. and Gallagher, J.S. III. 1997. AJ 117, 75

Condon, J.J. 1989. ApJ 338, 13

Condon, J.J. 1992. ARA&A 30, 575

Condon, J.J. 1984. 284, 44

Condon, J.J. et al. 1998. AJ 115, 1693

Cotter, G. private communication

Cotton, W.D. 1998 <ftp://nvss.cv.nrao.edu/pub/nvss/CATALOG/README>

Couch et al. 1994

de Bernardis, P. et al. 2002. ApJ 564, 559

de Propriis, R. et al. 2002. MNRAS 329, 87

Danese, L.; Franceschini, A.; Toffolatti, L. and de Zotti, G. 1987. ApJ 318, 15

- Donahue, M. 1998. ApJ 502, 550
- Dressler, A. "Star Formation Near and Far: Seventh Astrophysics Conference. Edited by Steven S. Holt and Lee, G. Mundy. (Woodbury N. Y. : AIP Press, 1997) p.535
- Dressler, A.; Oemler, A. Jr., Sparks, W.B. and Lucas, R.A. 1994. ApJ 435, 23
- Dressler, A.; Gunn, J.E. and Schneider, D.P. 1985. 1985. ApJ 294, 70
- Dressler, A. and Gunn, J.E. 1983. ApJ 270, 7
- Dressler, A. and Gunn, J.E. 1982. ApJ 263, 53
- Eales, S.A. 1985. MNRAS 217, 149
- Ebeling, H. et al. 2000. MNRAS 318, 333
- Ebeling, H. et al. 1998. MNRAS 301, 881
- Efstathiou, G et al. 2002 MNRAS 330, 29
- Eke, V.R. et al. 1998. MNRAS 298, 1145
- Ellingson, E.; Lin, H. Yee, H.K.C. and Carlberg, R.G. 2001. ApJ 547, 609
- Fairley, B.W. et al. 2002. MNRAS 330, 755
- Feigelson, E.D., Maccacaro, T. and Zamorani, G. 1982. ApJ 255, 392
- Franceschini, A.; Danese, L.; Toffolatti, L. and de Zotti, G. 1988. MNRAS 233, 157
- Fukugita, M.; Shimasaku, K. and Ichikawa, T. 1995. PASP 107, 945
- Fujita, Y. 1998. ApJ 509, 587
- Garnivich, P.M et al. 1998. ApJ 509, 74
- Gay, P.L 2002 FindOD: Overdensity search software.
- Gioia, I.M. et al. 1990 ApJ 356, 35
- Glaspey, J.W. et al. 1998. SPIE 3349, 50

Gonzalez, A.H.; Zaritsky, D.; Dalcanton, J.J. and Nelson, A. 2001 ApJS 137, 117

Gunn, J.E. and Gott, J.R. III. 1972. ApJ 176, 1

Gurvits, L.I. et al. 1994. ApJ 425, 442

Henriksen, M. and Byrd, G. 1996. ApJ 459, 82

Hill, G.J. and Lilly, S.J. 1991. ApJ 367, 1

Hoessel, J.G. 1980. ApJ 241, 493

Humason, M.L.; Mayall, N.U. and Sandage, A.R. 1956. AJ 61, 97

Icke, V. 1985. A&A 144, 115

Kauffmann, G. 1995. MNRAS 274, 153

Kim, R.S.J. et al. 2002 AJ 123, 20

Kodama, T.; Bower, R.G. and Bell, E.F. 2001. Ap&SS 276, 877

Krauss, L.M. 1998. ApJ 501, 461

Kron, R.G. 1980 ApJS 43, 305

Lacy, M.; Bunker, A.J. and Ridgeway, S.E. 2000 AJ 120, 68

Landolt, A.U. 1991 AJ 104, 340

Laing, R.A.; Railey, J.M. and Longair, M.S. 1983. MNRAS 204, 151

Lavery, R.J. and Henery, J.P. 1988. ApJ 329, 21

Lavery, R.J., Pierce, M.J. and McClure, R.D. 1992. AJ 104, 2067

Lilly, S.J.; McLean, I.S. and Longair, M.S. 1984. MNRAS 209, 401

Lineweaver, C.H. and Barbosa, D. 1998. ApJ 496, 624

Lubin, L.M. 1996. AJ 112, 23

Machalski, J. and Condon, J.J. 1999. ApJS 123, 41

- Maddox, S. et al 1998. "Large Scale Structure: Tracks and Traces." Proceedings of the 12th Potsdam Cosmology Workshop, held in Potsdam, September 15th to 19th, 1997. Eds. V. Mueller, S. Gottloeber, J.P. Muecket, J. (Wambsganss World Scientific, 1998). p. 91-96.
- Magliocchetti, M. et al. 2000. MNRAS 318, 1047
- Margoniner, V.E. and deCarvalho, R.R. 2000. AJ 119, 1562
- Margoniner, V.E.; de Carvalho, R.R.; Gal, R.R. and Djorgovski, S.G. 2001. ApJ 548, 143
- Martel, Hugo 2002 private communication
- Mauskopf, P.D. et al. 2000, ApJ 536, L63
- Machalski, J. and Condon, J.J. 1999. ApJS 123, 41
- McLean, B.J., Greene, G.R., Lattanzi, M.G. and Pirenne, B. 2000. ADASS 9, 145
- Melchiorri, A. et al. 2000 ApJ 536, 63
- Metevier, A.J.; Romer, A.K. and Ulmer, M.P. 2000. AJ 119, 1090
- Miller, A.D. and Owen, F.N. 2001. ApJS 134, 355
- Miller, A.D. et al. 1999 ApJ 524, L1
- Navarro, J.F.; Frenk, C.S. and White, S.D.M. 1997. ApJ 490, 493
- Nelson, A.E. et al 2001. ApJ 563, 629
- Nelson, A.E. et al. 2002. ApJ. 566, 103
- Netterfield, C.B. et al. 2002 ApJ 571,604
- Newman, J.A. et al. 2002 PASP 114, 29
- Oemler, A. Jr.; Dressler, A. and Butcher, H.R. 1997. ApJ 474, 561
- Owen, F.N. 1996. IAUS 175, 305
- Owen, F.N. and Laing, R.A. 1989. MNRAS 238, 357

Owen, F.N. and White, R.A. 1991. MNRAS 249, 164

Perlmutter, S. et al. 1999 ApJ 517, 565

Postman, M. et al. 1996. AJ 111, 615

Postman, M. and Lauer, T.R. 1995. ApJ 440, 28

Premadi, P.; Martel, H. and Matzner, R. ApJ 493, 10

Quilis, V., Moore, B. and Bower, R. 2000. Science 288, 1617

Rakos, K.D.; Schombert, J.M.; Odell, A.P. and Steindling, S. 2000. ApJ 540, 715

Renyue, C. 1998. ApJ 509, 494

Retzlaff, J. et al. 1998. New Astronomy 3, 631

Riess, A.G. et al. 2001. ApJ 560, 49

Sadler, E.M. et al. 2002. MNRAS 329, 227

Sandage, A.; Kristian, J. and Westphal, J.A. 1976. ApJ 205, 688

Schuecker, P., et al. 1998. ApJ 496, 635

Schindler, S. 2001. "Frontier Objects in Astrophysics and Particle Physics, Vulcano Workshop" ed. F. Giovannelli and G. Mannocchi. Italian Physical Society, 2001., p.33

Shectman, S.A. et al. 1996 ApJ 470, 172

Slee, O.B.; Roy, A.L. and Andernach, H. 1998 AuJPH 51, 971

Stoeckel, J.T. et al. ApJS 76, 813

Tyson, J.A. and Seitzer, P. 1988. ApJ 335, 552

van Dokkum, P.G. et al. 2001 ApJ 552, 101

Vikhlinin, A. et al. 1998. ApJ 502, 558

White, M. 1998. ApJ 506, 495

Windhorst, R.A.; Miley, G.K.; Owen, F.N.; Kron, R.G. and Koo, D.C. 1984.
A&AS 58, 1

Yamada, T. et al. 2001. PASJ 53, 1119

Yee, H.K.C.; Ellingson, E. and Carlberg, R.G. 1996. ApJS 102, 269

Zanichelli, A. et al. 2001, A&A 379, 35

Zirbel, E. L. 1997 ApJ 476, 489

Vita

Pamela Lynn Gay was born in California on December 12, 1973 to Donald and Eileen Gay. At age 8 she moved to Massachusetts where she later attended Westford Academy for high school. She went on to study astrophysics at Michigan State University and graduated with honors in May 1996. She next attended the University of Texas, where she completed her Masters of Arts in Astronomy in December 1998. Ms. Gay's research interests are variable stars and galaxy evolution. She has authored or co-authored papers in both these fields.

Throughout her graduate career, Ms. Gay was active in teaching and public service. She has written various popular and educational astronomy materials, was assistant instructor for AST103L: Observational Astronomy for five semesters, advised the Astronomy Students' Association for five years and volunteered for Tomorrow's Women in Science and Technology for six years. She is a two-time recipient of the Goettings Presidential Endowed Fellowship, and of the American Association of University Women Graduate Fellowship.

In her spare time, Ms. Gay rides her horses Quantum Leap, Hayley and Don Lazarus Red. Upon completion of writing this dissertation, she accepted a position as an editor at *Astronomy Magazine* in Brookfield, Wisconsin.

Permanent address: 8324 W. Dana St. #4, Milwaukee, WI 53214

This dissertation was typed by the author.